REVEALING COMPOSITIONAL DIVERSITY ON THE MARTIAN SURFACE FROM REMOTE SENSING OBSERVATIONS AND THERMAL INFRARED LABORATORY ANALYSES: IMPLICATIONS FOR ANCIENT HYDROLOGICAL AND CLIMATOLOGICAL SYSTEMS

A DISSERTATION SUBMITTED TO
THE GRADUATE DIVISION OF THE UNIVERSITY OF HAWAI'I
IN PARTIAL FULFILLMENT OF THE REQUIREMENTS FOR THE DEGREE OF

DOCTOR OF PHILOSOPHY

IN

GEOLOGY AND GEOPHYSICS

December 2010

By
Mikki Michele Osterloo

Dissertation Committee:

F. Scott Anderson, Chairperson
Victoria E. Hamilton
G. Jeffrey Taylor
Robert Wright
David W. Muenow

We certify that we have read this dissertation and that, in our opinion, it is satisfactory in scope and quality as a dissertation for the degree of Doctor of Philosophy in Geology and Geophysics.

DISSERTATION COMMITTEE

_____
Chairperson

_____

_____

_____

_____

This dissertation is dedicated to Keith. The only person who was able to actively support this endeavor while espousing that I should quit on almost a daily basis.

ACKNOWLEDGEMENTS

First and foremost, I thank my parents for imparting to me the love of the natural world. I thank my father for supporting me in all my endeavors and building my confidence to continually ask the difficult questions and never accept the easy solutions. I thank my mother for pushing me to always strive for excellence. My sisters have always been there for me, despite my absence from their lives. My grandfather is an inspiration, his steadfastness in his work has set such a standard that this dissertation pales in comparison.

I could not have asked for a better, more fundamental geology education than I received from the Geological Sciences Department at Indiana University. From the many professors, and especially Drs. James Brophy and Bruce Douglas in particular, I learned how to think critically and look at the many angles of a problem, but never lose site of the big picture at hand. My mentors at Los Alamos National Laboratory were instrumental in encouraging me to further my education; Drs. William Feldman, David Bish, Steven Brumby, and most especially Dr. Herbert Funsten, who served as role model, adviser, and friend. Thank you.

I would like to thank the professors in the Geology and Geophysics Department and Hawai‘i Institute of Geophysics and Planetology at the University of Hawai‘i for the excellent classes and interesting scientific discussions. I would also like to thank Drs. Bruce Houghton, Eric Gaidos, and Kathleen Ruttenberg for their incredible support and essential advice during my yearly graduate reviews. For logistics, especially in the years since I have not been physically located in Hawai‘i, I could not have managed to complete my degree without Leona Anthony and Rena Lefevre. I

especially want to thank Dr. Charles Fletcher for continual support and encouragement throughout this process.

I have been fortunate to have collaborated with and learned from an outstanding group of scientists. I would like to thank Drs. Philip Christensen, Joshua Bandfield, Timothy Glotch, Brian Hynek, Alice Baldridge, Livio Tornabene and Christopher Dreyer. Much of the actual work of this dissertation would not have been possible without Chris Edwards, Saadat Anwar, Eric Engle, and Scott Dickensheid, who provided essential guidance with Davinci and JMARS. Kim Murray and Dale Noss generously provided assistance in accessing and targeting THEMIS data.

I would like to formally thank my dissertation committee for working with me in a less than ideal situation, Drs. F. Scott Anderson, Victoria Hamilton, G. Jeffrey Taylor, Robert Wright, and David Muenow. I have greatly valued our discussions and appreciate all the support and encouragement you have provided me over the last few years.

I have benefited from being surrounded by an amazing and dynamic group of people whom I am fortunate to call my friends as well as colleagues. Many of you provided essential moral support in addition to stimulating scientific and philosophical discussions, for which my experience has been greatly improved: Meryl McDowell, Deon Van Niekerk, Laurie Rogers, Chris Edwards, Will Koeppen, Josh Bandfield, David Finkelstein, Deanne Rogers, Brian Hynek, Lisa Mayhew, Tim Glotch, Kim Brandstetter, Alison Moore, Alice Baldridge, Scott Anderson, and Vicky Hamilton. I could not have completed this dissertation without the support of my husband, Keith. Thank you.

ABSTRACT

This dissertation focuses on two topics; 1) quantifying the effects of roughness on the thermal infrared spectra of rock surfaces and 2) the identification and geologic context of proposed chloride-bearing materials on the Martian surface. Using thermal infrared (TIR) multi-spectral and hyperspectral data in concert with elevation and geomorphological information, I investigated the composition and global distribution of spectrally distinct surfaces on Mars. I identified the materials based on their spectral distinctiveness in false-color decorrelation stretched multi-spectral day infrared radiance data from the 2001 Mars Odyssey Thermal Emission Imaging System. Infrared emissivity data over the materials show relatively featureless spectra that slope towards lower wavenumbers. Based on the spectral observations, in concert with ancillary geomorphological observations, I concluded that the spectrally distinct deposits contained a component attributable to chloride-salts. Chloride salts are relatively spectrally featureless and commonly display non-unit emissivities, which could cause an incorrect temperature derivation and introduce a slope in the emissivity spectrum. I identified ~640 distinct sites dispersed throughout the low albedo Noachian and Hesperian aged terrains of the southern highlands. The materials show a range of sizes (~0.33 to ~1300 km^2) and morphologies and are typically lighter in tone and more consolidated relative to the surrounding terrain. Based on topographic analyses, I found that the majority of materials occur in local lows, although cross-cutting relationships indicate that some sites are located in 'geologic windows', implying that the materials may be older than the terrains in which they

are situated. Once exposed, the materials appear to undergo erosion, which may be the reason we do not observe large laterally extensive materials at the surface. The materials are predominantly local in nature, yet their prevalence across the southern highlands suggests that they represent one or more globally ubiquitous process and that formation of chloride salts on Mars has been an important process. Most observations are consistent with formation via ponding of surface runoff or groundwater upwelling. The materials' inferred ages suggest that the conditions that enabled the formation of the materials persisted for up to a billion years.

I present results of a laboratory study that focuses on investigating the effects of rough surfaces on the infrared spectra of different natural rock samples. The results indicate that: 1) the roughening process is highly repeatable across rock types, 2) rock types vary in the degree that they are susceptible to abrasion, 3) features in emissivity spectra do not change shape or position with increasing surface roughness, 4) reduction of spectral contrast is observed with increasing roughness across all rock groups until a threshold roughness (which varies across rock types) is achieved, whereupon further reductions do not occur or in some cases, spectral contrast begins to increase, 5) spectra from the roughened surfaces are well explained by few surface reflections, and 6) I do not observe complete obscuration of features in any of our roughened spectra, and 7) surfaces created through the roughening process could be considered analogs to materials roughened by aeolian abrasion, a dominant process on the surface of Mars. This study suggests that spectral contrast, strictly speaking, is not dependent upon surface roughness but upon the morphology of the surface. I found that rough surfaces may display morphologies that are well modeled by low

reflection cavities (LRCs), as investigated here, which would reduce spectral contrast, but not obscure spectral features.

TABLE OF CONTENTS

ACKNOWLEDGEMENTS ..... **IV**

ABSTRACT ..... **VI**

LIST OF TABLES ..... **XI**

LIST OF FIGURES ..... **XII**

CHAPTER 1: INTRODUCTION **1**

CHAPTER 2: CHLORIDE–BEARING MATERIALS IN THE SOUTHERN HIGHLANDS OF MARS **11**

ABSTRACT: **12**

SUPPORTING ONLINE MATERIAL (SOM) **20**

ACKNOWLEDGEMENTS **33**

FIGURES **34**

CHAPTER 3: THE GEOLOGIC CONTEXT OF PROPOSED CHLORIDE-BEARING MATERIALS ON MARS **40**

ABSTRACT: **41**

1.0 INTRODUCTION **42**

2.0 DATASETS AND METHODS **45**

2.1 THEMIS 45
2.2 ANCILLARY DATA AND SOFTWARE 47

3.0 RESULTS **49**

3.1 MORPHOLOGY 49
3.2 GLOBAL ELEVATIONS AND LOCAL TOPOGRAPHY 54
3.3 RELATIONSHIPS BETWEEN LOCATIONS OF PROPOSED CHLORIDE-BEARING MATERIALS WITH PREVIOUSLY MAPPED THERMOPHYSICAL, COMPOSITIONAL, AND MORPHOLOGICAL PROPERTIES .. 55

4.0 DISCUSSION **65**

4.1 FORMATION MECHANISMS FOR TERRESTRIAL CHLORIDE AND SULFIDE MINERALS 65
4.2 MORPHOLOGY 66
4.3 ELEVATION AND TOPOGRAPHY 70
4.4 CORRELATIONS BETWEEN THE LOCATIONS OF PROPOSED CHLORIDE-BEARING MATERIALS AND GLOBALLY MAPPED PROPERTIES 72
4.5. GLOBALLY MAPPED PROPERTIES THAT DO NOT CORRELATE WITH THE LOCATIONS OF PROPOSED CHLORIDE-BEARING MATERIALS 77
4.6 LOCAL AND REGIONAL MINERALOGICAL COMPOSITIONS 81
4.7 ASTROBIOLOGICAL SIGNIFICANCE OF POSSIBLE CHLORIDE-BEARING MATERIALS 84

5.0 CONCLUSIONS **86**

ACKNOWLEDGEMENTS: **90**

TABLES **91**

FIGURES **101**

CHAPTER 4: A LABORATORY STUDY OF THE EFFECTS OF ROUGHNESS ON THE THERMAL INFRARED SPECTRA OF ROCK SURFACES **119**

ABSTRACT: **120**

1.0 INTRODUCTION **122**

2.0 BACKGROUND **123**

3.0 METHODS. **127**

4.0 RESULTS **133**

4.1 REPEATABILITY AND INITIAL SPECTRAL CHARACTERISTICS 133
4.2 SURFACE ROUGHNESS 134
4.3 ROUGHNESS EFFECTS ON TIR SPECTRA OF ROCK SURFACES 137

5.0 DISCUSSION **144**

5.1 CAUSES OF SPECTRAL CONTRAST CHANGES 145
5.2 APPLICABILITY TO NATURAL SURFACE ROUGHNESSES 153
5.3 SUGGESTIONS FOR ADDITIONAL WORK AND IMPROVED STUDIES 156

6.0 CONCLUSIONS **158**

ACKNOWLEDGMENTS: **161**

TABLES **162**

FIGURES **166**

REFERENCES **183**

LIST OF TABLES

Chapter 3
Table 3.1. THEMIS infrared band characteristics 91
Table 3.2. Global maps used in analysis 92
Table 3.3. Geologic ages of the proposed chloride-bearing materials 93
Table 3.4. Proportion of chloride materials' areas 94
Table 3.5. Crater size-frequency determinations 95
Table 3.6. THEMIS thermal inertia and single detector albedo 96
Table 3.7. Formation hypothesis for the proposed chloride-bearing 98
Table 3.8. Minimum required halite wt% 100

Chapter 4
Table 4.1. Rock samples 162
Table 4.2. Wavenumber positions 163
Table 4.3. Fine-grained materials 164
Table 4.4. Intermediate- to coarse-grained materials 165

LIST OF FIGURES

Chapter 2.
Figure 2.1. THEMIS 8/7/5 DCS radiance images 34
Figure 2.2. Global distribution of spectrally distinct materials 35
Figure 2.3. THEMIS and TES emissivity spectra 36
Figure 2.4. HiRISE image PSP_003160_1410 37
Figure 2.S1. Assuming a maximum emissivity of 0.95 38
Figure 2.S2. Laboratory emission spectra for a variety of chlorides 39

Chapter 3.
Figure 3.1. Spectra of chloride materials and candidates 101
Figure 3.2. THEMIS decorrelation stretch images 102
Figure 3.3. Morphology from THEMIS 103
Figure 3.4. Differences in spatial resolution 104
Figure 3.5. Fluvial associations in Terra Sirenum 105
Figure 3.6. HiRISE composite of materials 106
Figure 3.7. HiRISE showing etched morphology 107
Figure 3.8. HiRISE showing variations in fractures 108
Figure 3.9. MOLA elevations of materials 109
Figure 3.10. Topography of three sites 110
Figure 3.11. DCI and Geologic terrains 111
Figure 3.12. Age and area of materials 112
Figure 3.13. Size-frequency crater plots for three sites 113
Figure 3.14. Thermal inertia and albedo for the materials 114
Figure 3.15. THEMIS radiance and thermal inertia for three sites 115
Figure 3.16. Valley network density map showing materials in red 116
Figure 3.17. GRS Cl, H_2O, and K/Th global maps 117
Figure 3.18. GRS Cl, H_2O, and K/Th values for the materials 118

Chapter 4.
Figure 4.1. Examples of the twelve groups of rock samples 166
Figure 4.2. Averages of spectra collected for reproducibility 167
Figure 4.3. Spectra of the abrasives 168
Figure 4.4. Average spectra for each group with standard deviations 169
Figure 4.5. Initial R_a values for three samples 170
Figure 4.6. Elevation profiles for roughened surfaces 171
Figure 4.7: Roughened R_a values for groups 172
Figure 4.8. Log-log plots of R_{qe} (μm) vs. Epsilon (μm) 173
Figure 4.9. Emissivity of initial and roughened surfaces 175
Figure 4.10. Delta emissivity values versus R_{qes} 177
Figure 4.11. Percentages of normalized delta emissivities versus R_{qes} 179
Figure 4.12. Height of feature (in microns) required for observation 181
Figure 4.13. Average number of reflections versus R_{qes} 182

CHAPTER 1: INTRODUCTION

One of the primary goals of acquiring spectroscopy observations of Mars is to determine surface mineralogy. Understanding the mineralogy of a surface is critical because it can record evidence of hydrothermal activity and past climatic conditions, including aqueous and aeolian processes. From the surface mineralogy, the composition of the planet interior and the degree of variation in magma compositions may also be inferred. In this work, I used orbital infrared emission data to map the distribution of terrains proposed to contain a chloride-bearing mineralogical component. Using ancillary information such as topography, geomorphology, thermophysical characteristics, and previously published geological and geochemical maps, in concert with the spectroscopic data, I investigated the composition, age, geologic setting, and global distribution of the proposed chloride-bearing materials. In order to investigate the composition of a surface, a solid basis in laboratory spectroscopy is fundamental. To this end, I systematically, under controlled conditions, investigated roughness effects on the thermal infrared spectra of a wide variety of natural rock surfaces.

Thermal emission spectroscopy is fundamentally based on vibrational spectroscopy. Molecular vibrations that occur within a crystal lattice at frequencies that are directly related to the crystal structural and elemental composition cause the absorption and emission of infrared radiation [e.g.,*Wilson et al*., 1955; *Farmer,* 1974]. Several factors affect the frequency, shape, intensities, and number of internal vibrational modes including valences of the cations and anions, mass of the atoms, degree of covalency of the bond, bond length, and type of symmetry of the vibration

modes (e.g., stretching or bending) [e.g., *Gaffey et al.,* 1993]. These variables are determined by the composition, location, and polymerization of the anions and cations within a crystal lattice. Because all minerals have unique compositions and/or structures, virtually every mineral contains a unique set of absorptions and therefore also has a distinct spectrum in the thermal infrared. Vibrational spectroscopy has been used extensively to determine quantitative mineralogy and petrology in many studies [e.g., *Lyon*, 1965; *Vincent and Thompson*, 1972; *Farmer*, 1974; *Salisbury et al.,*1987, 1991; *Salisbury and Walter*, 1989; *Salisbury*, 1993; *Christensen and Harrison*, 1993; *Feely and Christensen*, 1999; *Christensen et al.,* 2000a; *Hamilton and Christensen*, 2000; *Hamilton et al.,* 2001; *Koeppen and Hamilton*, 2008].

The overall goal of this work was to investigate in detail the surface composition and global distribution of spectrally distinct materials on Mars that had not previously been identified in orbital data. The results in turn could be incorporated into the current understanding of the compositional diversity and geologic history of the Martian surface. For my dissertation, I analyzed local-scale variability in surface compositions, in the context of morphology, relative age/stratigraphy, thermophysical properties, geographic province, regional compositions, elevation and topography, and latitude, in an effort to constrain the origin of the observed materials and decipher their similarities and differences globally. Additionally, I analyzed surface roughness effects on thermal infrared emission laboratory data in an effort to understand how surface texture may obscure the diagnostic spectral signatures of a material in the infrared wavelength region. The work presented in this dissertation is divided into three main chapters and each chapter describes an individual research project with its

own set of results and conclusions. However, chapters 2 and 3 could be considered companion chapters, as the results from the second chapter are the basis for the analysis in the third.

Mars has long been the object of detailed spectroscopic studies that have largely suggested a planet shaped primarily by volcanic processes, but modified by aqueous alteration. Early spectroscopic investigations showed that the difference between the low and high albedo region spectra was well modeled using basalts that were oxidized to different degrees [*Adams and McCord,* 1969], indicating that the bright regions are more highly oxidized or altered and composed of finer particles [*Singer et al*. 1979]. Mineral mapping using data from the Mars Global Surveyor Thermal Emission Spectrometer (TES) [*Christensen et al*., 2001a] instrument as well as data returned from the Mars Express Observatoire por la mineralogie, i'Eau les Glaces et l'Activite (OMEGA) [*Bibring et al.*, 2005] have supported earlier hypotheses, yet added a higher degree of compositional and mineralogical complexity. TES data demonstrated that basalt is the primary rock type on Mars [*Christensen et al.*, 2000a], but deconvolution results indicate that there is regional scale igneous compositional variability within the low-albedo regions [*Rogers and Christense*n, 2007; *Rogers et al.*, 2007]. Additionally, local compositional variations have been identified using higher spatial resolution data from the Thermal Emission Imaging System (THEMIS) onboard Mars Odyssey [*Christensen et a*l. 2004, 2005; *Bandfield et al*., 2004; *Bandfield*, 2006; *Hamilton and Christensen*, 2005; *Rogers et al.*, 2005; *Edwards et al*. 2008].

Spectroscopic evidence for hydration, weathering or alteration of surface components, and aqueously derived minerals has accumulated since early spectroscopic observations. However, limited spatial and spectral resolution in early data sets as well as partial obscuration due to the atmosphere made it difficult to definitively identify specific minerals. Spectroscopic data from OMEGA and the Compact Reconnaissance Imaging Spectrometer for Mars (CRISM) [*Murchie et al.*, 2006] has provided evidence for a diversity of phyllosilicate spectral detections in isolated occurrences throughout the Noachian aged terrains [*Bibring et al.*, 2005; *Poulet et al.*, 2005; *Bibring et al.*, 2006; *Mustard et al.*, 2008; *Bishop et al.*, 2008; *Ehlmann et al.*, 2009]. Additionally, crystalline, coarse-grained, "gray" hematite was one of the first aqueously formed minerals identified on the Martian surface from orbit [*Christensen et al*., 2000b; *Christensen et al.,* 2001b]. A variety of sulfates have been identified in OMEGA and CRISM data associated with light-toned layered units in Valles Marineris and in Aram Chaos, as large regional units in Terra Meridiani, and close to the perennial northern polar cap [*Bibring et al*., 2005; *Gendrin et al*., 2005; *Milliken et al.,* 2008; *Bishop et al*., 2009; *Murchie et al*., 2009; *Lichtenberg et al.*, 2010; *Roach et al*., 2008, 2009]. *Bandfield* [2008] identified a high silica material that is likely the product of aqueous alteration and *Milliken et al.*, [2008] identified hydrated opaline silica using data collected from CRISM. Furthermore, analysis of CRISM data has provided evidence for detection of magnesium carbonate-bearing bedrock [*Ehlmann et al.,* 2008].

Multiple lines of evidence suggest that chloride salts are also a component of the Martian regolith. Principally, chloride salts are predicted to form in a Martian

evaporative environment that is dominated by basaltic weathering [*Tosca and McLennan*, 2006]. Analyses of SNC (shergottite, nakhlite, and chassignite) meteorites indicate traces of volatile compounds that suggest either accommodation of vestigial magmatic volatiles or late-stage interactions with aqueous liquids [*Gooding*, 1992]. Specifically, trace amounts of NaCl (halite) have been documented in various Nakhla and Shergotty meteorite specimens [*Gooding et al.*, 1990; *Gooding et al.*, 1991; *Bridges and Grady*, 1999, 2000; *Rao et al.,* 2005]. Based on analysis and Cl/Br modeling and alteration assemblages within Nakhla, a formation mechanism involving evaporation (or concentration via freezing) of low-temperature brines with chemistry similar to terrestrial marine halite-rich brine solutions has been suggested [*Bridges and Grady*, 2000; *Rao et al.*, 2005]. Additionally, elevated levels of chlorine (~1%) in cohesive soils (duricrust) have been reported from chemical analysis at the Viking landing site 1 and 2 [*Clark et al*., 1976; *Baird et al.,* 1976; *Clark and VanHart,* 1981], Pathfinder [*Rieder et al.,* 1997; *Wänke et al.,* 2001; *Foley et al*., 2003; *Bruckner et al.,* 2003] and MER [*Gellert et al*., 2004; *Rieder et al.,* 2004] landing sites. Furthermore, the Gamma Ray Spectrometer has mapped chlorine from orbit (mean concentration of 0.49%) [*Keller et al.*, 2006], which suggests that the upper few centimeters of regolith is enriched relative to estimates for the bulk composition of the planet.

Both MERs, *Spirit* and *Opportunity*, have provided evidence for elevated levels of halogens, specifically Cl and Br, and various chloride salts [*Gellert et al.*, 2004; *Rieder et al*., 2004]. *Clark et al*. [2005] evaluated the chemical mass balance of data from the Burns formation and suggested that late-forming evaporitic minerals, such as

chlorides or bromides, may have formed in the system. Additional modeling from *Marion et al.* [2009] of the Br/Cl partitioning in chloride minerals within the Burns formation supports the theory of salt upwelling through groundwater evaporation. The suggested chlorides, and sometimes specifically halite, are present as interstitial cements [*McLennan et al*., 2005] or inferred from secondary porosity features such as crystal shaped molds or vugs interpreted to represent molds of an earlier formed evaporitic mineral (possibly magnesium or iron chloride) [*McLennan et al*., 2005]. Additionally, NaCl found in the veneers of some of the outcrops at Meridiani Planum are hypothesized to have formed from dissolution of soluble salts by a thin film of water under transiently favorable environmental conditions (presumably from outcrops blanketed by soil), and then re-precipitated on the outcrop surface [*Knoll et al*., 2008].

Water and acid volatiles also appear to have played a significant role in the alteration and formation of rocks and soils in and near the Columbia Hills of Gusev Crater [*Ming et al.*, 2006]. Clovis, Wishstone, and Watchtower source materials appear to have been altered by fluids rich in the volatile elements S, Cl, and Br [*Ming et al*., 2006]. Minor amounts of halite (~2%) were also inferred to be present in the light toned Paso Robles soil and the additional mineralogy and chemistry strongly suggest that the salts are precipitates from gas condensates and hydrothermal fluids associated with the nearby Home Plate [*Yen et al*., 2008; *Squyres et al.*, 2007]. Additionally, a number of the rock classes observed in the Inner Basin of Columbia Hills also show elevated levels of halogens presumably from hydrothermal alteration [*Haskin et al*., 2005; *Yen et al*., 2005, 2008; *Schmidt et al.*, 2008].

In Chapter 2, I present the initial identification and distribution of the spectrally distinct materials. I report on the spectral signature of the materials, as well as their thermophysical and morphological properties from a type locality in Terra Sirenum. The materials are identified based on their spectral distinctiveness in false-color, decorrelation stretched (DCS) THEMIS daytime infrared radiance images. The spectrally distinct materials show THEMIS emissivity spectra that are unlike any previously studied surface type. The materials are characterized by a relatively featureless spectrum that slopes towards lower wavenumbers. The initial survey of the THEMIS dataset revealed ~200 of the deposits located throughout the Noachian and Hesperian low-albedo, southern highlands. The deposits identified were typically small (< ~25 km^2) isolated patches, that were generally topographically lower than the surrounding terrain. Additionally, the spectrally distinct materials in Terra Sirenum were light-toned and displayed polygonally fractured surfaces that cross cut morphologies suggestive of dune forms. These morphological observations, in addition to the elevated THEMIS-derived thermal inertias suggested that the materials were cemented. The spectral and morphological observations indicated that the most likely component of the Martian materials were chloride salts. Chapter 2 was published in the journal *Science*, in March 2008.

In Chapter 3, a comprehensive global survey of the proposed chloride-bearing materials discovered in Chapter 2 is presented. Here, I expand on the characterization of the materials from ~200 to ~640 distinct sites using a variety of orbital datasets and previously published maps. I considered sulfides as an alternative hypothesis for the minerals responsible for the relatively featureless, sloped spectra. And though they

can not be eliminated based on the results of the work presented, I conclude that they are less likely candidates given the lack of morphological indicators for volcanic processes or compositional evidence for parent lithologies and associated weathering products. The materials are predominantly local in nature, yet their prevalence within the southern highlands suggests that they represent a globally ubiquitous process. Observations over many sites shows characteristics consistent with deposition via precipitation from a ponded evaporating brine derived from upwelling groundwater and/or surface runoff. The correlation between the proposed chloride-bearing materials' locations and ages with the locations and ages of the valley-networks and paleobasins further supports this hypothesis. The results of the survey are consistent with the presence of chloride salts as the component of the spectrally distinct materials on the Martian surface and their presence has the potential to shed light on the history and evolution of water and paleoenvironmental conditions on Mars. Chapter 3 is in press in the *Journal of Geophysical Research-Planets*.

An underlying theme of this dissertation is to compare remotely acquired infrared emission data with laboratory-derived infrared emission spectra of rocks and minerals. However, previous studies have suggested that surface roughness effects can change the contrast or obscure the diagnostic spectral signatures of materials in the infrared wavelength region [e.g., *Kirkland et al*., 2003]. If the detectability of all minerals in the infrared may be dependent in part on their surface roughness, it is critical to establish which classes of rocks display this effect and to what degree. In Chapter 4, I present a laboratory study on the effects of surface roughness on the infrared emission spectra of diverse suite of natural rock surfaces, including igneous,

metamorphic, and sedimentary compositions. Previous studies have attributed all surface roughness to blackbody cavity effects where multiple reflections reduce the number of photons measured at the sensor, resulting in shallowing of spectral features. However, not all rough surfaces have morphologies that can be approximated by blackbody cavities. Here, I focus on investigating the effects of more geologically common rough surfaces on the infrared spectra of natural rock surfaces. I roughened the samples with abrasives, which created average roughnesses that ranged from > ~1 μm to < ~10 μm and compared infrared emissivity spectra from initial and roughened surfaces. I used profilometer data to calculate the length scale-dependent root mean square deviation of the initial and roughened surfaces. The results show that for the roughness and morphologies created through the abrasion process utilized here, reduction of spectral contrast occurs with increasing roughness across all groups until a threshold roughness (that varies across rock types) is achieved, whereupon further reductions do not occur and in some cases, spectral contrast begins to increase. The results of this study suggests that spectral contrast, strictly speaking, is not dependent upon surface roughness but upon the morphology of the surface. Chapter 4 will be submitted for publication to the journal *Icarus*.

Overall, the work presented here is another piece of the complex Martian geologic puzzle. The identification of chloride-bearing materials adds yet another aqueously derived mineral to the compositional diversity and complexity of the Martian surface. The ages of the proposed chloride-bearing materials, proximity to valley networks, and locations within topographic lows, suggest that they may have been deposited during a punctuated time of abundant surface water when climatic conditions were

more conducive to longer-lived ephemeral surface brines. The results of the work presented here is a step towards gaining a more complete view of these interesting and important materials. The purpose of this study was to lay a firm ground work upon which future investigations of the proposed chloride-bearing materials may build. If future analyses of the materials continue to support and yield evidence for chloride-salts on the Martian surface, the materials have important implications regarding the role water has played in altering the surface of Mars, as well as, astrobiological potential and thus are a high priority for future landed missions.

CHAPTER 2: CHLORIDE–BEARING MATERIALS IN THE SOUTHERN HIGHLANDS OF MARS

Published in its present form as Osterloo, M. M., Hamilton, V. E., Bandfield, J. L., Glotch, T. D., Baldridge, A. M., Christensen, P. R., Tornabene, L. L., and Anderson, F. S. (2008), Science, 319, 1651, DOI: 10.1126/science.1150690.

Abstract:

Chlorides commonly precipitate during the evaporation of surface water or groundwater and during volcanic outgassing. Spectrally distinct surface deposits consistent with chloride-bearing materials have been identified and mapped using data from the 2001 Mars Odyssey Thermal Emission Imaging System. These deposits are found throughout regions of low albedo in the southern highlands of Mars. Geomorphologic evidence from orbiting imagery reveals these deposits to be light-toned relative to their surroundings and to be polygonally fractured. The deposits are small (< ~25 km^2) but globally widespread, occurring in middle to late Noachian terrains with a few occurrences in early Hesperian terrains. The identification of chlorides in the ancient southern highlands suggests that near-surface water was available and widespread in early Martian history.

On Earth, chlorides are formed by precipitation from evaporating surfaces (e.g. saline lakes) or groundwater/hydrothermal brines, as volcanic sublimates (e.g., at fumaroles) and by efflorescence (direct crystallization onto sediment grains forming crusts) [*Goodall et al.*, 2000]. Typically, chloride deposits produced by precipitation have large surface relief and polygonal to blocky morphologies, whereas efflorescence tends to produce thin crusts [*Goodall et al.*, 2000]. For terrestrial evaporite systems, the most important variable for the resultant brine composition and saline mineral assemblages is the composition of the dilute water at the onset of concentration (evaporation) [*Eugster and Hardy*, 1999]. Generally, chlorides in terrestrial settings occur in alkaline environments and are the last minerals to precipitate out of saline brines, preceded by various carbonates, sulfates, and silica. On Mars, saline minerals (including various chlorides) are predicted to form from acidic fluids derived from basaltic weathering [*Tosca et al.*, 2006]. Geologic environments that contain saline minerals are of key interest to the exobiology community because they are potentially areas of biological activity and chemical sedimentation, which is optimal for the preservation of biological signatures and a high priority for future exploration by orbiting and landed missions [*Farmer and Des Marais*, 1999].

Using Mars Odyssey Thermal Emission Imaging System (THEMIS) data [*Christensen et al.*, 2004], as well as supporting data from the Mars Global Surveyor [*Malin et al.*, 1992] and Mars Reconnaissance Orbiter [*McEwen et al.*, 2007], we have identified a compositional unit on Mars that contains a mineralogical component likely attributable to chloride salts. We initially identified these deposits because of

their spectral distinctiveness in false-color, decorrelation stretched (DCS), THEMIS daytime infrared radiance images [*See Supporting Online Material (SOM)*]. The deposits range in area from ~1 km_2 to ~25 km^2 and generally are topographically lower than the immediate surrounding terrain. The spectrally distinct deposits commonly exhibit irregular outlines (Figure 2.1A) and occur less commonly in small craters and sinuous channels (Figure 2.1, B to D). Our examination of the THEMIS daytime infrared data set has revealed ~200 of these deposits throughout the low albedo, mid-to-low latitude southern highlands (Figure 2.2), corresponding to mid-Noachian [~3.9 to ~3.8 billion years ago (Gya)] terrains and the Hesperian ridged plains unit (~3.7 to ~3.5 Gya) [*Hartmann and Neukum*, 2001].

THEMIS surface emissivity spectra [*Bandfield et al.*, 2004] of the deposits show that they have a spectral shape that is unlike any previously studied surface type [*Bandfield et al.*, 2000; *Hoefen et al.*, 2003; *Christensen et al.*, 2000a,b; *Bandfield and Smith*, 2003]. Whereas the regional materials (2.3A) exhibit a basaltic spectral shape, the distinct deposits are characterized by higher emissivity across the 1260 to 900 cm^{-1} range and exhibit a featureless spectral slope toward lower wave numbers. Higher spectral resolution (10 cm^{-1} sampling) Thermal Emission Spectrometer (TES) data can be used to further constrain the mineralogy of these surfaces, although at lower spatial resolution (~3 × 6 km minimum) [*See SOM*]. In Terra Sirenum, the spectrum of the distinct material is similar to that of the surrounding terrain, in that it exhibits a shape similar to that of basalt, but it differs in having a negative spectral slope (Figure 2.3B). The basaltic shape is attributable to the large spatial area measured by TES relative to THEMIS, which leads to sub-pixel mixing and dilution

of the spectrally distinct material by the regional basaltic materials. Spectral ratios were used to remove features common to both spectra and derive a residual spectral shape that represents the difference between the two materials [*Ruff and Christensen*, 2002]. The resulting ratio spectrum is relatively featureless and slopes toward lower wave numbers, as shown in Figure 2.3B. A slight residual "hump" in the ratio spectrum between ~1330 and 830 cm^{-1} resembles the basaltic shape (inverted) and is attributable to a difference in spectral contrast between the two spectra, both of which include basaltic materials. Therefore, we conclude that the spectral character of the spectrally distinct deposits is nearly featureless and inconsistent with previously derived TES surface shapes [*See SOM*] [*Bandfield et al.*, 2000; *Hoefen et al.*, 2003; *Christensen et al.*, 2000b; *Bandfield and Smith*, 2003]. Quantitative linear deconvolution and factor analysis/target transformation analyses of the TES data also indicate that phases with weak spectral features and negative slopes are candidates for the component that is responsible for the spectrally distinct materials, although there is no phase in our spectral library (which contains >200 rock and mineral phases, including phyllosilicates and sulfates, [*Christensen et al.*, 2000c]) that results in a good model fit [*See SOM*].

A negative spectral slope in mid-infrared emissivity spectra can arise from errors in the derivation of temperature in the process of converting radiance (a temperature-dependent parameter) to emissivity (which is independent of temperature) [*See SOM*] [*Ruff et al.*, 1997]. The separation of temperature and emissivity relies on the assumption that the observed radiance represents a single or narrow range of temperatures (e.g., a few degrees K) and that the emissivity of the materials is unity at

some point in the spectral range. We find no evidence for large temperature variations at the 100m/pixel scale of the THEMIS instrument that would introduce such temperature errors [*See SOM*]. However, if the observed materials do not exhibit unit emissivity (as assumed at some point in the wavenumber range used to determine the target temperature), incorrect temperatures may be derived during the conversion of radiance to emissivity [*See SOM*]. For materials having a maximum emissivity less than unity, the target temperature will be underestimated and a slope will be imparted to the resulting emissivity spectrum [*Ruff et al.*, 1997].

Virtually all silicate phases (and most carbonate, sulfate, and oxide phases) exhibit near-unit emissivity at some point in the 1350 to 300 cm^{-1} range used for the TES temperature-emissivity separation [*Christensen*, 1999]; however, some chlorides have relatively featureless spectra in this range [*See SOM*] [*Lane and Christensen*, 1998; *Farmer*, 1974]. One or more chlorides as a component of the Martian materials would reduce emissivity, causing incorrect temperature derivation and introducing a slope in the emissivity spectrum. Chloride salts have been identified on Earth in infrared multispectral data on the basis of similar observations; for example, the presence of halite was accurately inferred in Death Valley, California, by a lack of spectral features in high-resolution MODIS (Moderate Resolution Imaging Spectroradiometer)/ ASTER (Advanced Spaceborne Thermal Emission and Reflection Radiometer)Airborne Simulator (MASTER) which covers a similar wavelength range as the THEMIS instrument [*See SOM*] [*Baldridge et al.*, 2004]. Based on the observed Martian spectra, the assumption of unit emissivity during TES and THEMIS data reduction, the laboratory measurements of the behavior of chloride

salts, and similar terrestrial identifications, we interpret these spectrally distinct materials to be chloride-bearing deposits.

Further insight into the nature and origin of the putative chloride-bearing deposits is provided by visible images from THEMIS [*Christensen et al.*, 2004], the High Resolution Imaging Science Experiment (HiRISE) [*McEwen et al.*, 2007], and the Mars Orbiter Camera (MOC) [*Malin et al.*, 2002], topography from the Mars Orbiter Laser Altimeter (MOLA) [*Zuber et al.*, 1992], and thermal inertia from THEMIS nighttime data [*Bandfield*, 2007]. MOC images (~2.95m/pixel) of the Terra Sirenum deposit and other deposits across the southern highlands show that the chloride-bearing materials are light-toned; in addition, they exhibit patterned-ground and etched terrain morphologies. Higher spatial resolution (~25.3 cm/pixel) HiRISE images of the materials in Terra Sirenum also show the putative chloride bearing materials to be light-toned and highly fractured and to have an etched morphology that may indicate cemented Aeolian bedforms (Figure 2.4,A and B). The chloride-bearing materials appear to have been exposed by erosion of dark materials, which are observed bordering the light-toned deposit (Figure 2.4A).

The pervasive polygonal fracturing observed in the HiRISE image is irregular, with variable diameters (Figure 2.4B.). The fractures defining the polygons crosscut ridges and valleys and occur along ridge crests, indicating that the surface is an indurated material (Figure 2.4C). Thermal inertia derived from THEMIS nighttime infrared observations indicates that the chloride-bearing material in Terra Sirenum has a thermal inertia close to 400 $Jm^{-2}\ K^{-1}s^{-1/2}$, whereas values for the surrounding terrain are substantially lower (180 to 280) [*Bandfield*, 2007]. The values for the

putative chloride-bearing deposits are consistent with a mean particle size of fine gravel (2 to 4mm) [*Presley and Christensen*, 1997]. However, thermal inertia is not a uniquely interpretable parameter, and values in this range also are consistent with smaller-grained particles that are cemented together [*Palluconi and Kieffer*, 1981]. The latter is consistent with the generally crusty to indurated appearance for the chloride-bearing deposits observed in the MOC and HiRISE imagery.

The relationship between the putative chloride-bearing materials and craters is complex. A number of small (<300 m diameter), highly degraded craters appear to predate the chloride-bearing materials in Terra Sirenum, indicated by polygonal fractures crosscutting the crater rims and sidewalls (Figure 2.4C). Larger craters (~300 to 900m) in the same area appear to have excavated through the materials, covering them with ejecta (Figures 1A and 4A). In other locations, chloride-bearing materials fill the floors of degraded craters but do not fill nearby, less degraded craters (Figure 2.1C). In Terra Sirenum, a small crater ~500 m in diameter shows the light-toned, putative chloride-bearing materials in cross-section and reveals that the stratigraphic unit containing the putative chloride-bearing materials has a substantial thickness (Figure 2.4E) [*See SOM*].

On a global scale, the chloride-bearing materials occur at a wide range of elevations, ranging from roughly −3 to 3 km. MOLA gridded elevation data show that individual deposits not located in crater floors commonly occur in local topographic lows relative to the immediate surrounding terrain. As described previously, many of the deposits occur as small, isolated patches; in conjunction with their locally low elevations, this suggests they most likely represent incontiguous units. Additionally,

within a region containing several deposits, the putative chloride-bearing materials may occur at different elevations relative to each other, indicating that the formation postdates the stratigraphy, although it may also suggest the presence of multiple units in the stratigraphy.

On the basis of our observations, a number of inferences can be drawn about how the putative chloride-bearing deposits might have formed on the Martian surface. The widespread distribution of the deposits suggests that the climatological/ hydrological conditions that facilitated their deposition were global in scale. However, ocean-scale bodies of water would appear to be inconsistent with the deposits' concentration in the cratered southern highlands. Alone, local-scale processes such as fumarolic activity are unlikely to produce the observed global distribution and differing morphologies of the deposits. Similarly, efflorescence alone does not account for the observed polygonal morphologies of the deposits, which are more consistent with desiccation cracks in thick salt deposits forming through precipitation. The occurrences of putative chloride-bearing materials in crater floors and in association with sinuous channels suggest that many of the putative chloride-bearing materials were precipitated from brines. Crater floors are ideal locations for ponding and evaporation of brines trapped from surface runoff or by the intersection of groundwater with the surface. Additionally, impact melting and mobilization of subsurface groundwater (or ground ice) could also be a viable mechanism for the production of chlorides. Based on our observations, we believe that the majority of the deposits were formed by chloride precipitation processes, although it is likely that in various locations, some of the materials are efflorescent salts or volcanic sublimates or were precipitated from

hydrothermal brines [*See SOM*]. Locations where the stratigraphic relationship between the putative chloride-bearing materials and surrounding terrain is not clear (Figure 2.4D) may be candidates for reactivation and/or modification of the original deposits by efflorescence.

The abundance of these deposits indicates that the formation of chloride salts on Mars has been an important process [*Brass*, 1980; *Knauth and Burt*, 2002]. The deposition of widespread chloride-bearing materials in the ancient southern highland terrains of Mars is further evidence of the presence of extensive reservoirs of surface and/or subsurface groundwater in the planet's early history [*See SOM*].

Supporting Online Material (SOM)

Identification of spectrally distinct units

The spectrally distinct deposits display consistent coloration in the three 3-band combinations used to produce Thermal Emission Imaging System decorrelation stretched images (http://themis-data.mars.asu.edu). The deposits appear blue in stretches using bands 8, 7, and 5 (11.75 μm, 10.99 μm, and 9.30 μm) for the red, green, and blue channels, respectively; they are green when bands 9, 6, and 4 (12.55 μm, 10.17 μm, and 8.51 μm) are used, and yellow or orange in a stretch using bands 6, 4, and 2 (10.17 μm, 8.51 μm, and 6.77 μm).

Atmospheric correction of TES data

The TES spectrum over the spectrally distinct unit in Terra Sirenum is an average of 4 spectra from orbit 2274, incremental counter keeper (ICK) 1365, detectors 4 and

5, and ICK 1366 detectors 2 and 3. The spectrum of the regional terrain is an average of ICKs 1368-1370 from orbit 2274. Surface emissivity was retrieved assuming the atmospheric model and dust opacity shape of [*Bandfield and Smith*, 2003 . The magnitude of the dust opacity was determined from a nearby high albedo surface assuming the high albedo surface emissivity at 9 microns is the same as the high albedo dusty surface of [*Bandfield and Smith*, 2003]. The dust is assumed to be well mixed in the atmosphere and is scaled to account for elevation differences between the two surfaces. Similar surface spectral characteristics of the region of interest were acquired from the deconvolution atmospheric correction technique and from spectral ratios [*Ruff and Christensen*, 2002]. This technique was chosen because it allows for extended wavelength coverage, is not dependent on reference spectral libraries, and does not convolve spectra of multiple surfaces.

Linear deconvolution results from TES

Linear deconvolution, a quantitative spectral technique for deriving surface mineralogy of thermal infrared data [*Ramsey and Christensen*, 1998; *Feely and Christensen*, 1999; *Hamilton and Christensen*, 2000; *Gillespie*, 1992; *Christensen et al.,* 2000a], indicates that the spectrally distinct unit spectrum is dominated by high abundances of Fe-oxides (primarily magnetite), as well as pyroxene (augite), plagioclase feldspar (bytownite), and olivine (fayalite). Linear un-mixing of the regional terrain results in surface spectra with a basaltic shape and a composition similar to that derived for the spectrally distinct unit with the exception of lower abundances of Fe-oxides (dominantly augite, bytownite, K–rich glass, and olivine Fo-

35). The end member spectral library included quartz, plagioclase feldspars (microcline, albite, oligoclase, andesine, labradorite, bytownite, and anorthite), high and low Ca pyroxenes (enstatite, bronzite, diopside, augite, hedenbergite manganoan, and pigeonite), several olivines (forsterite, Fo-68, Fo-53, Fo-39, Fo-18 [*Koeppen and Hamilton*, 2008], and fayalite), sulfates (gypsum, kieserite, and anhydrite [*Lane*, 2007]), carbonates (calcite and dolomite), phyllosilicates (illite, Ca-montmorillonite, and clinochlore), glasses (alkali-rich), and iron oxides, including the target transformation-derived average global Martian hematite [*Glotch et al.,* 2004], magnetite, ilmenite, and goethite. The results indicate that the component that is giving the material the characteristic blue color in the decorrelation stretch image is only one component of many within the pixel of the TES instrument, though it must be abundant or have strong spectral character to cause the distinct spectral slope. The observed slope towards lower wave numbers appears to favor the modeling of various oxides, which exhibit no (or few) features at higher wave numbers (~1300 – 800 cm^{-1}) and strong features at low wave numbers. However, if the spectrally distinct unit's spectral signature were the result of oxides on the surface, the ratio of the distinct unit to the regional terrain would result in a spectrum closely similar to that of the oxide. The results of TES spectral ratios yield a featureless spectrum that slopes towards lower wave numbers and not a spectrum that is indicative of an oxide. Furthermore, decreasing particle size effects can be ignored due to the lack of observed transparency features and characteristic "roll off" or decrease in emissivity towards higher wave numbers [*Hunt and Vincent*, 1968].

To further investigate the spectra, we utilized factor analysis and target transformation [*Bandfield et al.,* 2000], which has been used in previous studies to isolate occurrences of hematite in TES and mini-TES data [*Glotch et al.,* 2004; *Glotch and Bandfield,* 2006]. Factor analysis is used to determine the number of independently varying components present in the spectral data (represented by eigenvectors), and target transformation uses the eigenvectors to reconstruct trial spectra using a linear least squares model. If a trial spectrum is reproduced well by the eigenvectors, then that trial spectrum is a component of the data. If the trial spectrum is not fit well by the eigenvectors, the best-fit spectrum commonly is close to an actual component [*Bandfield et al.,* 2000]. We used a library of mineral spectra as trial spectra; none were reproduced well, but the spectra that were most closely reconstructed (and not attributable to atmospheric components) include oxides, sulfates, and some phyllosilicate clays. These minerals have low contrast spectral features and some exhibit slopes towards lower wave numbers [*Christensen et al.,* 2000b; *Lane,* 2007]. Sulfates and phyllosilicates, like oxides, typically have features that are distinguishable in the infrared and thus could be identified in a TES ratio of the spectrally distinct unit to the surrounding terrain. As these features are not apparent in the TES ratios, it is unlikely that they are abundant on the surface.

Effects of varying temperature on emissivity

Emissivity is an intrinsic property of a material; it is wavelength dependent, and is defined as the ratio of the calibrated radiance of the material to that of a perfect emitter (a blackbody, defined by the Planck equation) at the same temperature (and

thus, dimensionless). For geomaterials measured in emittance (e.g., via passive remote sensing, such as with TES and THEMIS), the sample kinetic temperature must be determined radiometrically.

The relationship between observed radiance (L), emissivity (e), and the radiance from a surface with no spectral character (a blackbody, L_B) is: $L(\lambda,T) = e(\lambda)L_B(\lambda,T)$, where, λ is wavelength, T is brightness temperature, h is Planck's constant, c is the speed of light, k is the Stephan-Boltzmann constant. On Mars we convert radiance measured by THEMIS and TES to emissivity using a radiance to brightness temperature look-up table that assumes a maximum emissivity of one between 1350-300 cm^{-1} in the spectrum. The brightness temperature is converted to a Planck function, the calculated radiance for a given brightness temperature of a spectrally featureless blackbody material. Dividing the observed radiance by the Planck function at the observed brightness temperature results in a spectrum normalized around unit emissivity showing the spectral absorptions from the non-blackbody surface. The peak of the Planck function shifts both in amplitude and in spectral position as a function of temperature, hence, a mis-identification of the brightness temperature shifts the predicted peak radiance spectrally, and following the division of observed by predicted radiance, causes a sloped emissivity spectrum [*Ruff et al*., 1997]. This effect potentially could occur if the temperature of the materials in the field of view are wide ranging (e.g. > 5 – 10 K), however THEMIS-derived brightness temperatures at 100 m / pixel spatial resolution within the TES spatial footprint over the spectrally unique deposits do not indicate that there are sufficiently large temperature differences to produce the slope observed in the TES spectrum.

Furthermore, THEMIS spectra from within the spectrally distinct materials also show a strong spectral slope, and there is no indication that surface temperatures vary significantly at 100-meter scales.

To demonstrate the temperature variation required to introduce the slope observed in the THEMIS spectrum, we have modeled the effects of wide ranging temperatures within the THEMIS 100 m pixel. A temperature variation on the order of ~47 K difference between the warmest and coldest materials over ~60 to 70 % of the pixel would be the minimum temperature variation required to induce the slope observed. This is beyond the temperature ranges expected within the THEMIS 100 m pixel. Temperature variations of this order are generally observed for shadowed versus sunlit regions (i.e., resulting from large surface variations associated with topography such as crater walls, cliffs, or fault scarps). High resolution imagery (~25 cm / pixel) from HiRISE over the deposit in Terra Sirenum do not give evidence for such large scale surface variations which would subsequently result in large shadow effects within the THEMIS pixel. Furthermore, if the sloped signature were the result of temperature variations within the THEMIS pixel, we would expect a basaltic spectral shape with a slope towards lower wavenumbers however, this is not observed.

To further test the hypothesis that the spectral signature of these spectrally distinct deposits is not a function of temperature effects, we calculated spectral ratios over a spectrally distinct unit and the regional terrain for the same location on the planet using three different THEMIS images. The solar longitude of these images varied from 262 to 328, and the local solar time varied from 15.99 to 16.23. Due to orbital constraints of the 2001 Mars Odyssey spacecraft, this is the largest variation available

with the THEMIS data at this time. We would expect that if the spectral signature were due to surface temperature effects that the spectral ratio would change with differing local solar times and solar longitudes. The result of this study was that no discernible differences were found within the ratios. Therefore, we can conclude confidently that the slope observed in the THEMIS data is not due to wide ranging temperatures and is instead due to a material with maximum emissivity that is not near unity.

Non-unit emissivity effects

We find that assuming a maximum emissivity of ~0.95 over the 1350 to 800 and 500 to 300 cm^{-1} wavenumber regions removes the slope observed in the TES data as shown in Figure 2.S1. Taking a ratio of this corrected emissivity spectrum to that of the regional basaltic terrain shows a ratio similar to that shown in the manuscript of the spectrally distinct unit to the regional terrain, but does not exhibit the slope towards lower wavenumbers. To fully remove the slope observed in the THEMIS emissivity spectrum of the spectrally distinct unit, a maximum emissivity of ~0.92 is needed for the conversion. The variation of the maximum emissivity needed to remove the observed slopes differs in the TES and THEMIS data due to the different spatial scales of the two instruments. The spectral signature of the distinct unit is somewhat masked due to the larger pixel size of TES which incorporates the regional basaltic materials (which have a maximum emissivity near unity) into the scene. This spatial mixing is not apparent in the THEMIS data and thus the spectral character is likely more representative of the spectrally distinct unit.

Laboratory chloride spectra

The laboratory-measured emissivity spectra (Figure 2.S2) demonstrate the relatively featureless spectral shapes of chlorides over the TES wavelength range. These spectra were corrected non-unit emissivity effects either by using a known maximum emissivity or by using the measured kinetic temperature to derive the Planck function. The maximum emissivity corresponds to the minimum reflectance via Kirchoff's law, $E = 1 - R$, where E is emissivity and R is reflectance [*Hapke,* 1993b]. Reflectance measurements are insensitive to temperature and can be used to constrain the absolute maximum emissivity. Therefore these laboratory spectra do not exhibit spectral slopes. This spectral region is particularly important because silicates have near-unit emissivity in this wavelength range, and, as a result, virtually all silicate mixtures have maximum emissivity values located in this region. In portions of the wavelength range where the chloride emissivity is relatively high, silicates are strongly absorbing (emissivity is low). Consequently, mixtures of silicates and chloride salts will therefore have a maximum emissivity significantly less than unity throughout the spectrum, leading to an incorrect estimate of true kinetic temperature as discussed previously. Experiments with mixtures of halite and silicate minerals show a common trend toward decreased effective emissivity with increasing abundance of halite [*Eastes*, 1989]. One or more chlorides as a component of the Martian materials would reduce emissivity by an unknown amount causing incorrect temperature derivation and introducing a slope in the emissivity spectrum.

As stated, assuming a maximum emissivity of ~0.95 instead of 1 in the conversion from radiance to emissivity removes the slope from the TES spectrum. Previous work with granular mixtures of halite and quartz indicated that a 50/50 mixture increases the minimum reflectance to ~45% (i.e., maximum emissivity ~0.55) [*Eastes*, 1989]. We have made reflectance measurements of granular mixtures of 50% basalt and 50% halite that yield a minimum reflectance of ~20% (i.e., maximum emissivity ~0.80). Linear deconvolution of these granular mixtures using pure basalt and pure halite as end members, consistently underestimate the abundance of halite in the mixed spectrum, indicating a nonlinear relationship. However, if we assume a roughly linear relationship between maximum emissivity and abundance of halite within the mixture, a maximum emissivity of 0.95 (our best estimate of the TES emissivity maximum) indicates a ~15% abundance of halite, while a maximum emissivity of 0.92 (estimate of the THEMIS emissivity maximum) indicates an abundance of ~20% halite. However, if there are roughness effects, the abundance of chloride may be greater [*Kirkland et al.,* 2003]. Mixtures of chlorides and/or chloride cements and silicates are expected to also decrease the maximum emissivity in mixtures, however specific trends may be different. Laboratory work is ongoing to investigate the behavior of chloride mixtures and cements in the infrared.

Many anhydrous chlorides are also spectrally neutral in the visible and near infrared wavelength regions. Minerals commonly are identified in the near infrared region due to O-H, H-O-H, and metal-OH bonds, which anhydrous chlorides do not contain. Obtaining data over these ranges may help to substantiate the inference of the

presence of a chloride-bearing material, however, if the materials are anhydrous chlorides, it is unlikely that a definitive identification can be made.

Terrestrial observations of halite deposits in Death Valley

There are terrestrial observations of chloride deposits that are based upon similar remote sensing observations as described in this study of Mars. MODIS/ASTER Airborne Simulator (MASTER) data covers a similar wavelength range as the THEMIS instrument and has been used to infer the location of halite deposits within the Badwater Basin, Death Valley, California [*Baldridge et al.,* 2004]. The inference of halite is based on the lack of spectral features over the MASTER wavelength range. The halite spectrum has a maximum emissivity of ~0.98 and exhibits a relatively flat featureless spectrum. MASTER emissivity was derived using the temperature emissivity separation algorithm of [*Gillespie et al*., 1998] which begins by assuming a maximum emissivity of 0.96 for rocks and soils, therefore there is no slope observed in the emissivity spectrum because the algorithm does not assume a maximum emissivity of 1.0.

Spatial extent of putative chloride materials

In visible data of Terra Sirenum, small areas of similar looking, light-toned, fractured material not discernable at THEMIS 100 m/pixel resolution outcrop further to the south of the larger chloride-bearing deposits. The limits of THEMIS spatial resolution and geographic coverage, as well as the presence of superposing units

suggests that the localities we have identified to date likely represent a fraction of the true extent of these materials.

Estimate of stratigraphic thickness

HiRISE image PSP_003160_1410 over a putative chloride deposit in Terra Sirenum shows a ~500 m diameter crater excavating through the deposit to darker-toned materials that are stratigraphically lower. A first order analysis of the relationships observed in the crater wall can yield important information regarding the stratigraphic thickness of the unit bearing the putative chloride materials. The light-toned unit is visible in the crater wall and there is a clear contact between the putative chloride-bearing materials and the darker-toned unit beneath it (dark boulders appear to be eroding from this lower unit). Based on a simple crater morphology, and assuming a slope of ~30˚ (consistent with the angle of repose for most materials regardless of gravity) for the crater wall [*Melosh*, 1989] and combining this with a measurement of the lateral width of the exposed unit, a rough estimate of the thickness of the unit is achieved applying trigonometric relationships. A thickness of ~32 m is estimated using the following relationship: $T = \tan(30°) * 57m$. This rough calculation is a first order estimate of the thickness of the unit containing the putative chloride bearing material. This unit may contain other minerals or it could represent a thick chloride deposit. The layer does not necessarily represent one depositional event, and could represent multiple episodes of deposition in this location.

Correlations with previously defined surface materials and elemental chemistry

Chemical progressions of saline evaporite phases that are expected in the course of acidic (pH ≤6) basaltic weathering on Mars have been predicted for an "acid fog" model [*Tosca and McLennan*, 2006]. The progression begins with carbonates, progresses to sulfates, and concludes with chlorides. We have not yet identified carbonates or sulfates in direct association with any of the deposits. However, it is possible that other evaporite phases were precipitated but have not been preserved, are difficult to discern due to their physical properties [*Kirkland et al*., 2003], or are located stratigraphically below the putative chloride-bearing materials and are hidden from view.

There are no first order correlations with publicly available surface material maps from TES [*Bandfield,* 2002; *Rogers and Christensen,* 2007] Observatoire pour la Minéralogie, l'Eau, les Glaces, et l'Activité (OMEGA) [*Bibring et al.,* 2005, 2006], or elemental abundance maps from the Gamma Ray Spectrometer (GRS) [*Boynton et al*., 2002; *Keller et al*., 2006; *Taylor et al*., 2006]. Special attention was paid to the lack of correlations with the distribution of water equivalent hydrogen and chlorine weight percent from the GRS instrument [*Boynton et al.,* 2002; *Keller et al.,* 2006]. One explanation for this lack of correlation is the size of these chloride-bearing materials (~1 km^2 to ~25 km^2) relative to the footprint of the Gamma Ray Spectrometer (GRS) instrument (~440 km to ~540 km in diameter) results in significant dilution of the elemental signal from these deposits, as observed in other data sets such as TES. Another reason for the lack of correlation may be that if these

putative chloride-bearing materials were formed in the Noachian and are largely buried, they may not represent or be related to the processes that are responsible for the current distribution of water equivalent hydrogen or chlorine in the upper ~65 cm of the surface sensed by the GRS suite of instruments.

Aqueous alteration products have been identified via in-situ and remote sensing observations. The Mars Exploration Rover (MER) Opportunity has identified sulfate minerals in the Meridiani Planum region [*Squyres et al.,* 2004] and OMEGA [*Gendrin et al*., 2005; *Bibring et al.,* 2007 and has observed a variety of sulfates remotely. In addition, OMEGA has identified phyllosilicates in Noachian terrains [*Poulet et al.,* 2005; *Bibring et al*., 2006]. Based on publicly available location maps of these minerals from OMEGA, there is no overlap between the putative chlorides and the sulfates and phyllosilicates that would indicate either of those materials as spectral components of the distinct deposits. It is possible that either there was not sufficient coverage of these deposits when these maps were produced or that because OMEGA is on a similar spatial scale as TES, these deposits were not identified due their spatial extent and neutral spectral features. Furthermore, it has been shown that sulfates as well as phyllosilicates have spectral features in the infrared region and many can be identified in THEMIS and TES data [*Lane*, 2007; *Michalski et al.,* 2006]. However, we find no evidence that the infrared spectral characteristics of these deposits are consistent with laboratory trends of sulfates or phyllosilicates.

Implications for current hydrologic model of Mars

A model has been proposed for the evolution of the early aqueous history of Mars that is grounded in the hypothesis of an early neutral pH (via identification of phyllosilicates) weathering environment in the Noachian which transitions to a low pH (via identification of sulfates) alteration environment in the Hesperian and finally to arid conditions [*Bibring et al.,* 2006]. Because many chlorides can form under a variety of pH conditions (alkaline in terrestrial environments and acidic predicted for Martian environments), these results cannot support or refute the claim that the pH conditions were neutral for much of the Noachian with a later trend towards more acidic weathering in the Hesperian. However, the identification of putative chloride-bearing materials associated with ancient terrains is consistent with the model put forth by [*Bibring et al.,* 2006] that the early history of Mars had greater aqueous activity.

Acknowledgements

We are grateful to the members of the THEMIS team at Arizona State University and the Mars Odyssey team at the Jet Propulsion Laboratory. We thank K. Nowicki for help with THEMIS data processing and M. Lane for the use of chloride samples and spectra. We also thank our anonymous reviewers for insightful, thorough, and constructive comments. Funding for this work was provided by NASA grant NNX06AE15G and the Mars Odyssey Science Office. Funding for V.E.H. was provided by grants from the Mars Odyssey Participating Scientist, the Mars Data Analysis, and the Planetary Geology and Geophysics programs.

FIGURES

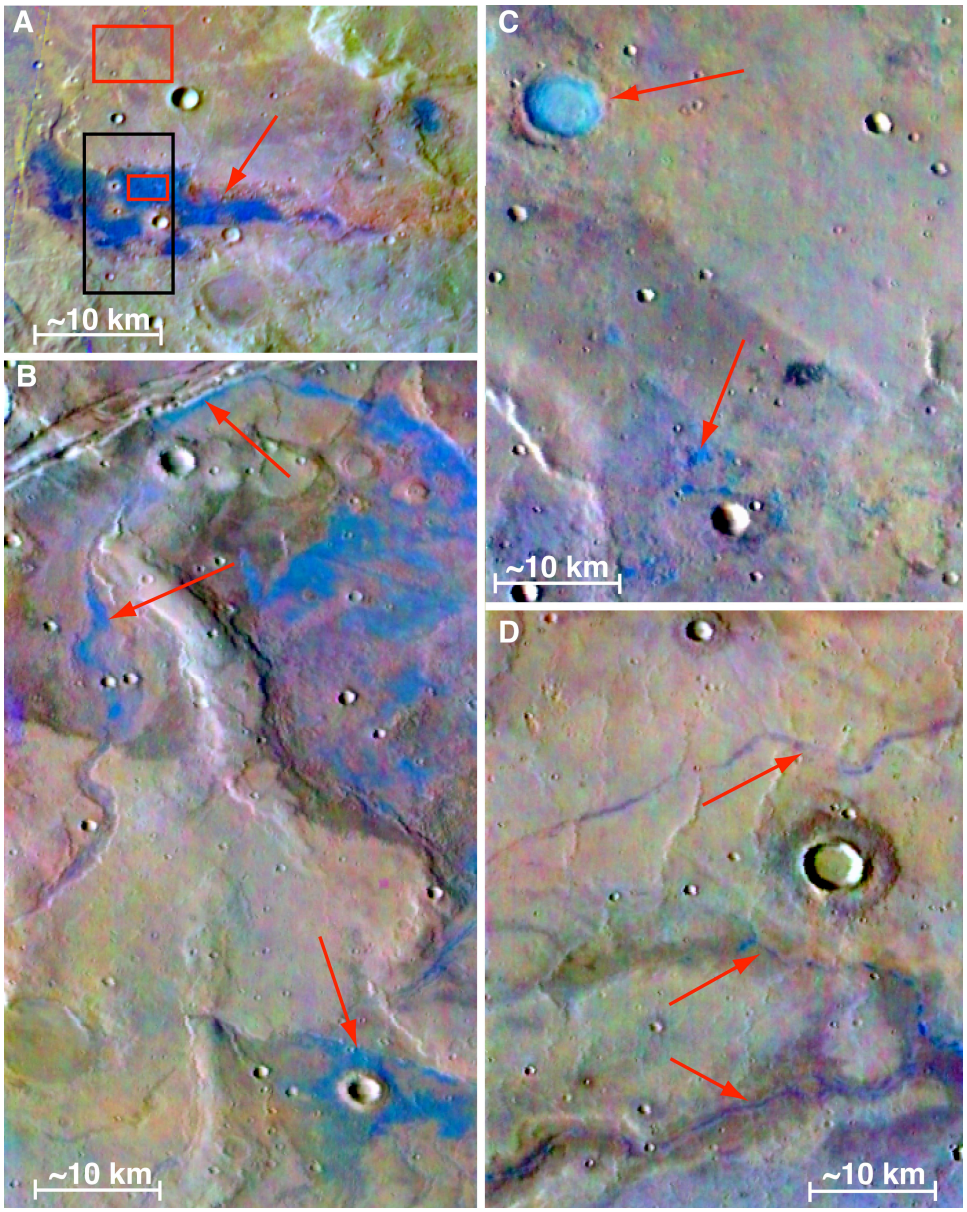

Figure 2.1. All images are THEMIS 8/7/5 DCS radiance images. (A) I08831002 (~221.0° E, –38.8° N) showing spectrally distinct materials in blue. Red boxes indicate areas averaged for spectral analysis, and the black box indicates HiRISE coverage. (B) I07808003 (~205.5°E, –32.7 °N) showing spectrally distinct materials following sinuous paths, abutting Sirenum Fossae, and occurring in low-lying areas near craters. (C) I07815002 (~4.1° E, –28.0° N) showing spectrally distinct materials filling a small crater, as well as occurring as patches. (D) Spectrally distinct materials following sinuous path in I07830004 (~290.8° E, –34.0° N).

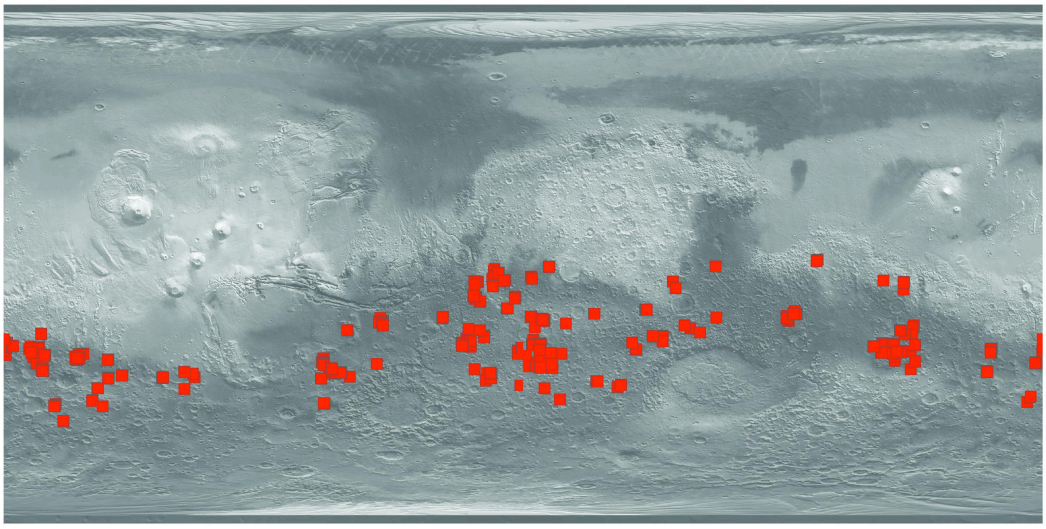

Figure 2.2. Global distribution of spectrally distinct materials overlain on TES Lambert albedo and MOLA shaded relief.

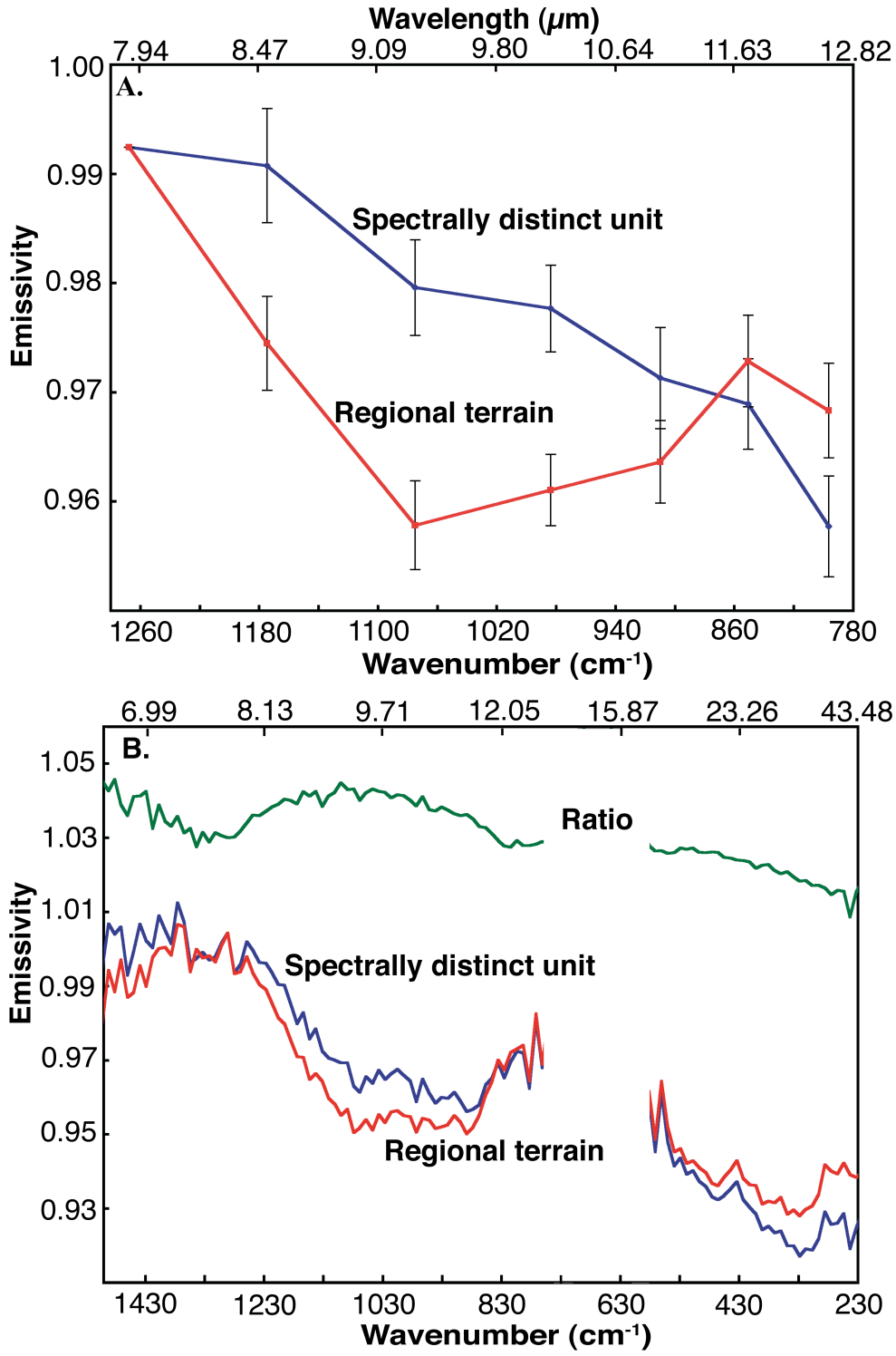

Figure 2.3. (A) THEMIS surface spectra from image I08831002 in Terra Sirenum. (B) TES data for the spectrally distinct materials and the surrounding terrain. The ratio of the spectrally distinct surface to the surrounding terrain is shown at top.

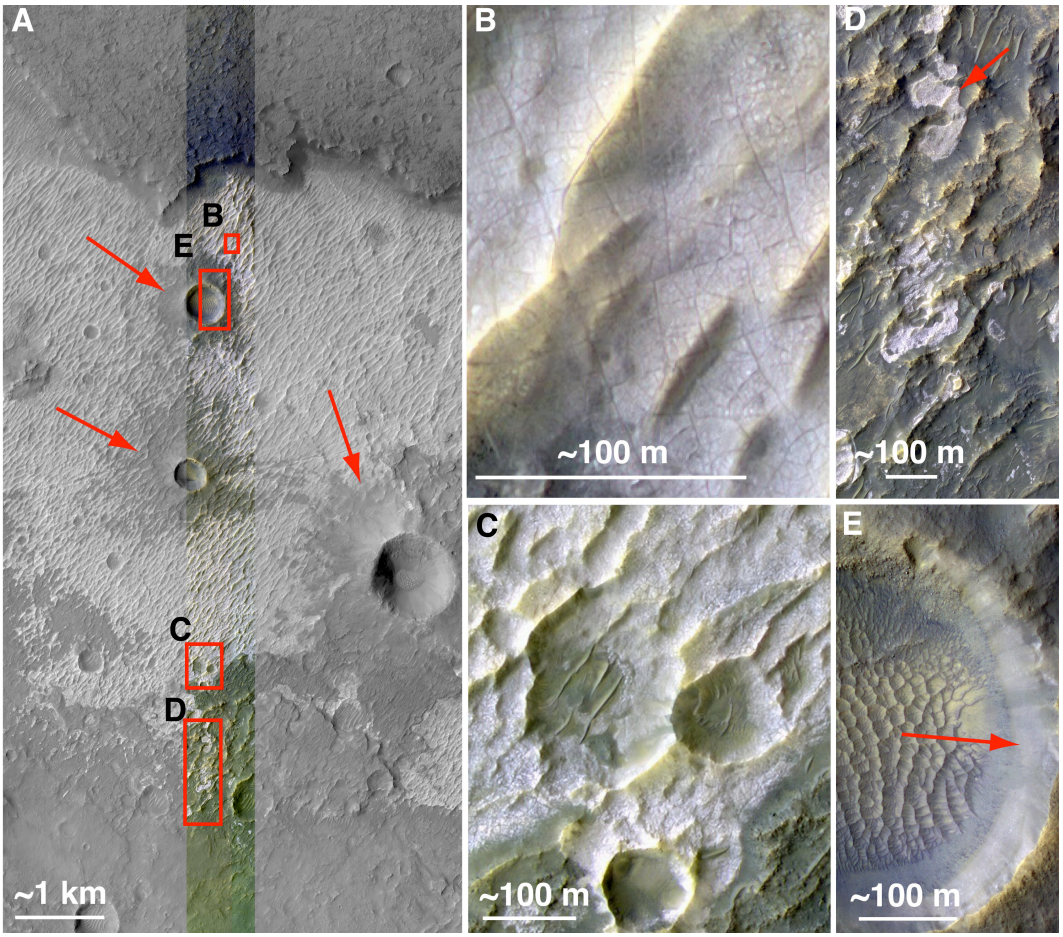

Figure 2.4. (A) HiRISE image PSP_003160_1410, which includes the location of color data; locations of color inset images are indicated by red boxes. Crater ejecta overlie the light-toned materials, as indicated by the red arrows. (B) Polygonal fractures. (C) Chloride-bearing material appears to post-date small, degraded craters. (D) Small patches of chloride-bearing material with ambiguous stratigraphic relationships. (E) Light-toned materials are visible in the wall of this ~500-m-diameter crater.

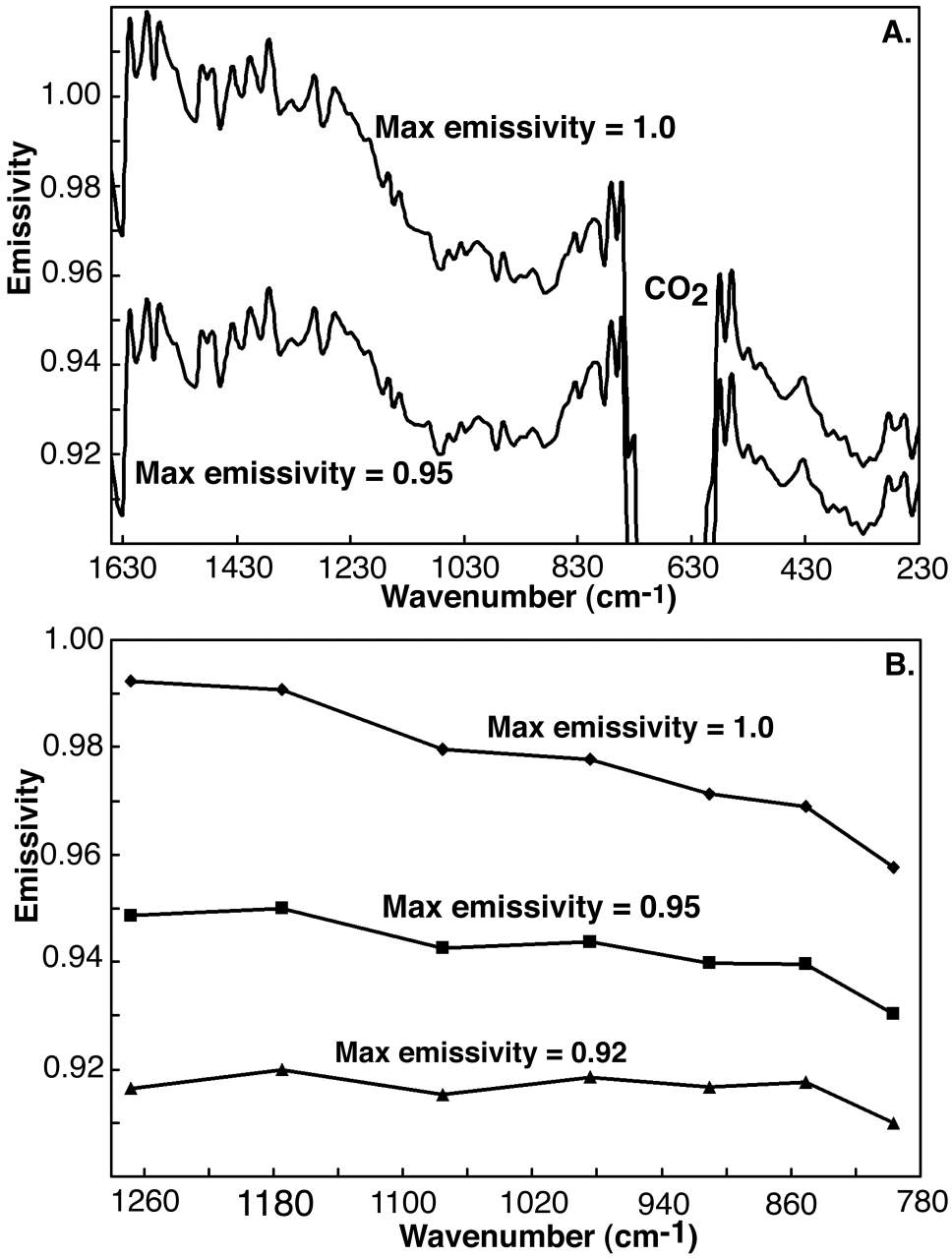

Figure 2.S1. A) Assuming a maximum emissivity of 0.95 removes the slope observed in the TES data over the spectrally distinct unit in Terra Sirenum. B) We assume a maximum emissivity of 0.95 for the THEMIS data, but observe that the slope is not fully removed until the maximum emissivity is reduced to 0.92 for the radiance to emissivity conversion.

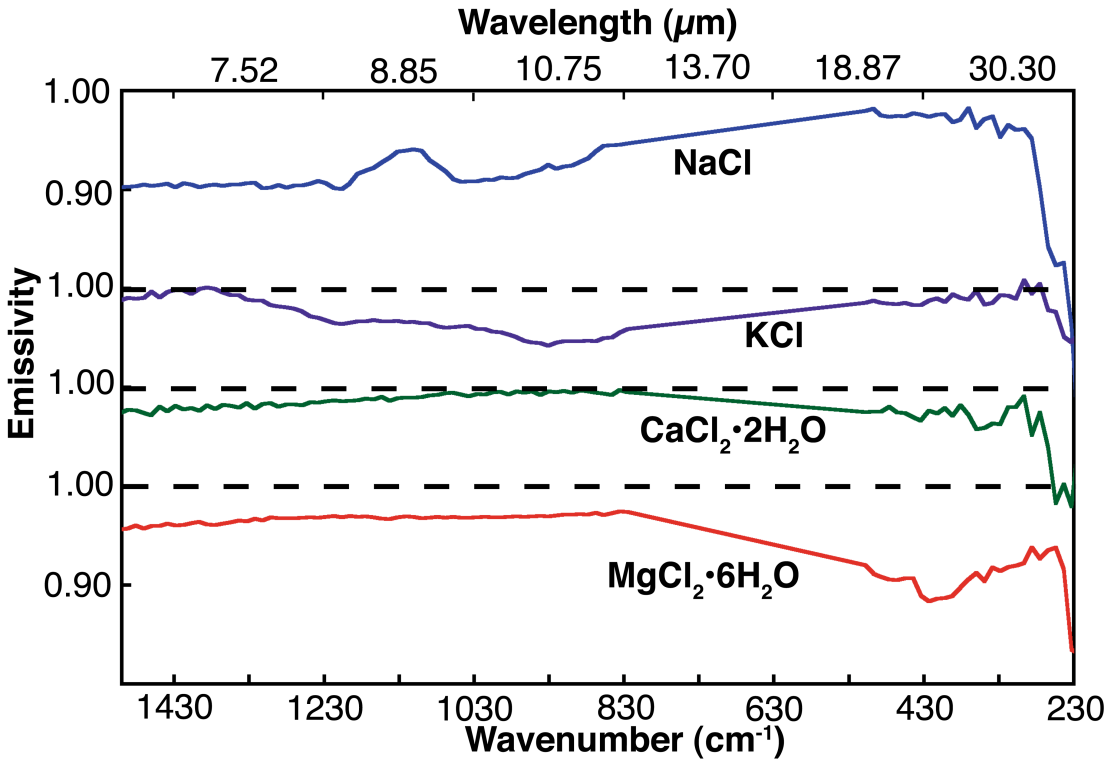

Figure 2.S2. Laboratory emission spectra for a variety of chlorides (halite- NaCl, sylvite- KCl [*Lane and Christensen,* 1998], sinjarite- $CaCl_2 \bullet 2H_2O$ [Sample graciously provided by Melissa Lane], and bischofite- $MgCl_2 \bullet 6H_2O$) reduced to TES resolution with the CO_2 band removed and offset for clarity.

CHAPTER 3: THE GEOLOGIC CONTEXT OF PROPOSED CHLORIDE-BEARING MATERIALS ON MARS

Published in its present form as Osterloo, M. M., Anderson, F. S., Hamilton, and Hynek, B. M. (2010), Journal of Geophysical Research-Planets, DOI:10.1029/2010JE003613.

Abstract:

We use Thermal Emission Imaging System (THEMIS) data to identify and characterize the global distribution of distinct materials interpreted to contain chloride salts on the Martian surface. Previously mapped global geochemical and physical properties are used in concert with thermophysical and morphological observations to assess the materials' local and regional characteristics. The results of our survey have expanded the characterization of the materials from ~200 to ~640 distinct sites dispersed throughout low albedo Noachian and Hesperian aged terrains. Our survey also shows that the materials are detected in locally thermophysically distinct terrains and display a range of morphologies. Topography indicates that the majority of the materials occur in local lows, although cross-cutting relationships indicate that some sites are located in 'geologic windows' implying that the materials may be older than the terrains in which they are situated. Once exposed, the materials appear to undergo erosion, which may be the reason we do not observe large laterally extensive materials at the surface. The materials are predominantly local in nature, yet their prevalence across the southern highlands suggests that they represent one or more globally ubiquitous processes. We consider a number of formation hypotheses, but find that most observations are consistent with formation via ponding of surface runoff or groundwater upwelling, although efflorescence and hydrothermal activity may also be possible in some locales. The materials' inferred ages suggest that the conditions that enabled the deposition of the materials persisted for up to a billion years.

1.0 Introduction

Osterloo et al. [2008] discovered a compositional unit on Mars that contains a component attributed to chloride salts. These materials were identified based on their spectral distinctiveness in false-color, thermal infrared (TIR) images from the Mars Odyssey Thermal Emission Imaging System (THEMIS). *Osterloo et al.* [2008] found that the materials were dispersed throughout the low-albedo ancient southern highland terrains. Geomorphologic observations indicated that the materials were typically light-toned, spatially small (< ~25km^2) discontinuous materials. Using higher- resolution visible imagery, *Osterloo et al*. [2008] found that at least one proposed chloride-bearing material was highly polygonally fractured, which was interpreted to be suggestive of desiccation cracks. The materials blanketed the underlying topography, which consisted of roughly aligned undulating ridges that appeared to be similar to cemented dune forms. THEMIS thermal inertia data indicated elevated values for the materials, suggesting they were relatively consolidated. Using the spectral data, morphological, and thermophysical observations, *Osterloo et al*. [2008] concluded that the materials were at least partially composed of a chloride salt.

The proposed chloride-bearing materials exhibit featureless, sloping emissivity spectra in THEMIS (~672 to 1475 cm^{-1} or ~14.88 too 6.78 μm) and Mars Global Surveyor (MGS) Thermal Emission Spectrometer (TES) data (~300 to 1300 cm^{-1} or ~33.33 to 7.70 μm) (Figure 3.1B). The observed spectral slope suggests an erroneous assumption of an isothermal surface and/or a surface with unit emissivity in the

conversion of measured radiance to emissivity. Either of these assumptions, if incorrect, will lead to negative slopes in the emissivity spectra [*Ruff et al.*, 1997; *Osterloo et al.*, 2008]. *Osterloo et al.* [2008] and *Bandfield* [2009] did not find evidence for anisothermalities on the Martian surface and attributed the relatively featureless sloped spectra to a material with non-unit emissivity, such as chloride salts.

We used compositional information obtained by the Mars Reconnaissance Orbiter's (MRO) Compact Reconnaissance Imaging Spectrometer for Mars (CRISM) to investigate the distinct materials and found that a site in the Terra Sirenum region (~38.8°S, ~221°E) has a surface that is distinctly brighter when compared to the typical background soils, lacks the negative infrared continuum slope characteristic of dusty background materials, and has a weak (or non-existent) 3-μm H_2O absorption feature (Figure 3.1A). Our observations are consistent with those of *Murchie et al.* [2009] and *Wray et al.* [2009] who have interpreted spectra from other sites to be consistent with a high albedo, anhydrous phase such as chloride salts.

There are relatively few minerals other than chlorides (e.g., halite**,** Figure 3.1C and 1D) that can explain the relatively featureless sloped spectrum observed in both the TIR and NIR data. *Murchie et al.* [2009] indicated that the materials displayed either a weak or non-existent 3 μm hydration feature and it should be noted that there are significant hydration features in the spectrum of halite shown here (1.9 and 3 μm) that may not be consistent with the apparently anhydrous Martian material. However, preliminary laboratory studies of halite and labradorite mixtures are able to reproduce the observed CRISM spectra fairly well [*Jensen and Glotch*, 2010]. Thus, it is

possible that the Martian chlorides may have weak hydration features that are significantly subdued due to mixtures with regional materials. Additionally, Martian chlorides may be significantly less hydrated than their terrestrial counterparts due to less atmospheric water available for hydration. The spectral signature may also be explained by other less common halides than chlorides, such as bromides, fluorides, and iodides that also are relatively featureless and have a maximum emissivity less than one. Some sulfides can also lack spectral absorptions in the infrared and near infrared wavelength region (e.g., chalcopyrite and galena, Figure 3.1C and 3.1D). There are a number of additional minerals, such as those that are strictly homopolar compounds (e.g., diamond), that could be considered potential matches to the observed spectrum, but which are not geologically plausible. Hence, the most likely mineralogical explanation for the observed spectral signature is a common halide such as a chloride, or a spectrally featureless sulfide.

If chloride salts are indeed the component responsible for the observed spectra of the Martian materials, we could expect thermophysical, morphological, and topographical characteristics consistent with one or more depositional environments conducive to chloride salt formation (i.e., ponding via surface runoff or groundwater upwelling, or via hydrothermal brines). Alternatively, if the materials contain sulfides, we could expect materials to form in stratabound lenses or thinly disseminated sheets at the base of magnesian ultramafic lava flows, or thicker deposits located in isolated structural depressions and observe evidence of weathered gossan assemblages [*Burns and Fisher*, 1990]. Oxidative weathering of the exposed surface of sulfide-rich veins can form gossans, a coherent iron (e.g., oxides, limonite,

goethite, and jarosite) and quartz-rich residue, which remains after sulfide removal [*Klein and Hurlburt*, 1985]. Sulfides also occur in large masses or veins of hydrothermal origin as well as accessory minerals in a wide range of felsic igneous rocks [*Deer et al.,* 1992]. Silica-rich compositions and ancillary hydrothermal minerals and morphologies near the sites may be evident if the Martian materials are sulfides produced by hydrothermal processes.

In this paper, we greatly expand the initial survey of *Osterloo et al.* [2008] by: (1) documenting all sites with similar TIR spectral character, (2) documenting the physical properties of the materials, and (3) seeking correlations with other globally mapped properties to help infer their origin. Due to the lack of features in both the VNIR and TIR spectral data of the materials, investigating their physical characteristics and integrating the datasets can provide constraints on the interpretations and inferred formation mechanisms for these distinct materials.

2.0 Datasets and Methods

2.1 THEMIS

The THEMIS instrument is a multi-spectral imager that contains both visible/near infrared (VIS/NIR) and thermal infrared (TIR) cameras [*Christensen et al.*, 2004]. The TIR portion of THEMIS acquires images at a spatial resolution of ~100 m/pixel in ~1 μm-wide bands centered at nine wavelengths between ~6.8 and 14.9 μm (~1475 to 670 cm^{-1}) for the identification of geologic materials. The visible camera collects higher spatial resolution data (~18 m/pixel) in up to five channels from 0.425 to 0.86 μm.

Calibrated THEMIS daytime TIR images with a minimum average surface brightness temperature of 220 K were processed to produce three combinations of decorrelation-stretched images. A decorrelation stretch (DCS) is an image color enhancement technique that amplifies the contrast of uncorrelated multispectral information [e.g., *Gillespie et al*. 1986]. DCS images display the selected bands in red, green, and blue (RGB) channels, respectively, with available variants including bands 8, 7, and 5 ("8/7/5"), 9/6/4, and 6/4/2. These band combinations are the standard DCS images provided publicly by the THEMIS team and cover the wavelength range of the surface sensing bands of the THEMIS instrument to provide the maximum potential for identifying compositional variations on the surface. The THEMIS bands and their respective wavelengths are summarized in Table 3.1. The proposed chloride-bearing materials are easily distinguishable in these DCS images, appearing blue in the 8/7/5, green or teal in the 9/6/4/, and orange or yellow in the 6/4/2 stretch (Figure 3.2). At present, the data processed as DCS images cover ~94% of the Martian surface.

Using the colors from the DCS images, we manually searched every processed THEMIS image (through orbit 35162) for the proposed chloride-bearing materials and logged the image identification number and site location. Our search resulted in the identification of 641 distinct sites. We assigned the identifications a subjective quality rating from 1 - 5 to indicate our confidence that the materials were similar to previously studied putative chloride-bearing materials that contain a spectrally neutral phase. We found no physical variation (i.e., thermal inertia, albedo, morphology, spatial location) between the materials with different quality ratings other than the

area of the material, indicating that we had less confidence in smaller exposures. We also investigated the extent to which the quality assignments were due to variations in THEMIS image quality, but found that there were no discernible differences in the average and standard deviations of the atmospheric dust and water ice opacities, average surface temperatures, image ratings, or local acquisition times between the different DCS quality groups. Therefore, at this time, we assume that all identifications are positive and similar in spectral character to those studied in detail by *Osterloo et al.* [2008] and *Bandfield* [2009]. Further detailed spectral analysis of all the sites may provide additional information on the degree that the materials vary in their spectroscopic signature from the type localities.

2.2 Ancillary Data and Software

We studied the proposed chloride-bearing materials using thermal and visible bolometer data from TES and imagery from the High Resolution Imaging Science Experiment (HiRISE) and the MGS Mars Orbiter Camera (MOC), as well as global datasets of composition and geology using Geographical Information System (GIS) software, as described below. At the time we began our study there was limited Context Camera (CTX) data [*Malin et al.,* 2007] publicly available and therefore we did not incorporate the imagery into our analysis. CTX images may be useful in future work that aims to investigate intermediate scale morphology between HiRISE and THEMIS-VIS. The TES instrument was comprised of a Fourier transform Michelson interferometer and thermal and visible bolometers [*Christensen et al.,* 2001a]. The visible bolometer measured the integrated solar reflectance from 0.3 to

2.9 μm and the thermal bolometer measured the integrated thermal radiance from 5.1 to 150 μm. Only data from non-dusty seasons (L_s = 0-135º and 330-360º) were used due to the accompanying increase in albedo with greater abundances of atmospheric dust and water ice clouds. HiRISE is currently acquiring data onboard MRO and is capable of acquiring visible data with ~25 cm/pixel resolution [*McEwen et al.*, 2007]. MOC narrow angle (NA) images offer an intermediate scale view of the morphology between HiRISE and THEMIS VIS data, with variable spatial resolutions ranging from ~1.5 to 3 m/pixel [*Malin et al.,* 1992; *Malin and Edgett*, 2001].

We use apparent thermal inertia, a measure of the ability of a surface to absorb and re-emit heat energy [*Kieffer et al.*, 1973; *Kieffer et al.*, 1977; *Mellon et al.*, 2000], calculated from THEMIS nighttime temperature images using the method of *Fergason et al.* [2006] and from the thermal bolometer of TES [*Mellon et al.*, 2000]. Thermal inertia is strongly controlled by the effective particle size and porosity (e.g., larger effective grain sizes or lower porosities have higher thermal inertias) [*Kieffer et al.*, 1973]. Below, we use thermal inertia to assess the degree to which the materials vary with respect to the surrounding terrain materials and discuss the absolute values in relation to grain size estimates from *Presley and Christensen* [1997].

We used a number of published maps to investigate global as well as regional correlations between composition, geology, geomorphology, and the distribution of materials (Table 3.2). We masked all global maps to exclude regions of high surface dust (i.e., excluding regions with a dust cover index (DCI) <0.94 from *Ruff and Christensen* [2002]) that obscures the substrate from reflectance and emission spectroscopy. The DCI is the average emissivity from 1350 -1400 cm^{-1} and serves as

a gauge for surface-obscuring dust that impacts spectral measurements [*Ruff and Christensen,* 2002]. Despite the fact that THEMIS TIR has near global daytime coverage of the planet, there is a possibility that a spatial bias exists in the data due to lack of high quality (i.e., high signal to noise and low atmospheric dust and water ice opacities) coverage of the northern lowlands (Dale Noss, personal communication, September, 2009). THEMIS is currently in an earlier orbit than planned (~1545 Local True Solar Time (LTST) instead of ~1700 LTST), which will provide data with higher signal to noise and thus it is possible that additional materials will be identified in the northern lowlands.

We used the JMARS [*Gorelick et al.*, 2003] software to create regions of interest (ROI) around each site and geospatially register the different data used in this study. The ROI shape file that we created for this study is publicly available for use in JMARS (http://jmars.asu.edu). We also utilized ArcGIS to investigate global to local scale correlations between the materials and globally mapped geological and compositional properties.

3.0 Results

3.1 Morphology

Throughout the Results section we will refer to the materials as 'proposed chloride-bearing materials', but consider alternative interpretations in the Discussion section. We characterized the general morphology of the proposed chloride-bearing materials using THEMIS TIR DCS images and their detailed morphology with higher resolution images. The proposed chloride-bearing materials generally occur as small,

spatially isolated patches having a wide range of areal extent (~0.33 to ~1300 km^2, with an average of ~24 ±76 km^2) and the materials exhibit many different morphologies at the scale of the THEMIS TIR instrument. The materials commonly occur as small patches displaying irregular boundaries (50%) (Figure 3.3A), ~16% occur as spatially contiguous larger materials with irregular boundaries (Figure 3B), ~8% as narrow sinuous to linear occurrences, suggestive of channels (Figure 3.3C), ~4 % interior to degraded craters (Figure 3.3D), 20% in circular depressions that are likely degraded craters, and ~2% occur as clusters of small (a few pixels) isolated patches (Figure 3.3E). We did not observe any first order correlations between the different morphologies, areas, and their geographic regions.

In addition to THEMIS TIR DCS images, we have characterized the small-scale, detailed morphology of the materials using higher spatial resolution visible imagery, which reveals additional morphological details. An example of a proposed chloride-bearing material is shown at increasing spatial resolution in Figure 3.4. In this case, the coarse resolution THEMIS VIS data shows the chloride material in a shallow depression at this scale (Figure 3.4B), MOC NA data indicates that the materials are light-toned with a morphology that is distinct from the surrounding terrain (Figure 3.4C), and the highest resolution HiRISE images shows a rough terrain with small fractures on the surface at the meter scale (Figure 3.4D). THEMIS VIS has the most comprehensive coverage for the materials (~62%), followed by HiRISE (~8%) and MOC NA data (~5%). Despite the fact that the highest resolution imagery is only available for a fraction of the materials, our results, described in detail below, indicate

that most materials have a distinct surface morphology, which may extend to the majority of materials.

Thermal imagery provided the first evidence that some proposed chloride-bearing materials occur as sinuous ridges, suggestive of inverted channel deposits (Figure 3.3C). Visible imagery has provided additional evidence for the proposed chloride-bearing materials outcropping as thin sinuous and sometimes branching ridges that are reminiscent of inverted channels with a few meters of relief. Commonly, the sinuous ridges appear to connect with larger proposed chloride-bearing materials sometimes at the inferred downstream end of the inverted channel system. One example of a well-developed channel system is shown in Figure 3.5A. This proposed chloride-bearing material is located in a basin in the Terra Sirenum region (~32.70º S, 205.84ºE) and TIR observations indicate distinct sinuous features, indicative of fluvial channels, that flowed from higher elevations down into the basin (Figure 3.5B). Upon further inspection using HiRISE imagery, it is apparent that the fluvial channels transition to inverted channels that are composed of the proposed chloride-bearing materials (Figure 3.5C). These inverted channels coalesce downslope and appear to terminate at a larger proposed chloride-bearing site (Figure 3.5B and 3.5C). This proposed chloride-bearing basin material is partially composed of small buttes beyond the main patch, which indicates the materials may have been more laterally extensive in the past. The basin materials are connected to a larger occurrence of proposed chloride-bearing materials to the north by a subparallel chloride-bearing feature. We hypothesize that briny water spilled over and flowed into the larger more

northern material (shown in Figure 3.5A), which also contains evidence for inverted sinuous features reminiscent of inverted channels (Figure 3.5D).

Additional observations of the proposed chloride-bearing materials indicate that they are in situ and have undergone significant erosion. Some materials appear to be located in layers eroding out of darker-toned walls (Figure 3.6A) and small, isolated buttes are observed outcropping in proximity to the main deposit, indicating they were once more extensive and preserved due to the protective cap rock (Figure 3.6B). Some proposed chloride-bearing materials appear to be observed due to the removal of overlying sediments, indicating they are located within a 'geologic window' as shown in Figure 3.6A. However, the proposed chloride-bearing materials commonly have a complex relationship with adjacent terrain as shown in Figure 3.6C, where the materials appear to be thinly layered, and partially covered by darker units. Yet the eroded appearance of the isolated sections indicates they may have been more laterally continuous. Additionally, the proposed chloride-bearing materials are sometimes observed in close proximity to other non-chloride layered units. The proposed chloride-bearing materials' curvilinear boundary (Figure 3.6D) appears to be the result of erosion and removal of the overlying dark unit and not due to deposition. At this site, the material displays a highly fractured quasi-circular surface morphology. Overall, many proposed chloride-bearing materials appear to be relatively thinly bedded, superpose darker sediments, and display an eroded appearance (Figure 3.6E and 3.6F).

Using the higher resolution visible data we also found that many of the proposed chloride-bearing materials are located within small degraded craters. THEMIS VIS

observations indicate that ~74% of the relatively small 'spots' observed in the TIR (~131 materials) data are small degraded craters where the materials are constrained within the remnants of the roughly circular crater. Many of these locations suggest that the materials are slightly elevated with respect to the surrounding terrain and appear to have partially filled existing craters (Figure 3.7A). In addition to the proposed chloride-bearing materials' scoured or eroded appearance, the materials commonly display a distinctive surface expression that appears rough and is composed of ridges and/or scallops (Figure 3.7B and 3.7C). In some locations, scallops are nearly equidistantly spaced, trend quasi-linearly, and repeat with a high degree of regularity whereas in other locations they are more hummocky and trend irregularly. The ridges can be broader and/or wider than those shown in Figure 3.7B and 3.7C. These characteristics are similar to some of the morphologies observed in the light-toned, friable layers in Valles Marineris and Meridiani, which have been attributed to aeolian erosion [*Malin and Edgett.,* 2000]. Additionally, many ridges in the proposed chloride-bearing materials continue into underlying cap rock without interruption (not shown) similar to elongate yardangs, which is consistent with formation by erosion [*Ward*, 1979].

We have expanded on the observations of *Osterloo et al*. [2008], which found the proposed chloride-bearing materials in Terra Sirenum are highly fractured at the HiRISE scale. In our analysis, we considered ~50 locations globally with sufficient HiRISE coverage and found that the extent to which the materials are fractured is highly variable. Approximately 16% of the proposed chloride-bearing materials are pervasively fractured with well-defined polygonal cracks (Figure 3.8A), ~18% are

fractured to a lesser degree, ~42% show morphologies that are suggestive of fracturing, and ~24% of the materials show no fractures on their surfaces (Figure 3.8B). Fractures generally crosscut topographical features such as scallops and small degraded craters. Despite the presence or lack of fractures, the proposed chloride-bearing materials are relatively free of rocks and boulders on their surfaces in comparison to the materials immediately adjacent to the sites. For example, in Figure 3.8B, the proposed chloride-bearing materials are pale yellow to light grey in color and boulders are a darker blue color. Boulders appear on top of the proposed chloride-bearing materials in some places, though the abundance of boulders increases significantly towards the materials edges and grade into the darker-toned units atop or underlying the proposed chloride-bearing materials, indicating the adjacent regional terrain materials are likely their source.

3.2 Global elevations and local topography

The proposed chloride-bearing materials are typically found at elevations of ~1000 to 3000 m and are generally consistent with the elevation trend of the southern highlands excluding major impact basins or volcanic constructs (Figure 3.9). Based on north-south and east-west topographic profiles, as well as contour maps, we found that ~63% of proposed chloride-bearing sites occur in local lows (i.e., one of the profiles indicates a low, whereas the other profile indicates the terrain is flat or sloped, suggesting a trough or depression but not necessarily a basin). We found that ~31% of the proposed chloride-bearing materials occur in localized basins (i.e., both north-south and east-west profiles indicate a basin), though they may not be

hydrologically closed basins. Finally, ~6% are either located in relatively flat terrains or upon slightly elevated ridges. Figure 3.10 shows examples of north-south and east-west topographic profiles for three proposed chloride-bearing sites located southwest of Miyamoto crater in Meridiani Planum. The easternmost site (profiles B.1 and B.2 in Figure 3.10) is an example of a site that is located in a local basin as is the westernmost material (profiles D.1 and D.2 in Figure 3.10), whereas the other site (profiles C.1 and C.2 in Figure 3.10) is an example of a site located in a local low.

3.3 Relationships between locations of proposed chloride-bearing materials with previously mapped thermophysical, compositional, and morphological properties

3.3.1 Correlations between proposed chloride-bearing materials and globally mapped properties

The locations of the proposed chloride-bearing materials are overlaid on the DCI map of *Ruff and Christensen*, [2002] (Figure 3.11A), showing that the materials are identified throughout the dust-free regions at TES resolution. This result is expected because spectrometers cannot identify compositional differences among surface materials in regions that have high dust cover. A generalized geological age map (Figure 3.11B) was compiled using the simple cylindrical global geologic maps of *Scott and Tanaka* [1986] and *Greeley and Guest* [1987]. From this simplified map, it is evident that the materials are primarily located within the ancient Noachian and Hesperian terrains (> ~2.6 Ga) [*Tanaka and Hartmann*, 2008]. Our comparison of the locations of the materials and the detailed geologic maps indicate that there are ~170

sites in unit Npl1 (cratered unit), ~115 in Npld (dissected unit), ~105 in Hr (ridged plains material), and ~105 in Npl2 (subdued cratered unit), followed in decreasing order by Nplr (ridged unit), Hpl3 (smooth unit), Nplh (hilly unit), Hplm (mottled smooth plains unit), Nple (etched unit), with a few occurrences in Nf (older fractured material), Nh1 (basin rim unit in Hellas assemblage), and Hf (younger fractured material) (shown schematically in Figure 3.12). Additionally, we find that many proposed chloride-bearing materials straddle at least two geologic units (i.e., at least eight straddle Npl1 and Hr). In order to estimate the age of the proposed chloride-bearing materials, we correlated the crater size-frequencies for each geologic unit from the stratigraphic column of *Scott and Tanaka* [1986] to the crater size-frequencies of the chronostratigraphic series defined by *Tanaka* [1986], which are correlated to age determinations of *Tanaka* [1986] and *Tanaka and Hartmann* [2008] (Table 3.3). It is important to note that we have not identified materials in dust-free, younger Amazonian-aged terrains nor have we identified any materials across the dichotomy boundary within the northern lowlands. On average, we find that the cumulative areas of the proposed chloride-bearing materials within the Middle Noachian (Npl1), Late Noachian (Nplr) and Early Hesperian units (Hr) are larger than those located in the other geologic units (Table 3.4 and Figure 3.12). Normalizing the cumulative areas of the materials to the total areas of the geologic units in which they are located indicates that the materials are most representative of the Nplr, Hplm, Hpl3, and Hr terrains, although the total areal coverage of materials within each geologic terrain is extremely low (Table 3.4).

The aforementioned age determinations from *Tanaka* [1986] used geologic maps by *Scott and Tanaka* [1986] and *Greeley and Guest* [1987], which were drafted using Viking imagery at 10s to 100s of m/pixel. More recent data have prompted ongoing efforts to update the geologic maps of Mars [*Tanaka et al.,* 2009]. Because the timing of proposed chloride-bearing materials' formation is an important issue, we investigated six occurrences in greater detail to further constrain ages and validate the ages derived from the existing global geologic maps. Figure 3.13 shows proposed chloride-bearing material occurrences on the left side mapped as gray polygons. The black boundary shows the surrounding geologic unit as mapped with THEMIS TIR and MOLA data. In one case, *Greeley and Guest* [1987] mapped all of the surrounding terrain as Npl1. We concur that a single cratered unit is seen throughout this region of interest, thus we outlined a representative box that encompasses the proposed chloride-bearing materials (Figure 3.13a). In other cases, we used the units mapped by *Scott and Tanaka* [1986] and *Greeley and Guest* [1987] as a starting point but drafted our own local geologic units comprising the proposed chloride-bearing materials (e.g., Figure 3.13b-c). We note that the previously published mapped units were relatively accurate and our new mapping had only minor deviations from the original Hr unit in these two cases.

Following our mapping, we used the crater database of *Robbins and Hynek* [2010], which is complete down to 1.5-km in diameter, to estimate ages of the units. In each case, larger craters (>~5 km diameter) show a surface retention age of 3.83-3.92 Ga [*Hartmann and Neukum*, 2001] (Figure 3.13). At intermediate diameters, a downturn is seen in each plot; indicative of resurfacing in the Noachian that likely

corresponded to significant fluvial erosion [*e.g., Hynek et al.,* 2010 in press]. An upturn is seen at small diameters, indicating crater production after the resurfacing event and the resultant surface retention age is ~3.7 Ga or older [*Ivanov,* 2001]. Given that *Scott and Tanaka* [1986] and *Greeley and Guest* [1987] mapped the bottom two sites in Figure 3.13 as Hesperian (~2.6 to 3.6 Ga [*Tanaka and Hartmann*, 2008]) in age, our result is somewhat surprising. Nevertheless in all three cases shown here, and others we have examined, crater size-frequency determinations consistently place the units containing the proposed chloride-bearing materials in the Late Noachian during the time of significant valley network formation (e.g., *Hynek et al.* [2010] in press). For consistency with the ages derived from the geologic maps, we converted our crater size-frequency determinations to the chronostratigraphic series of *Tanaka* [1986] and find that the series also show ages of Late Noachian or Late/Middle Noachian (Table 3.5) and match the isochrons [*Hartmann and Neukum*, 2001; *Ivanov*, 2001] plotted on Figure 3.13. In the cases investigated in detail here, and others we have examined, we do not see conclusive evidence for exhumation. The materials are commonly located in relative lows and display complex stratigraphic relationships with the surrounding terrain (e.g., both atop as well as below the surrounding units near their edges). Although it is possible that some locations are undergoing exhumation and hence may be older than their derived ages, we find little conclusive evidence that would suggest the materials are significantly older or younger than their derived ages. It is beyond the scope of this paper to provide novel mapping and ages for all ~640 proposed chloride-bearing materials, yet this cursory analysis supports the age determinations from the published geologic maps of *Scott and Tanaka* [1986]

and *Greeley and Guest* [1987]. Therefore, we find that the global maps give a relatively accurate assessment of formation ages of the proposed chloride-bearing materials and indicate that most of the materials formed in the Middle to Late Noachian or Early Hesperian epochs.

Osterloo et al. [2008] found that the proposed chloride-bearing materials appear to be lighter toned than the surrounding terrain based on their appearance in visible images. Our survey expands on the previous observations; visible imagery qualitatively indicates that the materials are lighter-toned than the surrounding terrain (~77%), and display a range of colors in the HiRISE false color images (e.g., light blue, teal, white, pink). Most HiRISE observations reveal that the materials are partially covered by younger, darker mantling sediments, especially near the edges of the materials. To quantitatively assess the light-toned nature of the proposed chloride-bearing materials, we extracted TES albedo for each site using the map from *Christensen et al.* [2001a]. However, we found no reliable differences between the locations of the proposed chloride-bearing materials and the surrounding region, indicating that the global map is likely too coarse of resolution to distinguish the spatially small materials. We obtained single detector albedo derived from the visible/near-infrared bolometer of the TES instrument for ten large and spectrally distinct sites (locations given in Table 3.6). We choose the largest sites because they had sufficient areal size to incorporate numerous TES pixels fully within their boundaries. Most materials display TES single detector albedo values in the ~0.10 to ~0.20 range with an average and standard deviation of ~0.14 ± 0.02. We also found that the materials are rarely significantly brighter than the surrounding terrain,

generally varied with the regional terrain values, and also fell within the average for the low-albedo regions on Mars (Figure 3.14A). These results indicate that regional terrain sediments are possibly obscuring the single detector TES albedo measurements for the proposed chloride-bearing materials. Therefore, future work would likely benefit from quantitative THEMIS-VIS or CRISM albedo measurements.

We extracted thermal inertia for each proposed chloride-bearing site from the map of median nighttime thermal inertia from *Putzig and Mellon* [2007] to investigate the thermophysical properties of the materials. We found that the values varied with the background terrain, which indicated that the areal extents of the proposed chloride-bearing materials are likely too small for representation in the global map. However, apparent thermal inertias derived from single detector TES thermal bolometer observations of the same ten sites as the albedo study indicated that thermal inertia values range from ~164 to 496 $Jm^{-2}K^{-1}s^{-1/2}$, with an average and standard deviation of ~295 ± 45 $Jm^{-2}K^{-1}$ $s^{-1/2}$ (Figure 3.14B). We also investigated the ten sites using THEMIS thermal inertia and observed elevated thermal inertias for materials with respect to the surrounding terrain in all instances (examples are shown in Figure 3.15). The proposed chloride-bearing materials generally display a thermal inertia of at least ~400 $Jm^{-2}K^{-1}s^{-1/2}$ and up to 509 $Jm^{-2}K^{-1}s^{-1/2}$ and appear to have relatively homogeneous thermophysical properties. Given the elevated THEMIS thermal inertia values with respect to the TES values, it is possible that the TES values are also being lowered (obscured) due to incorporation of regional fines within the TES pixel. The average THEMIS thermal inertia values (typically > ~300 $Jm^{-2}K^{-1}s^{-1/2}$, Table 3.6)

suggest that the proposed chloride-bearing materials have grain sizes that are generally greater than ~900 μm and/or are consistent with indurated materials [*Presley and Christensen*, 1997; *Mellon et al.* 2000; *Putzig et al.*, 2005].

Finally, we conducted a qualitative analysis using the "version 2" THEMIS 100m global nighttime temperature map available in JMARS [*Edwards et al*., in prep] as a proxy for thermal inertia to extend the general observation of increased thermal inertia to the full set of proposed chloride-bearing sites. Of the 623 sites having data coverage, ~90% occur as thermophysically distinctive terrains that are warmer than the surrounding regional materials. Sharp or distinct thermophysical boundaries at the THEMIS TIR scale are associated with most of the materials as was noted previously in the THEMIS thermal inertia observations. The remainder of the materials, which were typically smaller in size, occurred within terrains that had only slightly elevated brightness temperatures with respect to the regional materials, or showed a higher degree of variability in the vicinity of the materials. Thus, the thermophysical nature of these materials was difficult to distinguish (~8%). Only ~2% of the proposed chloride-bearing materials are not associated with thermophysically distinct terrains or they appeared to be similar in brightness temperature to the regional materials.

We used the valley network density map of *Hynek et al.* [2010 in press] and valley network-fed, open basin lakes map of *Fassett and Head* [2008a] to investigate the possible correlations between the proposed chloride-bearing materials and morphologies interpreted to be water-derived. We found a complex relationship between the locations of materials and terrains that contain morphological evidence for alteration by fluvial process. For example, though some materials appear to be

located in terrains that contain valley networks and paleobasins, there are almost an equal number located in terrains devoid of evidence for fluvial processes (Figure 3.16). There are only ~80 sites that occur within ten kilometers of a valley network-fed terrain, and ~40 that are within five kilometers. Additionally, there are only a few sites that occur within the mapped valley network-fed paleobasins of *Fassett and Head* [2008a], indicating that deposition via surface runoff and ponding may not be applicable for all the materials. As an example, the region near Meridiani Planum clearly shows evidence of valley networks and also contains numerous proposed chloride-bearing materials (Figure 3.10). The relationship observed in this region between the proposed chloride-bearing materials and the valley networks is typical of other localities where the materials are not directly related to the valley networks (i.e., they are not located in the valley troughs), but are located in close proximity, which suggests that they could have formed from ponded water as the valleys were incised. Moreover, some of the fine scale valleys we commonly observe flowing into local proposed chloride-bearing basins in the high resolution images are not included in the global map, but give significant supporting evidence for the presence of surface water near the proposed chloride-bearing materials (e.g., Figure 3.5).

3.3.2 Globally mapped properties that do not correlate with the locations of proposed chloride-bearing materials

We used Gamma Ray Spectrometer (GRS) maps of chlorine [*Keller et al*., 2006], hydrogen (H_2O) [*Boynton et al.*, 2007], and K/Th [*Taylor et al.*, 2006] to investigate the correlation between the proposed chloride-bearing materials and potentially

relevant elemental abundances or ratios that have been used to assess water alteration in the near surface crust [e.g., *Taylor et al.,* 2006]. Qualitatively, there do not appear to be any first order correlations between the materials and the chlorine, hydrogen, or K/Th maps (Figure 3.17). We extracted the average GRS Cl, H_2O, and K/Th value for each proposed chloride-bearing site from the published smoothed maps and calculated the average and standard deviations for all the materials (top values in each plot) (Figure 3.18A, 3.18B, and 3.18C) as well as the global average and standard deviations (bottom values in each plot and calculated from dust free areas using the DCI mask where data < 0.94 is excluded [*Ruff and Christensen*, 2002]). The range of chlorine values observed globally range from ~0.2 to 0.8 weight percent (wt%) and show peaks between ~0.4 to ~0.6 wt% [*Keller et al.*, 2006], and the majority of proposed chloride-bearing materials also appear to be within the peak range, displaying intermediate values around ~0.4 wt%. Excluding the polar regions, GRS H_2O ranges from ~1 to ~8 wt% on the Martian surface, and most proposed chloride-bearing materials display low to intermediate values (~3 to 3.5 wt%). Finally, K/Th ratios vary from ~3000 to ~10000 on the Martian surface but generally show peaks in the ~5000 to ~5500 range [*Taylor et al.*, 2006], and the majority of the proposed chloride-bearing materials occur within this average distribution. GRS estimates of Cl, H, and K/Th for the proposed chloride-bearing materials are uncorrelated with the size of the material. We consider different hypotheses for the lack of correlation in the Discussion section.

We investigated regional mineralogy derived from TES and the Mars Express Observatoire pour la Mineralogie, l'Eau, les Glaces et l'Activité (OMEGA) to shed

light on the possible formation mechanisms based on a search for possible co-occurring phases observed in terrestrial deposits. Both terrestrial chloride salts and sulfides can occur in stratigraphic sequences with ancillary minerals. For example, chlorides are commonly associated with sulfates, carbonates, and silica in successive playa evaporitic deposits [*Eugster and Hardie*, 1978] and terrestrial sulfides are commonly weathered to surficial gossan assemblages consisting of ferric-bearing oxide, oxyhydroxide, sulfate, and clay silicate phases [*Burns and Fisher*, 1993]. To investigate the extent to which the materials are correlated with phyllosilicates and sulfates, which could be common to both sulfide- and chloride- bearing deposits, we compared the locations of the proposed chloride-bearing materials with publicly available OMEGA maps [*Bibring et al.,* 2006]. At the time of publication of the phyllosilicate and sulfate maps, OMEGA had covered ~90% of the Martian surface at a spatial sampling of ~1.5 to 5 km, and ~5% at < 0.5 km over the 0.35 to 5.1 μm spectral range [*Bibring et al.*, 2006]. We found few proposed chloride-bearing materials in proximity to phyllosilicates deposits and no sites in close proximity to sulfates. Yet, previous studies using CRISM data [*Murchie et al.,* 2009; *Wray et al*., 2009] show that at least some of these distinct materials are found in association with phyllosilicates, indicating that detailed spectroscopic investigations are necessary to fully characterize the mineralogical diversity of the sites and future studies would greatly benefit from higher resolution spectroscopic data.

We investigated regional volcanic mineralogy derived from TES and OMEGA because sulfide deposits on Earth are commonly associated with lava flows (and many with ultramagnesian lava flows), and hydrothermal deposits and thus, may be a

way to distinguish chlorides from sulfides. However, locations of the materials do not strongly correlate with any one mineral phase [*Bandfield*, 2002; *Koeppen and Hamilton*, 2008; *Bibring et al.,* 2006], nor do they correlate with strictly Surface Type 1, Group 3, or Group 4 compositional units (which are the dominant regional compositions of the southern highlands) [*Bandfield et al.,* 2000; *Rogers and Christensen*, 2007], implying that deposition was unlikely to be associated with regional volcanic events or alteration processes.

4.0 Discussion

4.1 Formation mechanisms for terrestrial chloride and sulfide minerals

On Earth, chloride and sulfides can form in a wide variety of geological environments. Commonly, salts are observed as a dominant constituent of arid evaporative alkaline environments such as playas. Playas, or dry lakes, are generally located in hydrologically closed basins and subject to alternating wet/dry periods as well as high evaporation rates [*Eugster and Hardie,* 1978]. Formation of chloride salts via precipitation from evaporation in a basin could occur as the result of ponding of surface water runoff or groundwater upwelling, as has been proposed as the dominant formation mechanism for the salts in the Burns formation in Meridiani Planum [e.g., *McLennan et al.,* 2005]. Terrestrial massive salt deposits can form from deepwater closed basins, such as the Miocene Messinian evaporites of the Mediterranean region, where saturation occurs within the brine and salts are precipitated, but these basins rarely completely dry out [*Boggs*, 2001]. While the presence of large deep-water bodies on Mars is still controversial [*DiAchille and*

Hynek, 2010], it is possible that saturation occurred in smaller bodies of water and salt precipitated without complete evaporation of the brine. On Mars, deposition of chloride salts could also occur via hydrothermal brines where interaction of meteoric waters with heat from volcanism [e.g., *Schmidt et al.,* 2008], impact events [e.g., *Newsom et al.,* 1999], or heated ash deposits (either volcanic or impact related) [*Knauth et al.,* 2005]. Degassing of volatile elements from magmas or lava flows under high-temperature, reducing conditions can produce halide salt dominated surface encrustations near fumaroles [*Schmidt et al*., 2008 and references therein]. Finally, chloride salts can form by efflorescence via atmospheric interactions, similar to the relatively thin late stage veneers and surface rinds found by the rover *Opportunity* in Meridiani Planum [*Yen et al*., 2006; *Knoll et al.,* 2007].

Alternatively, sulphide mineral deposits associated with terrestrial komatiites include pyrrohotite-pentlandite (±chalcopyrite, pyrite) deposits in stratabound lenses or sheets up to a few meters thick at the base of magnesian ultramafic lava flows [*Burns and Fisher,* 1990]. On Earth, sulphides are also found as masses or veins in hydrothermal deposits associated with felsic intrusive rocks [*Deer et al.,* 1992]. They are also commonly an accessory mineral in a wide range of felsic igneous rocks and are a major ore mineral in volcanogenic and volcano-sedimentary deposits [*Deer et al*., 1992].

We summarize the possible depositional environments discussed above in Table 3.7 and use our observations to support or refute the different formation hypotheses.

4.2 Morphology

If we assume that the observed fractures (Figure 3.8) are related to the process that deposited the materials (i.e., they are not a product of the pre- or post-depositional stress regimes), the fracture morphology could shed light on their mode of formation. For example, salt crusts formed by efflorescence processes typically have a thin powdery or puffy texture and display raised ridged polygonal fractures, whereas salts produced by precipitation generally form thick deposits with polygonal or blocky morphologies with well developed fractures [*Goodall et al.*, 2000]. If the fractures we observe represent primary desiccation fractures, the wide range of fracture morphology suggests that both modes of deposition have operated to form the materials on the Martian surface. Our observations are consistent with deposition via ponding of surface runoff or groundwater upwelling as well as efflorescence from fumaroles or atmospheric interactions.

We found that ~25% of the proposed chloride-bearing materials are located within small, degraded and sometimes inverted craters, which could suggest formation during the impact process. Hydrothermal systems created from impact events would likely result in chloride deposition within crater walls and though this has been documented in a few locations in our study and within the location studied in detail by *Osterloo et al.* [2008], we do not observe widespread evidence of impact induced hydrothermal deposits. Additionally, most of the craters with proposed chloride-bearing materials are generally simple craters (< ~7 km in diameter) and therefore are unlikely to have created or supported a well-developed, long-lasting hydrothermal system [*Abramov and Kring*, 2005]. Moreover, we do not see evidence for fluidized ejecta or pedestal craters in most locations, nor do we see evidence for

proposed chloride-bearing materials on ejecta blankets, which may have supported a hydrothermal impact or surge deposit origin [*Knauth et al*., 2005]. Additionally, we would have expected to find more proposed chloride-bearing materials in craters given the ~250,000 craters > 1-km-diameter in the southern highlands if the materials were predominately from hydrothermal impact or surge deposit processes.

Alternatively, the proposed chloride-bearing materials could have formed in craters via a later infilling process that was not associated with the cratering event by: 1) groundwater upwelling, 2) hydrothermal brine upwelling, or 3) via ponding of surface runoff. This is also consistent with a formation scenario in which depressions impede the flow of advancing lavas, resulting in the deposition of sulfides via gravitational settling [*Burns and Fisher*, 1990]. Even though ~58% of the materials are located terrains that may have old Noachian and Hesperian lava flow regions (Nplh, Npl1, Nplr, and Hr, Table 3.4), most do not show similarities to the vast number of documented craters with clear lava flow inundation [e.g., *Leverington and Maxwell,* 2004; *Keszthelyi et al.,* 2010]. Additionally, we have not seen evidence for lava morphologies near the materials or any visible local heat sources [e.g., *Carr*, 1973; *Mouginis-Mark et al.,* 1992; *Bleacher et al*., 2007], thus deposition of sulfides via advancing lavas is less likely.

There are only a few locations with morphological evidence that suggests fluids originated from either above or below the surface, which could indicate upwelling from a brine or infill from surface runoff. Materials that appear to blanket underlying topography, including scallops and craters, may be good candidates for the upwelling scenario (Figure 3.7). In other cases, deposition via surface runoff is supported by our

observations of materials associated with sinuous features emanating into or out of local depressions (including craters), such as the proposed chloride material in Terra Sirenum (Figure 3.5). In this site, we observe a clear linkage between deposition and surface water features, with inverted channels throughout the material and dendritic valleys flowing into a local low (Figure 3.5). Locations of materials within sinuous channels could also indicate deposition of sulfides via gravitational setting in surface depressions. *Huppert et al.* [1984] suggested that sulfide deposits could have originated from assimilation of sulfur-rich sediments during thermal erosion by low viscosity ultramafic flows. Such low-viscosity lavas could have eroded vast portions of underlying sulfur-rich sediments and formed deep erosional channels into which the FeS liquids would subsequently be deposited. However, we see indications of surface water and ponding nearby for many locations (i.e., with respect to some proposed chloride-bearing materials in relative proximity to valley networks and valley-network fed paleobasins), but we have observed little evidence for local/regional volcanic activity, indicating that primary igneous deposits are unlikely.

Osterloo et al. [2008] noted that relatively small dark-toned dunes are commonly observed overlying the proposed chloride materials. However, we do not observe small dunes or ripples stratigraphically atop all the materials, nor do we observe large expanses of sand dunes near the sites. Many proposed chloride-bearing materials appear to be overlaid by darker sediments in patches, especially near the edges of the materials. Due to differences between the materials in tone, color in HiRISE false color images, and striking correlations with compositional boundaries from the THEMIS TIR data, it is unlikely that the sediments and dunes are geochemically

and/or physically related and the dark sediments are more likely derived from erosion of regional terrain materials.

Additionally, our observations indicate that the proposed chloride-bearing materials retain a fairly high angle of repose and typically do not form erosional morphologies that would suggest the materials are highly friable. We do not see evidence for boulders near the edges of the materials that could have suggested the proposed chloride-bearing materials were composed of massive competent bedrock (such as lava flows), which can produce boulders upon erosion. The materials are observed outcropping in buttes with somewhat steep topography (Figure 3.6A and 3.6B), inverted channels (Figure 3.5C) and craters (Figure 3.7A) and display well developed fractures with sharp edges in some localities (Figure 3.6D and 3.8A), suggesting that they are indurated and/or lithified materials. Materials are also commonly found to be thinly layered and appear to have been sections of a larger more laterally continuous layer, which indicates that they have undergone erosion (Figure 3.6E and 3.6F). Still, the observed scallops (Figure 3.7) may have formed in a similar erosional fashion to yardangs, and thus indicate the materials are erodible. We do not see evidence for dunes in the near vicinity for most locations, suggesting that the materials are not easily broken down into sand-sized particles. Therefore, it is likely that the materials are broken down into smaller particles and easily transported away. These observations suggest that the materials are likely fine grained, but somewhat cemented.

4.3 Elevation and topography

The proposed chloride-bearing materials could be genetically independent, or related and part of a laterally extensive subsurface unit that has undergone burial and subsequent exhumation in some localities to be exposed within 'geologic windows'. However, the small areal extent (~1340 km^2 to less than ~0.5 km^2) and variable elevation of the materials regionally and globally (Figure 3.9B), is inconsistent with regional deposits similar in context to the olivine-bearing layers in Nili Fossae (~30,000 km^2) [*Hamilton and Christensen,* 2005] or Eos and Ganges Chasma (which extend laterally greater than ~1100 km) [*Edwards et al*., 2008]. Nonetheless, there could be locally continuous layers in some places. For example, we have observed clusters of tens or fewer sites over areas ~10 km^2 that display similar elevations, indicating that they could be part of a laterally continuous layer. Outcrops of proposed chloride-bearing units show morphologies that are consistent with both removal by erosion, as well as burial by regional terrain materials. However, our observations do not support the hypothesis that the materials are thinly disseminated sulfide mineral layers produced by lava flows over large areas of Mars [*Burns and Fisher*, 1990].

A significant observation from this survey is that the majority of materials occur in local lows and/or regional basins (Figure 3.10). If the formation of topographic lows occurred before the deposition of the materials, it is possible that chloride salts could have precipitated through infilling of surface depressions with water via local runoff or intersection with a groundwater table or hydrothermal brine, as described above in Section 4.2. In addition, fumarole and sulfide deposits can occur as concentrated ore deposits a few meters thick (< 10's of meters) in isolated structural

or topographical depressions [*Burns and Fisher,* 1990], consistent with the observed materials. Morphological evidence in high-resolution images, such as inverted and fluvial channels (Figure 3.5C and 3.5D), suggests that the infilling by water from above or below, and not formation via fumarolic activity, is the most likely possibility.

Alternatively, it is possible that the occurrence of materials within topographic lows indicates that some materials have been exhumed by the removal of stratigraphically younger units. Crosscutting relationships observed in visible images suggest that some materials are visible through a "geologic window" in a relatively thick (few meters) darker overlying unit, and that the lateral extent of the material is likely greater than what is exposed. However, erosion of the proposed chloride-bearing materials is also commonly observed (Figure 3.6E and 3.6F). Therefore, it is possible that the lack of laterally extensive materials suggests that erosion is modifying or removing the materials from the surface.

4.4 Correlations between the locations of proposed chloride-bearing materials and globally mapped properties

The proposed chloride-bearing materials have elevated THEMIS thermal inertia (~400 up to 509 $Jm^{-2}K^{-1}s^{-1/2}$) and nighttime temperatures, which in conjunction with the presence of well developed fractures, is consistent with a homogeneous deposit composed of relatively rocky or cemented materials. Visible imagery suggests that the materials are lighter-toned than the regional materials, though TES albedo suggests they are not significantly brighter than the average of the southern highland

low-albedo terrains (proposed chloride-bearing materials have an average of 0.14 ±0.02, whereas the average for the low-albedo southern highlands is 0.15 ±0.02). The albedo and thermal inertia observations indicate that the materials generally fall into Unit B of *Putzig et al.* [2005], which is interpreted to be comprised of sand, rocks, bedrock and some duricrust. Yet, THEMIS thermal inertia observations indicate that some materials fall into Unit F (thermal inertias > 386 $Jm^{-2}K^{-1}s^{-1/2}$), which is interpreted to be comprised of rocks, bedrock, duricrust and/or ice in polar regions [*Putzig et al*., 2005]. The general lack of rocks observed in HiRISE images (which show rocks > 1 m in diameter) over the proposed chloride-bearing materials suggests that the higher thermal inertia is due to cementation rather than a rockier component. However, our observed thermal inertia values are inconsistent with initial theoretical results from *Piqueux and Christensen* [2009], which suggest chloride salt cement fractions in the range of 1% to 10-15% should yield thermal inertias in the range of 675 to 1025 $Jm^{-2}K^{-1}s^{-1/2}$. If these sites are chloride-bearing materials, one possible way to account for the discrepancy is that finer grained regional sands and dust located on top of the materials (which are commonly observed in visible images) reduce the apparent thermal inertias and/or nighttime temperatures.

In terms of age, the distribution of the proposed chloride-bearing materials in the Noachian (~76% of sites or ~61% of total area) to Hesperian (~24% of sites or ~39% of total area) aged units (Table 3.5 and Figure 3.12) suggests that the processes for formation were constrained to these geologic eras. Based on the occurrences within the series, formation processes may have started in the Early (~2%) to Middle Noachian (~46%), peaked in the Late Noachian (~28%) to Early Hesperian (~22%),

and ceased by the end of the Hesperian (~2%). Though it is possible that similar materials could be located in younger or older terrains, preferential erosion of the Late Noachian to Early Hesperian surfaces is probably unlikely. Additionally, Hesperian and Amazonian terrains have been well dissected by impacts, volcanism, tectonics, and chaos, thus it is unlikely that similar proposed chloride-bearing materials are present but have not yet been uncovered. We cannot rule out the possibility of materials located in younger dust covered areas or address the possibility that materials are or were located in the northern plains but were subsequently obliterated by a resurfacing event [e.g., *Frey et al.*, 2002; *Andrews-Hanna et al.* 2008]. The possibility that some materials may be observed at the surface because they are located in a 'geologic window', suggests that they could be slightly older than the mapped ages of the terrains in which they are located.

There have been a wealth of previous studies that suggested Mars experienced a major climate shift from "warm and wet" to "cold and dry" [e.g., *Craddock and Howard*, 2002] near the boundary between the Noachian and Hesperian epochs (~3.8 to ~3.5 Ga) [*Hartmann and Neukum*, 2001]. Regardless of the duration [*Howard et al.*, 2005; *Irwin et al.*, 2005; *Hoke and Hynek*, 2009] and exact mechanism that caused the transition [*Melosh and Vickery*, 1989; *Jakosky et al*., 1995; *Fairen et al.*, 2002], it is clear that this period in Martian history is marked by diminishing occurrences of well-developed valley networks [e.g., *Fassett and Head* 2008b; *Harrison and Grimm*, 2005] and an apparent reduction in phyllosilicate formation [*Mustard et al.*, 2007, 2008]. There is evidence that formation of fluvial valley networks, paleolakes, and deltas appear to have started in the Middle to Late

Noachian, peaked near the Noachian-Hesperian boundary, and precipitously declined thereafter [*Hoke and Hynek*, 2009; *Howard et al.,* 2005; *Irwin et al.,* 2005]. Given the ages of the terrains on which the proposed chloride-bearing materials occur, it is likely that they formed predominantly during this punctuated time of abundant surface water. The correlation between the ages of the proposed chloride-bearing materials and the peak of surface water activity suggests that water could have been available for deposition via surface runoff and ponding. This hypothesis is also supported by observations of some proposed chloride-bearing materials located in close proximity to valley networks and paleo basins.

Given the proposed chloride-bearing materials likely ages, proximity to the valley networks, and locations within topographic lows, it is possible they may have been deposited during a time when climatic conditions were more conducive to longer-lived ephemeral surface brines. Groundwater upwelling, discharge rates, and evaporite deposition have been predicted globally for Mars, as well as regionally for Arabia Terra and Meridiani Planum [*Andrews-Hanna et al.,* 2010]. Despite the observation that the highest potentials for thick evaporite deposits formed through groundwater upwelling and evaporation occur in areas with high surface dust (that obscures the underlying surface from imaging spectrometers), there are locations dispersed throughout the southern highlands that display some potential for groundwater upwelling and evaporite deposition. Many of these regions (e.g., Terra Sirenum) have proposed chloride-bearing materials identified within them and may benefit from higher resolution modeling and mapping. Additionally, regional modeling within the Meridiani region indicates a high potential for groundwater

upwelling and evaporite deposition [*Andrews-Hanna et al.,* 2010]. Proposed chloride-bearing materials are also found within this predicted high potential region indicating that groundwater upwelling, ponding, and deposition via evaporation may have played a role in their formation.

It appears that the proposed chloride-materials' formation span the time period between the hypothesized end of neutral-high pH, alkaline waters that were conducive to phyllosilicate deposition and the beginning of acidic alteration and sulfate deposition [*Bibring et al.,* 2006]. This hypothesized evolution was a result of the observed segregation of phyllosilicate and sulfate deposits temporally as well as spatially, with phyllosilicates located throughout the Noachian southern highlands and sulfate deposits located in Late Noachian to Hesperian terrains (e.g., Valles Marineris) [*Bibring et al*., 2006]. However, subsequent investigations have identified smaller sulfate deposits in close proximity to phyllosilicates in a number of localities [e.g., *Wiseman et al*., 2008a; *Milliken et al.*, 2009; *Wray et al.,* 2009]. Additionally, *Baldridge et al.* [2009] proposed contemporaneous deposition of phyllosilicates and sulfates on Mars by comparing the geochemical diversity observed to terrestrial acidic saline lake deposits. Terrestrial chlorides are typically associated with alkaline waters, however thermodynamic calculations predict chloride precipitation on Mars during the evaporation of fluids where the initial chemistry is controlled by basaltic weathering under acidic conditions [*Tosca and McLennan,* 2006]. Therefore, because chlorides may form on Mars under alkaline or acidic conditions, if the materials investigated here are partially composed of chloride salts, their presence neither supports nor refutes the neutral to acidic alteration transition proposed by *Bibring et*

al. [2006]. Regardless of the acidity of the precursory evaporating fluids, the occurrence of materials partially composed of chloride salts throughout the Noachian southern highlands would support the hypothesis that water was more abundant during their formation and the global decline of water limited their formation in younger terrains.

If the materials are comprised of sulfides produced by komatiitic lava flows, their occurrence may suggest distinct changes in the composition of magmatic reservoirs and volcanic processes around the Noachian/ Hesperian boundary. No spectroscopic study has yet investigated in detail the mineralogical differences between the various geologic terrains and their respective ages, though previous studies of regional and global mineralogical variability have shed light on the magmatic and crustal evolution. For example, *Rogers and Christensen* [2007] found that some Hesperian terrains exhibit a difference in mineralogy from Noachian terrains and from each other, suggesting variations in the degree of crystal fractionation, assimilation, and/or source region compositions. On the other hand, *Koeppen and Hamilton* [2008] did not find a clear trend between forsteritic-fayalitic compositions and their inferred geologic ages. Therefore, though there is not yet conclusive evidence for a major shift in the composition of lavas between the Noachian and Hesperian boundaries, there is evidence for mafic materials within the ancient crust as well as occurrences in younger terrains.

4.5. Globally mapped properties that do not correlate with the locations of proposed chloride-bearing materials

There is no clear correlation between the location of the proposed chloride-bearing materials and the distribution of Cl from the GRS data [*Keller et al*., 2006]; however, this can likely be attributed to the disparate spatial scales of the GRS and thermal observations. THEMIS has a spatial scale of ~100 m/pixel, whereas GRS has a spatial footprint of ~440 to ~540 km/pixel [*Boynton et al.,* 2004]. Assuming a simple linear addition model, we can approximate the abundance of chlorine required to elevate the signal above the average for the southern highlands using the following equation:

$$FA \times Cl_d + (1 - FA) \times Cl_b = Cl_b + Cl_{sd} \quad (1)$$

Where FA is the fractional areal contribution of the proposed chloride-bearing material to the GRS footprint, $1 - FA$ is the fractional areal contribution from the remainder of the GRS footprint, Cl_d is the weight percent of chlorine from the proposed chloride material, Cl_b is the weight percent chlorine of the background, and Cl_{sd} is the standard deviation of the background chlorine in weight percent. If we want to calculate the minimum amount of chlorine that would be necessary within the material to be detected, we assume that the total chlorine at the sensor must be above $Cl_b + Cl_{sd}$. Assuming the material is composed of a chloride with of relatively abundant chlorine atoms like NaCl (50% Cl), the equation becomes:

$$NaCl_d = 2\left(\frac{Cl_{sd}}{FA} + Cl_b\right) \quad (2)$$

We use the largest proposed chloride-bearing material as a "best case" scenario because it is greater in area than the cumulative areas of individual sites in any GRS

data grid (~5º by 5º area) [*Taylor et al.*, 2006; *Boynton et al.,* 2007; *Keller et al.*, 2006]. Using the area of largest material (~1340 km^2), we calculate the maximum fractional contribution for a single pixel (~152053 km^2, using a typical 440 km diameter), as well as 5º by 5º grid (~295500 km^2, at ~30ºS), to be 0.0088 and 0.0045, respectively. Typical GRS analyses have demonstrated measured Cl values of 0.48 ± 0.04 wt% for mid-latitudes from the smoothed gridded maps [*Boynton et al*., 2008], yet unsmoothed 5º by 5º gridded values for Cl range from ~0.2 to 0.8 wt% with uncertainties between 0.10 and 0.18 wt% for the southern highlands [*Keller et al.,* 2006]. Using the above equation (2), the two maximum fractional contributions, and the range of averages and uncertainties, we summarize the results of our calculations in Table 3.8.

Using the average and uncertainty from the smoothed data, it appears that halite at 18% would be required for detection in the 5º by 5º gridded data. However, the 0.04 wt% uncertainty is a result of smoothing the gridded data with 10º arc radius boxcar mean filter, which decreases numerical uncertainty and increases spatial area [*Keller et al*., 2006]. It is more realistic to assess the necessary abundance required to elevate the GRS gridded pixel (5° x 5°) above the background value using the unsmoothed averages and uncertainties for the southern highlands. The minimum required for a marginal detection using these parameters is ~45%. Preliminary laboratory studies estimate ~15 to 20% abundance of chloride salt [*Osterloo et al.,* 2008] thus, 45% is probably higher than the amount of proposed halite on the surface. Nevertheless, because we compare the proposed chloride-bearing material locations with smoothed global maps, even if there is a marginal detection for the grid with the largest

material, it would be reduced and obscured in the smoothed maps. This is because the signal from any other additional grid with sites in it would be lower due to smaller total area of the proposed chloride-bearing materials. At this time, there is little evidence to suggest these materials could be identified in the smoothed or unsmoothed gridded global maps. Similar arguments can be made to account for the lack of correlation between the proposed chloride materials and the GRS H_2O and K/Th distributions, though these elevated detections may be more representative of recent (~a few to ~1000 years) hydration and alteration processes than those producing the proposed chloride-bearing materials, which are likely ancient in age.

The lack of a Cl correlation between GRS and the materials can also be attributed to a variety of additional factors that do not preclude chloride salts, including:

1) The Cl content in the proposed chloride-bearing material is independent of the bulk composition of the near surface. For example, it is possible that aeolian deposition of Cl-rich dust, Cl-rich ash-flow tuffs, and ignimbrites through volcanic exhalation of HCl are more abundant in some regions (e.g., the Medusae Fossae formation [*Keller et al*., 2006]) which increases the total Cl content (as well as maximum wt%) independent of the proposed chloride-bearing composition. Essentially, other materials are significantly more Cl-rich than the proposed chloride-bearing materials, thus they are not displayed as areas of elevated chlorine. A similar hypothesis was proposed to account for the lack of correlation between the TES-derived olivine distribution and GRS Fe distribution by *Koeppen and Hamilton* [2008].

2) Dusty regions impenetrable to imaging spectroscopy obscure the correlation;

for example some of the highest Cl concentrations observed by GRS are located in dusty areas where spectrometers cannot measure surface composition (below the dust) with accuracy.

4.6 Local and regional mineralogical compositions

As previously described, spectral signatures consistent with phyllosilicates have been identified near the proposed chloride-bearing materials in some locations [*Murchie et al*., 2009; *Wray et al.,* 2009]. This observation suggests that the lack of correlation with OMEGA detections of phyllosilicate and sulfate signatures is likely related to the differences in spatial footprints between OMEGA and THEMIS. Some hydrated sulfate mineral detections have been found in close proximity to phyllosilicate detections in the southern highlands [*Wray et al.*, 2009], though at this time, no sulfates have yet been identified in CRISM data near the proposed chloride-bearing materials. Sulfate, and specifically jarosite, detections could be associated with weathered gossans or evaporative playa deposits, and thus may not be indicative of either chloride or sulfide deposition. Jarosite has been observed from orbit in a few localized areas [*Farrand et al*., 2009; *Milliken et al.,* 2008] but has not yet been observed near the proposed chloride-bearing materials. It is possible that sulfates are associated with the proposed chloride-bearing materials, but are sufficiently fine-grained and spectrally subdued or coated to hinder detection, similar to the sulfate terrains observed by *Opportunity* in Meridiani Planum [*Wiseman et al.,* 2008b]. It is also possible that sulfates still lie buried under regional terrain materials. If a stratigraphic sequence of sulfates and proposed chloride-bearing materials can be

identified through additional detailed spectroscopic or landed investigations, it may be possible to constrain the local depositional environment and geochemistry of the waters that precipitated the various salt assemblages. The different depositional environments that can produce chloride salts vary in terms of ancillary and sequential mineralogy that is expected. For example, saline lakes can be mineralogically zoned with carbonates, sulfates, and chlorides [*Eugster and Hardie,* 1978], whereas neutral-chloride hydrothermal brines are typically over-saturated with silica or carbonates and at surface conditions generally form sinter and/or travertine deposits [*Goff and Jank*, 2000]. Chlorides formed via volcanic sublimates typically occur in association with sulfates, oxides, and amorphous silica deposits (though lack of ancillary alteration products suggests that deposition occurred at relatively high temperatures (> ~400º C), high gas/ rock ratios, and under reducing conditions [*Schmidt et al., 2008*; *Getahun et al.,* 1996]).

The materials are not associated with volcanic magnesian or felsic compositions and hence are probably inconsistent with sulfide deposits. Hydrothermal mineralization of sulfide deposits on Earth are typically found near felsic igneous intrusions (commonly found as grains or veins in quartz-diorite to quartz-monzonite deposits), but can also occur as an accessory mineral in a wide range of felsic igneous rocks [*Deer et al.,* 1992]. High Si rocks (i.e., rhyolites and dacites) are rare on the surface of Mars [*Bandfield*, 2002], but even so, the proposed chloride-bearing materials are not correlated with the relatively silica-enriched surfaces, such as the Surface Type II interpreted basaltic-andesite [*Bandfield et al*., 2000]. Small, localized occurrences of high-silica materials, interpreted to be quartzofeldspathic granitoid

materials have been identified by TES and THEMIS in Syrtis Major [*Bandfield et al*., 2004; *Bandfield,* 2006]. Using CRISM data, *Ehlmann et al*. [2009] investigated these surfaces and concluded that they were most likely the products of hydrothermal processes instead of igneous in origin. Despite the differences in interpreted depositional processes, the proposed chloride-bearing materials are not associated with the high silica deposits, thus indicating that the materials are unlikely to be sulfide or chloride deposits associated with hydrothermal or fumarolic processes.

Terrestrial sulfide ore deposits can be associated with komatiites or ultramafic magnesian lava flows [*Burns and Fisher,* 1990], however, there has been no conclusive evidence of widespread exposed occurrences of komatiite compositions based on orbital spectral data [*Bandfield et al.*, 2000; *Christensen et al*., 2000a; *Rogers and Christensen*, 2007]. Extensive exposures of olivine-enriched rock layers near the Nili Fossae and Isidis Planitia have been investigated by a number of researchers [*Hamilton and Christensen,* 2005; *Mustard et al.*, 2007; *Tornabene et al.*, 2008] and although interpretations varied for formation mechanisms, none of the studies attributed the materials to komatiite lavas. Additionally, studies of olivine-enriched materials [*Koeppen and Hamilton*, 2008; *Rogers et al*., 2005; *Edwards et al.,* 2008] and mafic to ultra-mafic materials [*Schneider and Hamilton*, 2006; *Stockstill-Cahill et al*., 2008] have not yielded evidence for a direct compositional or spectral match to komatiite-type rocks. However, even if the olivine-enriched lavas produced sulfides, in general, we have not found that olivine-enriched materials are associated with the sites. Therefore, we see no direct evidence for a parent lithology consistent with sulfide deposition. Additionally, most terrestrial basalts associated with sulfide

mineralization are commonly weathered to surficial gossan deposits consisting of poorly crystalline ferric bearing oxide, oxyhydroxide, sulfate, and clay silicate phases [*Burns and Fisher,* 1993]. We do not find evidence for sulfates, ferric oxides or oxyhydroxides in close proximity to the materials, yielding further evidence indicating that these materials are not sulfides.

4.7 Astrobiological significance of possible chloride-bearing materials

If these sites are materials containing chloride salts as we infer, they may have astrobiological implications. A wealth of research indicates that many ancient terrestrial salt deposits contain a multitude of microbial fossils [e.g., *Huval and Vreeland,* 1991], cellulose fibers [e.g., *Griffith et al.* 2008], and microscopic prokaryotes, including both haloarchaea and halobacteria biomarkers [e.g., *Fredrickson et al.*, 1997; *McGenity et al.*, 2000; *Schubert et al.*, 2009; *Barbieri et al.,* 2006]. In addition, previous researchers have provided evidence that fluid inclusions in halite are a favorable refuge for short to long (possibly hundreds of millions of years) term survival of halophilic microorganisms [e.g., *Norton and Grant,* 1988; *Javor,* 1989; *Norton et al.*, 1993; *Vreeland et al.*, 2000; *Fish et al.*, 2002; *Satterfield et al.*, 2005; *Schubert et al.*, 2009].

Though the specific phase(s) of chloride mineral has yet to be determined based on orbital and laboratory spectroscopic observations and models, thermodynamic modeling indicates that halite would not precipitate in Meridiani with the observed assemblage of minerals until the H_2O activity was ≤ 0.50, which indicates an extreme salinity that would not be habitable for known terrestrial

organisms [*Tosca et al.,* 2008]. Nevertheless, it is possible that the chlorides were deposited under more alkaline conditions in some locations in the southern highlands and thus may not have precipitated at extreme salinities. Further orbital observations of ancillary mineralogy may aid in thermodynamic models for these locations to better ascertain the geochemical evolution and their exobiological potential. However, though the basaltic chemistry of Mars suggests very low water activity for chloride deposits [*Tosca and McLennan*, 2006], the low energy setting of terrestrial evaporite deposits suggests that such materials on Mars may have a high preservation potential. As such, even if the chlorides were precipitated at extreme salinity, the materials could have entrapped and preserved halophilic microorganisms present in a precursory lower salinity system. Finally, although microorganisms may not have been able to originate in such a high salinity system, they may have been able to adapt to survive in such a system [*Stivaletta et al.,* 2009; *Rothschild and Mancinelli*, 2001].

Therefore, in addition to providing information about the precursory liquid composition entrapped in inclusions and clues to the depositional environment and climate at the time of formation [*Lowenstein et al.*, 1999; *Roedder,* 1984], halite crusts may host traces of endolithic and/or fossils of halotolerant microorganisms. Furthermore the duration of the conditions that enabled the materials to form is important with respect to both the climatic and geologic evolution of Mars. Albeit the materials may only be representative of ephemeral bodies of water, such as the salt pans in Death Valley, the fact that the climatic and hydrologic conditions permitted

the existence of these ephemeral bodies of water to exist in localized occurrences throughout the southern highlands for ~0.5 Ga or more, is significant.

5.0 Conclusions

The geologic history of the planet Mars involves a complex interplay between volcanic, hydrologic, sedimentary, and erosional processes. The abundance of materials containing a spectrally featureless component dispersed throughout the southern highlands indicates that these distinct materials are important for understanding the processes and conditions that have shaped the surface of Mars. Detailed spectroscopic studies utilizing multiple wavelength regions and geomorphologic contextual observations of the sites, in addition to further laboratory studies, will help to gradually unravel the complex nature of these materials. However, it is possible that a landed mission will be the only way to unequivocally determine the mineralogy responsible for the spectral character of the materials and their formation mechanisms. If the materials are partially composed of chloride salts, locations where these materials occur within a diverse mineral assemblage could shed light onto the processes and environmental conditions that shaped similar sites on early Mars and should be considered a high priority for a landed mission.

If, as we infer, the materials are partially composed of chloride salts, our observations indicate that many of the sites show characteristics that are consistent with deposition via precipitation from a ponded evaporating brine derived from groundwater upwelling and/or surface runoff. The correlation between the proposed

chloride-bearing materials' locations and ages with the locations and ages of the valley-networks and paleobasins further supports formation via ponding from surface runoff and/or groundwater upwelling. The diversity of morphological observations and widespread occurrences throughout the southern highlands indicates that there were likely multiple formation mechanisms operating. However, efflorescence is unlikely to have been a dominant formation mechanism because materials commonly display distinct surface morphologies and appear to be relatively thick (~a few meters) based on our observations from visible imagery. Additionally, regional trends in mineralogy do not support evidence for widespread hydrothermal deposition of chlorides. Lack of evidence for parental lithologies (mafic and felsic igneous materials), limited evidence for ancillary weathering products (i.e., gossans), and lack of lava flow morphologies suggests that sulfides are less likely to be the mineral responsible for the relatively featureless spectral slope observed in the TIR and NIR data. However, our study cannot unequivocally determine the mineralogical component attributed to the featureless spectral slope of the materials, nor can we conclude a sole formation mechanism for the materials. Nevertheless, we have expanded the characterization of sites from ~200 to ~640 instances and from our detailed analyses, the following conclusions can be drawn:

1. The materials are predominantly local in nature, yet their prevalence around the planet suggests that they represent one or more globally prevalent processes.

2. Virtually all of the materials identified to date are dispersed in discrete locales throughout the low albedo Noachian to Hesperian aged terrains of the southern highlands. Their distribution indicates that their formation was most widespread in

the Middle/Late Noachian to Early Hesperian period of Martian history (our favored interpretation), and implies that resurfacing events may have obliterated their signatures in the geologic record of the northern lowlands. Additionally, the inferred ages of the materials suggests that the conditions (either hydrologic or volcanic) that enabled the materials to form had durations of up to a billion years.

3. The areal extent of the materials range from ~0.33 to ~1300 km^2 (per site), which could indicate variations in the degree to which materials have been exposed via erosion, or differences in depositional processes and fluid compositions. In addition, our observations suggest that there are a number of different dominant small-scale morphologies: 1) rough terrain consisting of scalloped surfaces, 2) exhumed layers exposed in geologic windows, 3) superposed sharp margin thinly layered materials, and 4) inverted channels and/or located within a drainage area of fluvial channels. Some morphological types can occur in concert together and fractures are commonly observed on their surfaces irrespective of morphological type. These differences could indicate variations in depositional, burial, and alteration environments. We have yet to identify spatial trends in morphology that could have would indicate regionally dominant depositional processes.

4. The materials are predominantly located in local lows (~63%) relative to the surrounding terrain, with a significant proportion occurring in basins (~31%). Some of these materials could be associated with topographic lows due to removal of overlying sediments, creating a 'geologic window' into the subsurface materials which could indicate they are more laterally extensive than their observed surface exposure would suggest. Additionally, our morphological observations indicate that the

materials occur as superposed buttes and eroded layers, which suggest a greater past extent of the material, though elevations globally do not suggest they constitute laterally extensive global or regional units.

5. Our THEMIS thermal inertia and nighttime temperature observations indicate that the materials are thermophysically distinct from the surrounding terrain materials, with elevated thermal inertia values and abrupt transitional boundaries that suggests the materials are relatively consolidated (cemented or indurated) and in situ.

6. If the materials are partially comprised of chloride salts, the lack of correlation between elevated GRS Cl abundances and their distribution is likely due to the small areal extent of the materials relative to the large spatial footprint of GRS.

7. Though we cannot eliminate sulfides as the minerals responsible for the relatively featureless, sloped spectra based on this work, we can conclude they are less likely candidates given that there is no morphological indicators for volcanic process and no compositional evidence for parent lithologies or associated weathering products.

8. These materials, if partially composed of chloride salts, have the potential to shed light on the history and evolution of water and paleoenvironmental conditions on Mars, and may have astrobiological potential.

Acknowledgements:

Funding for this work was provided by the NASA Mars Data Analysis (NNX06AE15G for F. S. Anderson, NNX06AE03G for V. E. Hamilton, and NNX06AE08G for B. M. Hynek) and Mars Fundamental Research (NNG05GL98G for F.S. Anderson) programs. Our manuscript was greatly improved by comments and suggestions from two anonymous reviewers. We would like to thank Keith Nowicki (Southwest Research Institute), Christopher Edwards, Saadat Anwar, Eric Engle, and Scott Dickenshied (Arizona State University) for assistance and development of Davinci and JMARS software. Dale Noss and Kimberly Murray (Arizona State University) graciously provided assistance in THEMIS targeting and data acquisition. Discussions with Meryl McDowell have been critical in shaping this work. Jeff Taylor provided helpful assistance and discussion of GRS chlorine data and detection limits. We also thank Robin Fergason for processing our THEMIS thermal inertia images. Lastly, we appreciate the exemplary efforts of the engineers and scientists involved in the development and continual operation of the THEMIS instrument and Mars Odyssey mission. This is Hawai'i Institute of Geophysics and Planetology publication 1855 and School of Ocean and Earth Science and Technology publication 7937.

TABLES

Table 3.1. THEMIS infrared band characteristics, modified from *Christensen et al.* [2004]

Band	Center Wavelength (μm)	Band Width (Full Width Half Max) (μm)
1	6.78	1.01
2	6.78	1.01
3	7.93	1.09
4	8.56	1.16
5	9.35	1.20
6	10.21	1.10
7	11.04	1.19
8	11.79	1.07
9	12.57	0.81
10	14.88	0.87

Table 3.2. Global maps used in analysis

Map	~ Map Resolution	Properties	References
GRS elemental abundance	5°x5°	H (H_2O), Cl, K/Th	*Boynton et al*. 2007; *Keller et al*., 2006; *Taylor et al*., 2006
TES mineralogy	8 ppd, and 16 ppd	Mineral maps	*Bandfield*, 2002; *Koeppen and Hamilton*, 2008
OMEGA mineralogy	3.5 ppd	Phyllosilicates, Sulfates	*Bibring et al.*, 2006
TES surface composition	8ppd	Regional compositions	*Bandfield et al*., 2000, *Rogers et al.*, 2007; *Rogers and Christensen*, 2007
TES Dust Cover Index	16 ppd	Abundance of surface dust	*Ruff and Christensen,* 2002
TES Albedo	8 ppd	Albedo	*Christensen et al.*, 2001a
TES Thermal Inertia	20 ppd	Thermal inertia	*Putzig and Mellon*, 2007
MGS Magnetic	1 ppd	Magnetic properties	*Connerney et al.*, 2005
Geologic	1:15 million or ~16 ppd	Morphology, age	*Scott and Tanaka*, 1986; *Greeley and Guest*, 1987
MOLA Topography	128 ppd	Regional topography, elevation, stratigraphy	*Smith et al.*, 2003
Open basin-lakes	~232 m/pixel	precipitation in standing water	*Fassett and Head*, 2008a
Valley Networks	~232 m/pixel	deposition via surface water	*Hynek et al.,* 2010 in press

Table 3.3. Geologic ages of the proposed chloride-bearing materials

Mapped geologic units and crater density (N = no. craters > (x) km diameter/10^6 km^2) from the stratigraphic column of *Scott and Tanaka* [1986]				Series from Table 2 of *Tanaka* [1986]	Age from *Tanaka* [1986] and *Tanaka and Hartmann* [2008]
Unit	~N(2)	~N(5)	~N(16)	E=early, M=middle, L=late, N=Noachian, H=Hesperian	~Age (in Ma)
Hf	500-1200	75-200	-	LH/EH	2600-3400
Hplm	550-1200	90-200	-	LH/EH	2600-3400
Hpl3	700-1200	125-200	-	EH	3400-3600
Hr	800-1200	150-200	-	EH	3400-3600
Npl2	-	200-400	25-100	LN	3600-3750
Nf	-	200-600	25-200	LN/MN	3600-3950
Nplr	-	300-600	75-150	LN/MN	3600-3950
Nple	-	400-600	100-200	MN	3750-3950
Npld	-	400-600	100-200	MN	3750-3950
Npl1	-	400-600	100-200	MN	3750-3950
Nplh	-	-	200-250	EN	3950-4100
Nh1	-	-	200-250	EN	3950-4100

Table 3.4. Proportion of chloride materials' areas within their geologic unit

Unit	~Total area of chloride materials (km^2)	~Total area of geologic unit (km^2)	~ % of Martian surface	~ % of geologic unit ($x10^{-4}$)
Nh1	1	1657663	0.011	0.00525
Nplh	23	2161460	0.015	0.107
Nf*	28	----------	----------	----------
Npl1	2872	20194700	0.139	1.44
Npld	1209	14114400	0.097	0.876
Nple*	34	----------	----------	----------
Nplr	3099	4240386	0.029	7.31
Npl2	1324	7394179	0.051	1.79
Hr	4139	12636868	0.087	3.28
Hpl3	1145	2885799	0.020	3.97
Hplm	209	21197	0.002	9.43
Hf	14	1146558	0.008	0.125

* Area of Nf is combined with area of Npld and area of Nple is combined with Npl1 because they are relatively small geologic units.

Table 3.5. Crater size-frequency determinations converted to the chronostratigraphic series of *Tanaka* [1986]

Location	19˚ S, 91˚ E	32˚ S, 205˚ E	3˚S, 350˚E
Area (km2)	20437	17870	31727
> 2 km	31	20	36
N(2)	1517	119	1135
N(2) age	LN	EH	EH
> 5km	12	8	16
N(5)	587	448	504
N(5) age	MN	MN	MN
> 16 km	3	1	1
N(16)	147	56	32
N(16) age	MN	LN	LN
Average age	MN/LN	LN	LN

Table 3.6. THEMIS thermal inertia in $Jm^{-2}K^{-1}s^{-1/2}$ and single detector albedo

Lat ˚S Lon ˚E	27.71 5.83	3.05 350.96	3.12 351.55	27.25 180.46	32.25 190.52
ID	I10392002	I02491006 I12776002 I20788002	I13687006 I05849012 I18292012 I12464002	I06629006	I11072004
Avg TI	358±58	377±45	455±27	406±56	349±12
Min TI	316	252	372	334	311
Max TI	413	437	504	453	380
Ave albedo	0.15	0.18	0.15	0.17	0.14
Min albedo	0.14	0.17	0.14	0.15	0.13
Max albedo	0.17	0.19	0.15	0.18	0.14

25.25 346.62	38.13 245.64	18.66 91.4	38.82 221.08	32.89 205.62			
NA	NA	I17128010	I06378009 I22727005	I16887006 I06366007			
		446±20	385±21	329±34			
		384	370	148			
		509	400	431			
0.15	0.17	0.14	0.12	0.13			
0.14	0.11	0.10	0.10	0.10			
0.18	0.20	0.19	0.13	0.15			

Table 3.6 (continued)

Table 3.7. Formation hypotheses for the proposed chloride-bearing materials

Proposed hypothesis	Potentially consistent observations	Potentially inconsistent observations
Precipitation in ponds from surface runoff or groundwater discharge	Locations in topographic lows and degraded craters; inverted and fluvial channels; close proximity to valley networks; polygonal fractures; clays; blanketing underlying topographic features such as scallops and craters; formation near peak of hypothesized surface water activity	No evidence of sulfates expected for playas
Hydrothermal brine via impact or volcanic activity	Located within and near craters; some observed within crater walls; locations in topographic lows	Lack of evidence for surge deposits, fluidized ejecta, pedestal craters; craters may not be sufficient in size to initiate long-lived hydrothermal region; observed in very few craters formed during this time period; no evidence for ancillary mineralogy (e.g., sulfur, silica)
Efflorescence via fumarolic activity or atmospheric interactions	Well developed fractures are not observed in some sites; located within topographic lows; some materials blanket underlying topography; pasted on terrain	No volcanic constructs observed; many materials have well developed fractures; no 'haloing' observed; morphology suggestive of well lithified materials
Sulfides via lava (present as either thinly disseminated layers or massive	Located in local lows (including craters); sinuous features that may be lava flows observed for some sites; 58% located on terrains interpreted to be partially volcanic in nature	Variations in elevation data does not suggest thin laterally expansive regional units; no evidence for parent material;

deposits located in local lows)	[*Scott and Tanaka*, 1986]	olivine-enriched materials not observed near materials; no evidence for lava flows or heat constructs; no evidence for weathering assemblages (i.e., gossans)
Sulfides via hydrothermal	Located in local lows; 58% located on terrains interpreted to be partially volcanic in nature [*Scott and Tanaka*, 1986]	No evidence for ancillary hydrothermal materials (i.e., quartz) or sulfide-derived weathering products (i.e., gossans), no volcanic constructs or heat sources evident

Table 3.8. Minimum required halite wt%

	Fractional area	Cl background average (wt%)	Cl background uncertainity (wt%)	NaCl (wt%)
Single pixel	0.0088	0.2	0.10	23.13
			0.18	41.31
		0.8	0.10	24.33
			0.18	42.5
Smooth gridded	0.0045	0.48	0.04	18.74
Unsmoothed gridded	0.0045	0.2	0.10	44.84
			0.18	80.4
		0.8	0.10	46.04
			0.18	81.6

*0.0088 is the fractional contribution for the largest proposed chloride-bearing material within a single GRS pixel, and 0.0045 is the fractional contribution for the largest proposed chloride-bearing material within a 5º by 5º gridded area (at ~30º S). Averages and uncertainties are from *Boynton et al.* [2008] (0.48 ±0.04 wt% for mid latitude southern highlands from smoothed maps) and *Keller et al*. [2006] (0.2 to 0.8 ± 0.10-0.18 wt% for mid latitude southern highlands from unsmoothed maps).

FIGURES

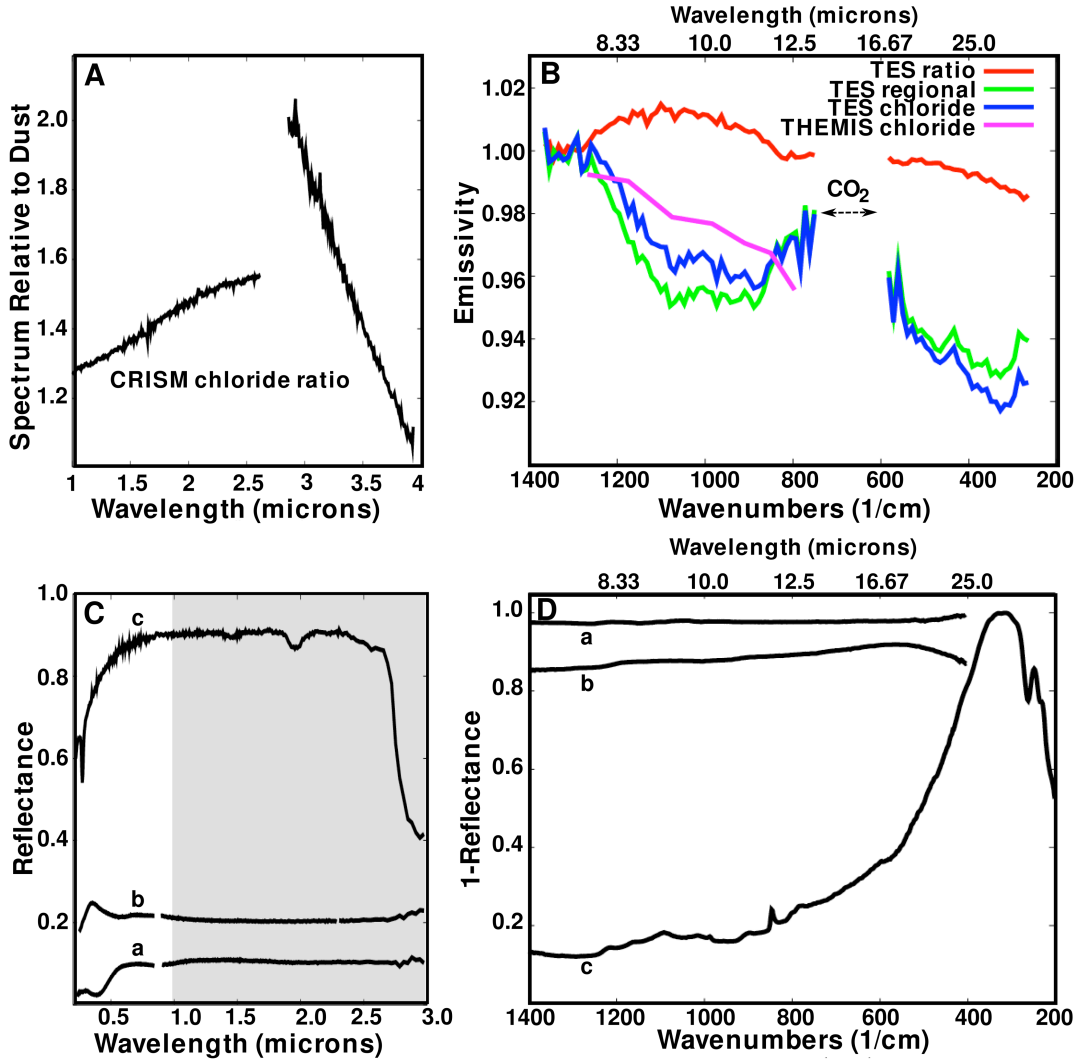

Figure 3.1. A) Relative spectrum of proposed chloride-bearing materials from CRISM FRT00010A4E at ~38.8ºS, ~221ºE. The spectrum has been ratioed to nearby spectrally neutral materials to highlight differences. B) Atmospherically corrected TES data (orbital counter keeper (ock) 3957) shown in red (ratio), green (regional material), and blue (proposed chloride-bearing materials), and THEMIS data (I08831002) in purple (proposed chloride-bearing material) from a site investigated in Terra Sirenum (from *Osterloo et al.* [2008]). C) NIR spectra for chalcopyrite (a), galena (b), and halite (c) from the Unites States Geological Survey (USGS) spectral library [*Clark et al.,* 2007]. Grey areas indicate CRISM long wavelength and TES wavelength regions. D) TIR spectra of chalcopyrite ($CuFeS_2$) (a), galena (PbS) (b), and halite (NaCl) (c) from the USGS spectral library [*Clark et al.*, 2007].

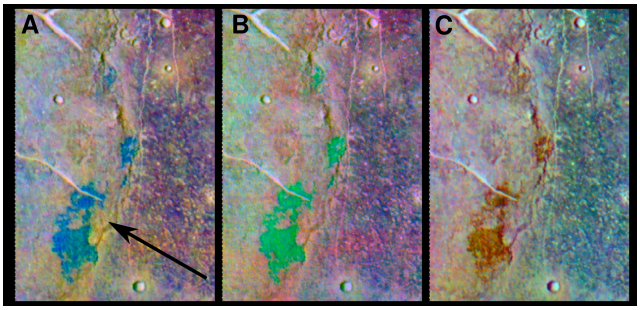

Figure 3.2. False color, decorrelation stretch image of THEMIS TIR radiance data I34346002 (~18.9°S, ~332.2°E). All subsequent TIR images begin with I and all subsequent THEMIS VIS images begin with V. A) Bands 8/7/5 as red/green/blue, arrow indicates proposed chloride-bearing materials that appear blue. B) Bands 9/6/4/ as red/green/blue, proposed chloride-bearing materials appear green or teal. C) Bands 6/4/2 as red/green/blue, proposed chloride-bearing materials appear yellow or orange.

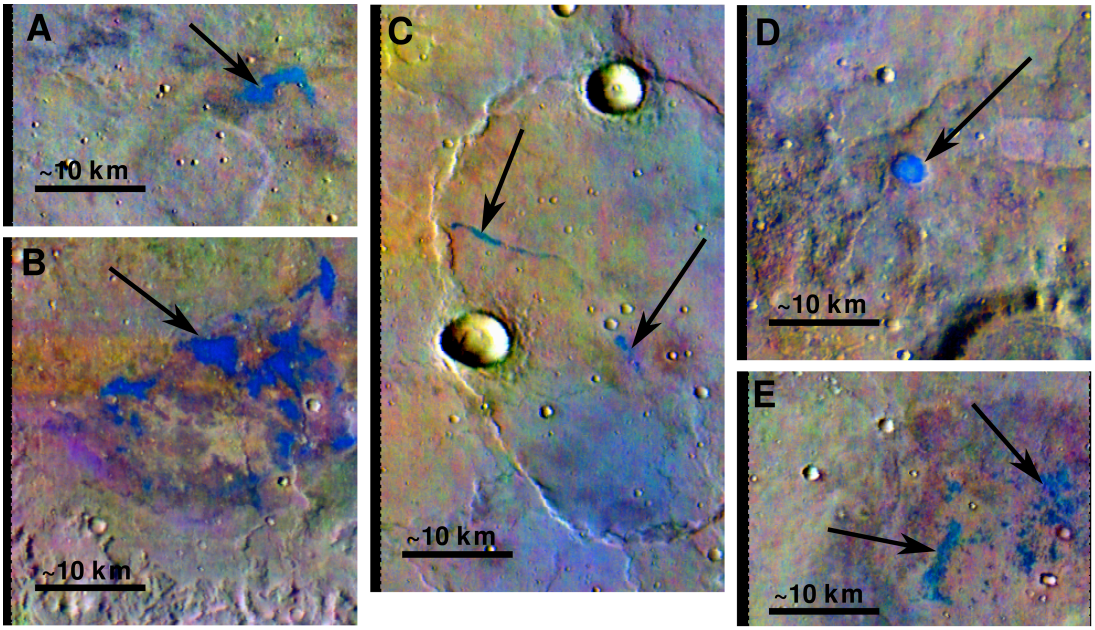

Figure 3.3. All THEMIS radiance data are displayed as 8/7/5 DCS images where proposed chloride-bearing materials appear blue. Arrows indicate locations of proposed chloride-bearing materials in each image and the black scale bar at bottom represents ~10 km. A) Spatially small patches of proposed chloride-bearing materials with irregular boundaries in I07890003 (~31.88°S, ~1.07°E). B) A larger proposed chloride-bearing site displaying irregular boundaries in I33877002 (~31.51°S, ~181.01°E). C) Thin semi-linear proposed chloride-bearing materials in I08123003 (~28.55°S, ~121.50°E). D) Proposed chloride-bearing materials infill a small degraded crater in I18063005 (~33.35°S, ~306.69°E). E) Cluster of small spatially isolated proposed chloride-bearing patches in I01224002 (~18.40°S, ~2.83°E).

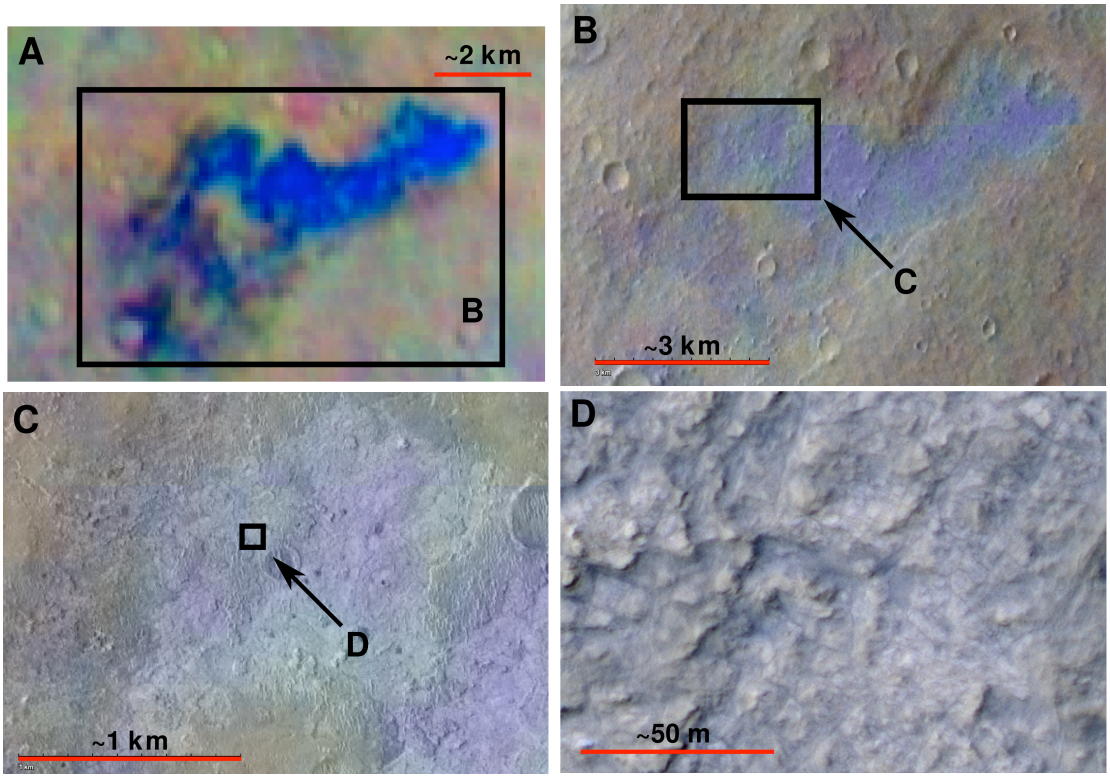

Figure 3.4. Example of the various spatial resolutions of different instruments used over a proposed chloride-bearing material near Meridiani Planum (~3.05ºS, ~350.96ºE). THEMIS TIR DCS images (8/7/5) are overlaid on THEMIS VIS and MOC images to highlight compositional differences (proposed chloride-bearing materials shown in blue in all images). A) THEMIS I34308001. B) THEMIS V12608001. C) MOC E0500659. D) HiRISE PSP_008851_1770.

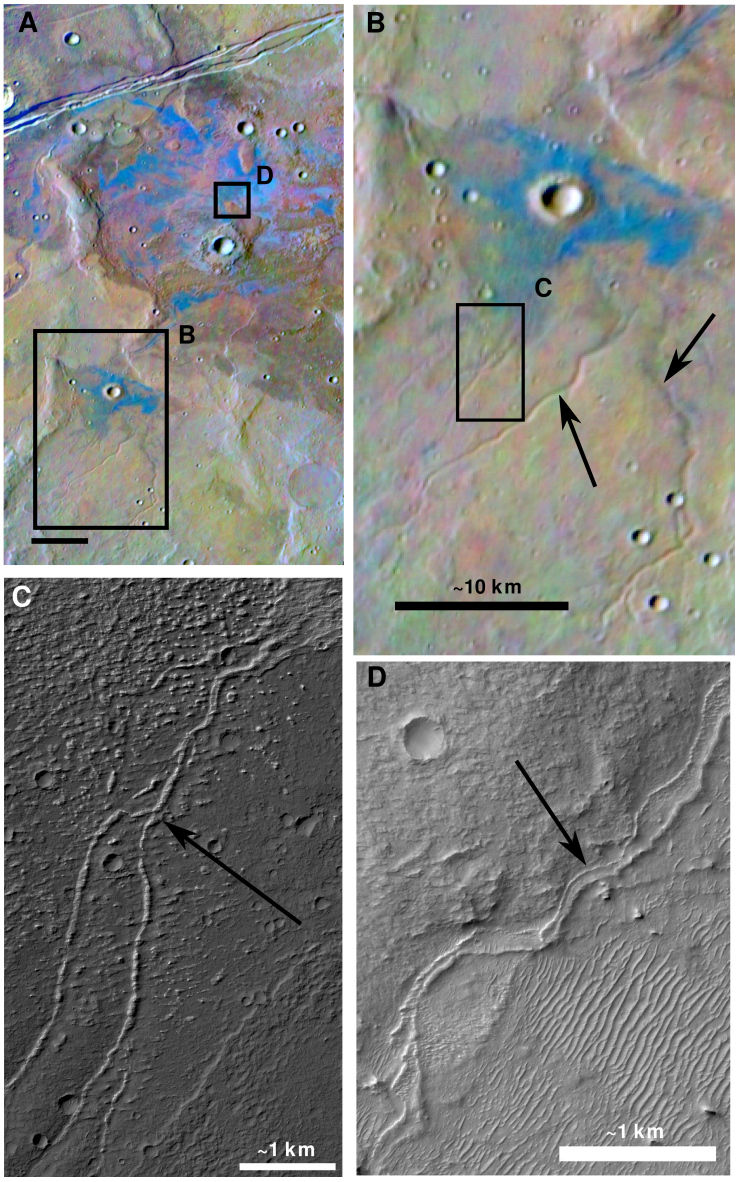

Figure 3.5. A) THEMIS 8/7/5 radiance DCS mosaic from ~205.31º to 206.18º E and ~32.15º to 33.86º S showing proposed chloride-bearing materials in blue. This location shows an example of sinuous features flowing into a closed basin containing the proposed chloride-bearing material. The thick black line indicates ~10 km and the black box indicates the location of Figure 3.5B and 5D. B) Close up of fluvial channels within the THEMIS DCS mosaic that transition to inverted channels containing proposed chloride-bearing materials. Black arrows indicate sinuous features indicative of fluvial channels and the black box indicates the location of Figure 3.5C. C) Section of HiRISE image PSP_009318_1465 showing inverted channels containing proposed chloride-bearing materials. The inverted channels are light-toned and show evidence of branching. D) Sinuous features are evident within the main proposed chloride-bearing material basin as well as shown here in HiRISE image PSP_007380_1470.

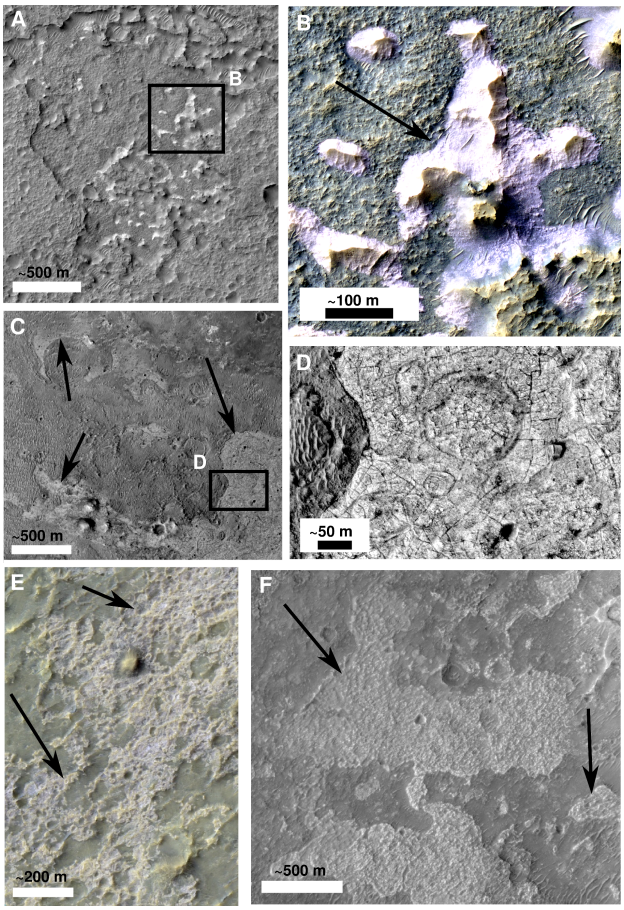

Figure 3.6. A) Some proposed chloride-bearing materials are observed within 'geologic windows' as seen here in HiRISE image PSP_007649_1575 (~22.46ºS, ~58.11ºE). Black box indicates location of higher resolution HiRISE color image in Figure 3.6B. B) The proposed chloride-bearing materials appear to be a distinct in situ layer under the erosion resistant cap rock, occurring between the darker terrain materials and as isolated buttes away from the main site. C) ESP_012741_1750 (~4.94ºS, ~349.82ºE) shows an example of proposed chloride-bearing materials as relatively thin beds that have likely undergone erosion, but are also partially covered by darker terrain materials near their boundaries. Black arrows indicate fractured, light-toned proposed chloride bearing materials and the black box indicates the position of the higher resolution image. D) The materials display curvilinear boundaries, well defined curved fractures, and semi-circular surface forms within the material. E) Example of proposed chloride-bearing materials in a relatively thin layer (indicated by black arrows) that appear to have an eroded morphology in HiRISE color image PSP_005680_1525 (~27.24ºS, ~180.48ºE). F) Proposed chloride-bearing materials are relatively thin and light-toned layers (indicated by black arrows) that appear to overlie darker terrain materials and have undergone significant erosion in HiRISE image ESP_012864_1405 (~39.34ºS, ~235.48ºE).

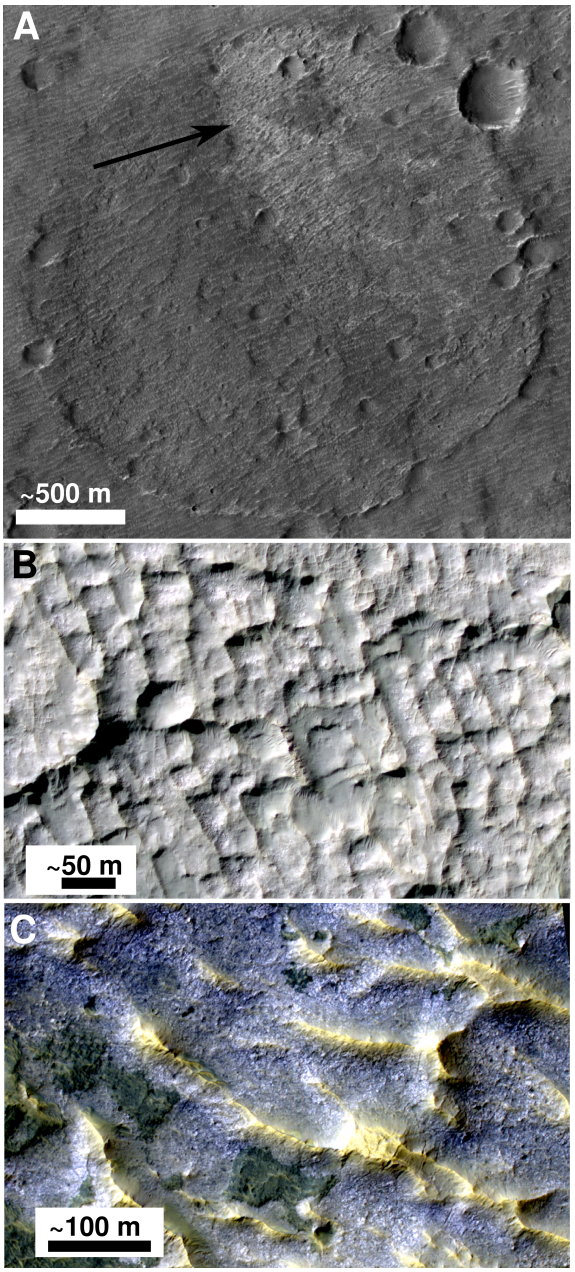

Figure 3.7. A) The proposed chloride-bearing materials located in this slightly inverted crater appear to have undergone erosion and have a scoured appearance (indicated by black arrow) in HiRISE image ESP_012847_1510 (~28.56ºS, ~338.92ºE). B) Proposed chloride-bearing materials often appear to have a scalloped surface. HiRISE color image PSP_009846_1475 over a proposed chloride-bearing material show an example of linearly trending, nearly aligned hummocks or ridges (~32.25ºS, ~190.52ºE). C) Some proposed chloride-bearing materials appear to be reminiscent of yardangs as shown in HiRISE color image PSP_008780_1735 (~6.37º S, ~131.94º E).

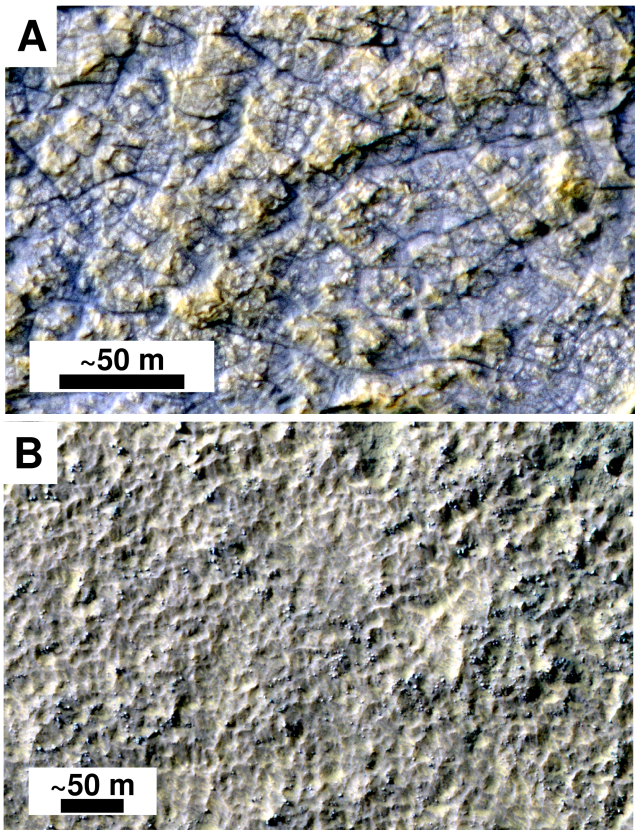

Figure 3.8. The proposed chloride-bearing materials display a wide range of fracturing at the HiRISE scale. A) PSP_007770_1770 shows a proposed chloride-bearing material with a highly fractured surface (~3.12ºS, ~351.55ºE). B) PSP_010460_1415 shows an example of a proposed chloride-bearing material that has a surface devoid of fractures (~37.95ºS, ~348.99ºE).

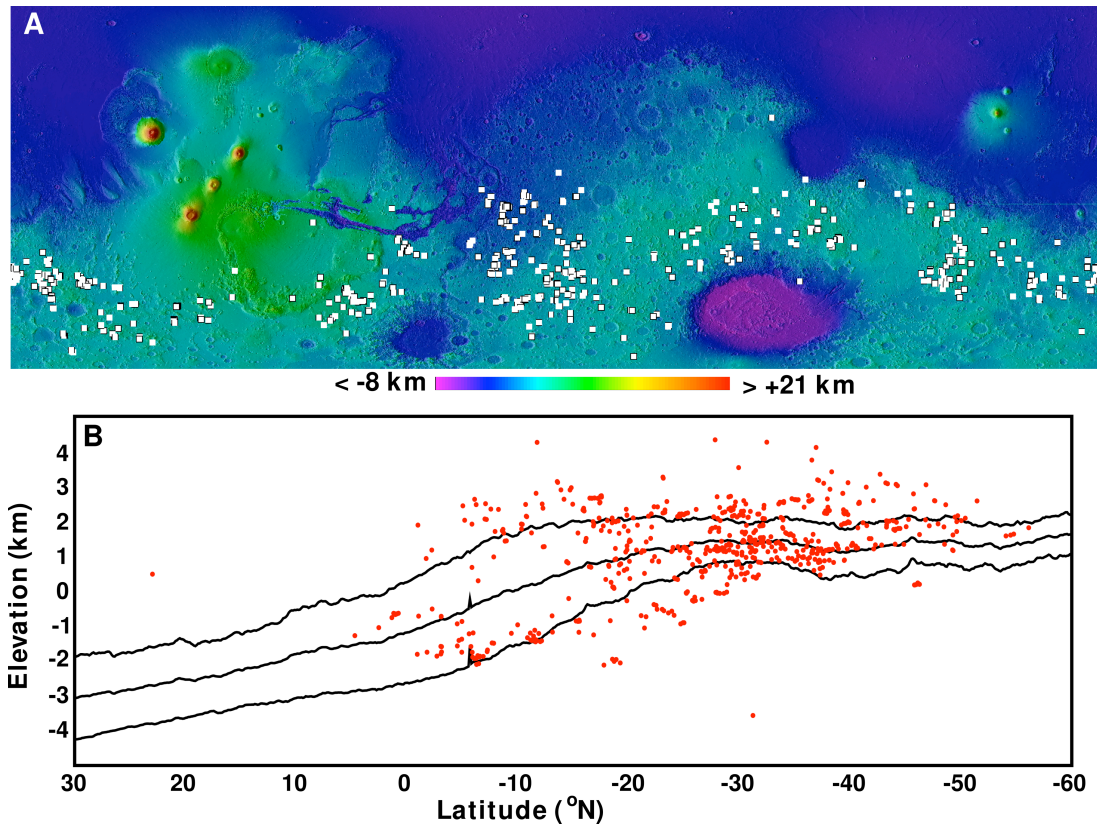

Figure 3.9. A) MOLA colorized elevation over shaded relief with locations of materials in white (boxes are enlarged for ease of viewing and do not represent true area at the surface). The map is simple cylindrical projection from 60°N to 60°S and 180°W to 180°E. B) Average MOLA elevation [*Smith et al.,* 2003] for all sites plotted (red) against latitude. Black trend lines indicate the average and standard deviation for the southern latitudes excluding major impact basins and volcanic provinces.

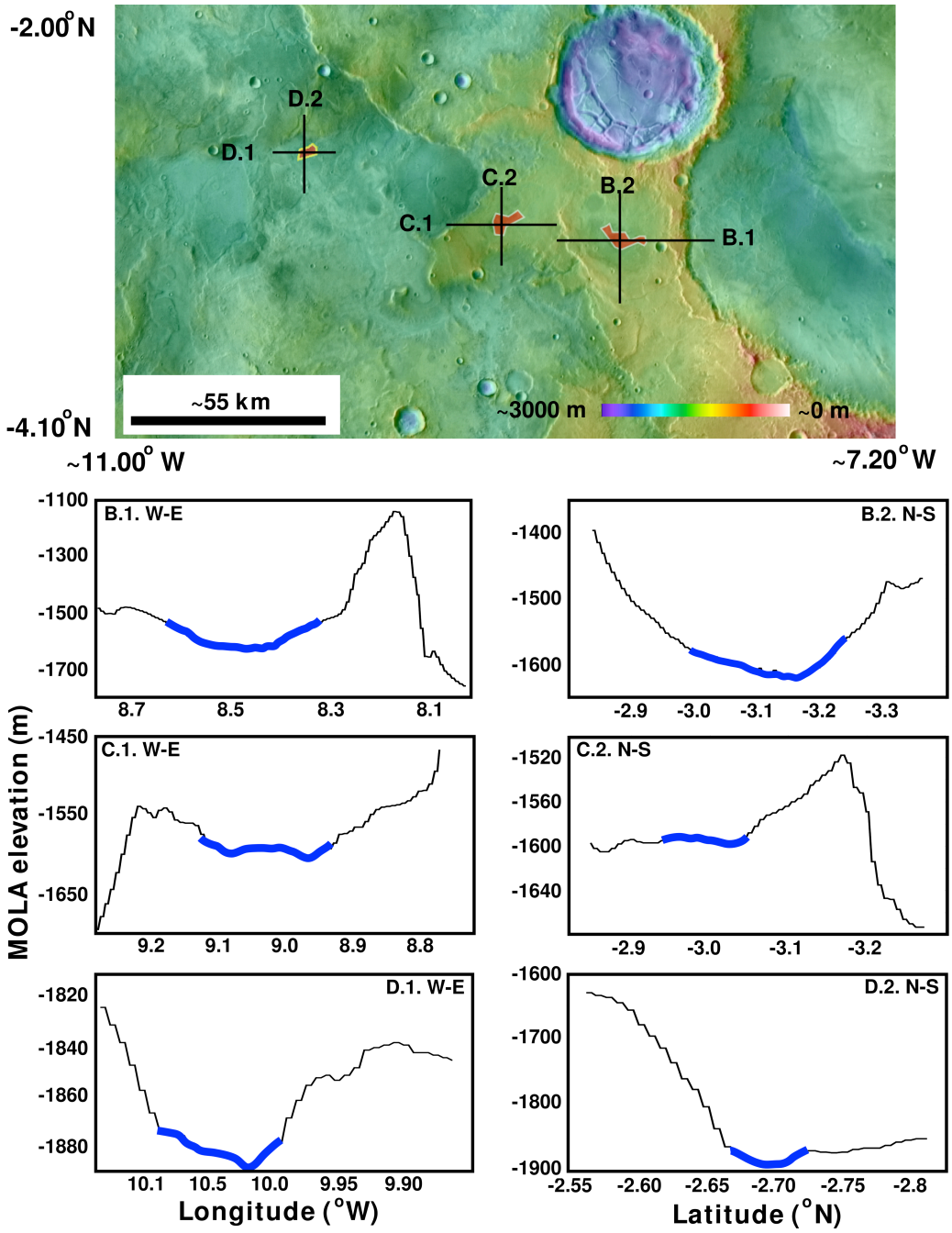

Figure 3.10. Profiles of three proposed chloride-bearing materials in the western Meridiani region (-2.00°N to -4.10°N, 11.00°W to 7.20°W). MOLA colorized elevation draped over a THEMIS band 9 daytime TIR mosaic [*Edwards et al.*, in prep], with locations of proposed chloride-bearing materials shown as red polygons. Black lines indicate approximate locations of topographic profiles (shown below the map). Plots on the left are east-west profiles and the plots on the right are north-south profiles. Thick blue lines indicate approximate location of materials within each topographic profile.

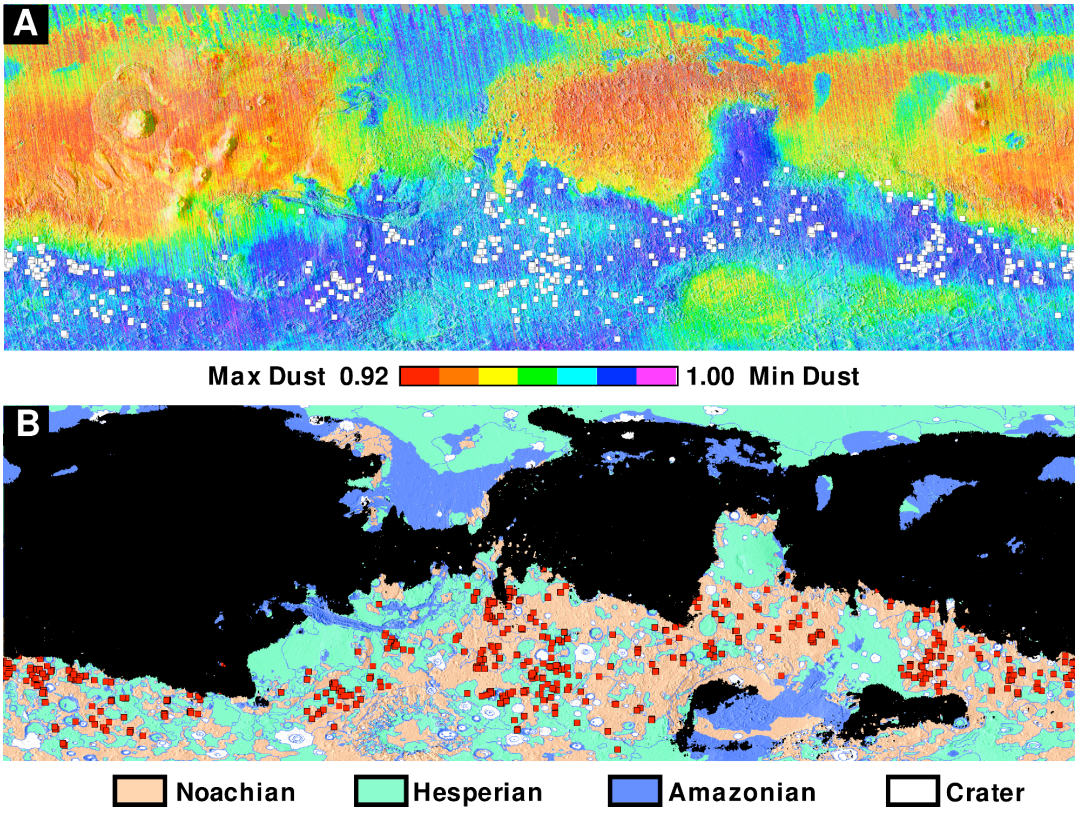

Figure 3.11. A) DCI map from *Ruff and Christensen* [2002] and proposed chloride-bearing materials shown as white boxes (boxes here and below are enlarged for ease of viewing). B) Simplified geologic map from *Scott and Tanaka* [1986], and *Greeley and Guest* [1987], with proposed chloride-bearing materials shown as red boxes. Black regions indicate masked out dusty regions (using the DCI values < 0.94 from *Ruff and Christensen* [2002]). Both maps are in simple cylindrical projection from 60°S to 60°N and 180°W to 180°E.

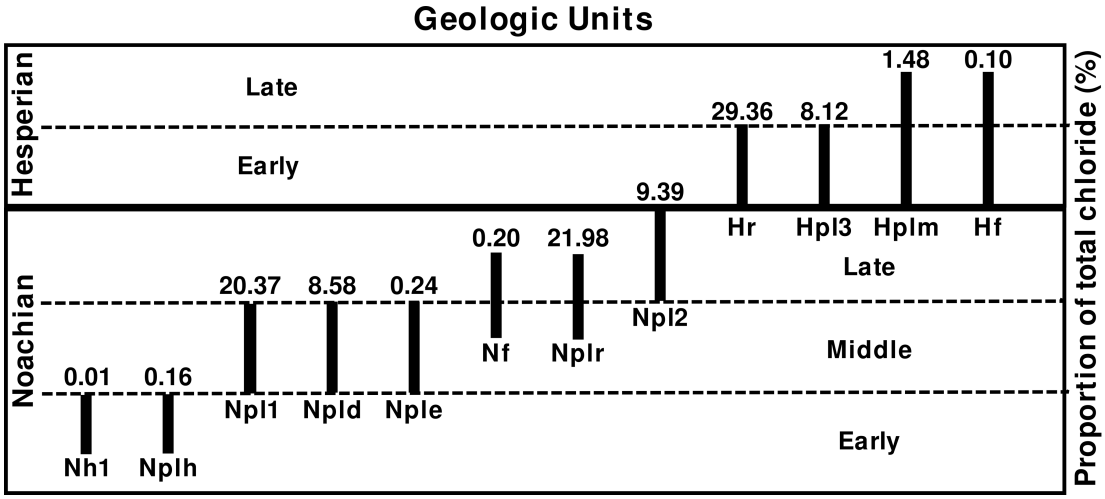

Figure 3.12. Schematic diagram showing the range of geologic units in which the proposed chloride-bearing materials occur. The areal percentage of proposed chloride-bearing materials identified within each unit are given above their respective geologic units (relative to total area of chloride-bearing materials). Geologic units from *Scott and Tanaka* [1986] and *Greeley and Guest* [1987] and series designations (e.g., Early, Middle, and Late) from *Tanaka* [1986].

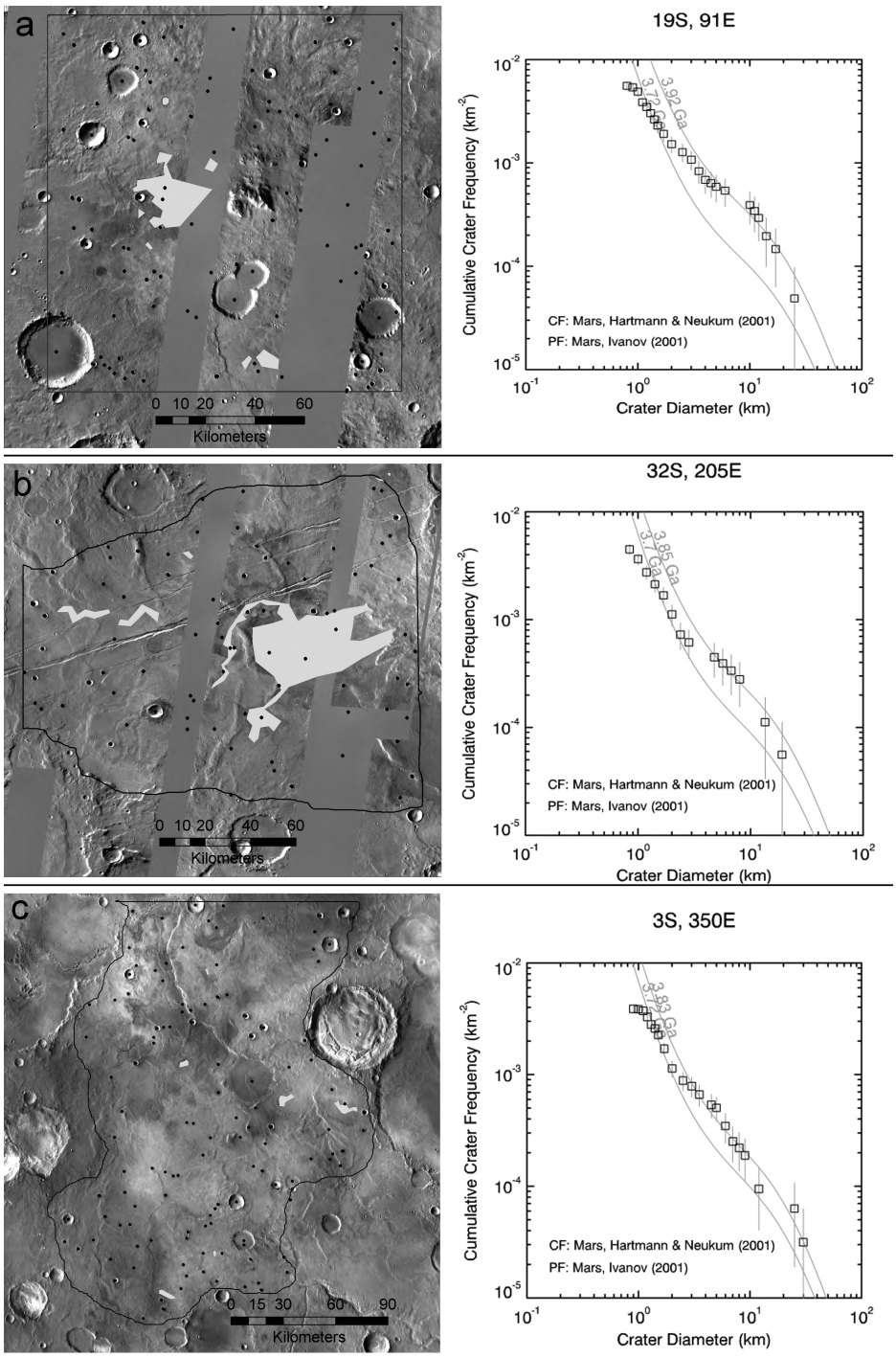

Figure 3.13. Size-frequency crater plots for three regions (black lines) surrounding significant chloride-bearing materials (gray polygons). Isochrons are plotted from *Hartmann and Neukum* [2001] and *Ivanov* [2001]. a) Proposed chloride-bearing materials in Terra Tyrrhena (~91°E, ~19°S). b) Proposed chloride-bearing materials in Terra Sirenum (~205°E, ~32°S). c) Proposed chloride-bearing materials in Meridiani Planum (~350°E, ~3°S).

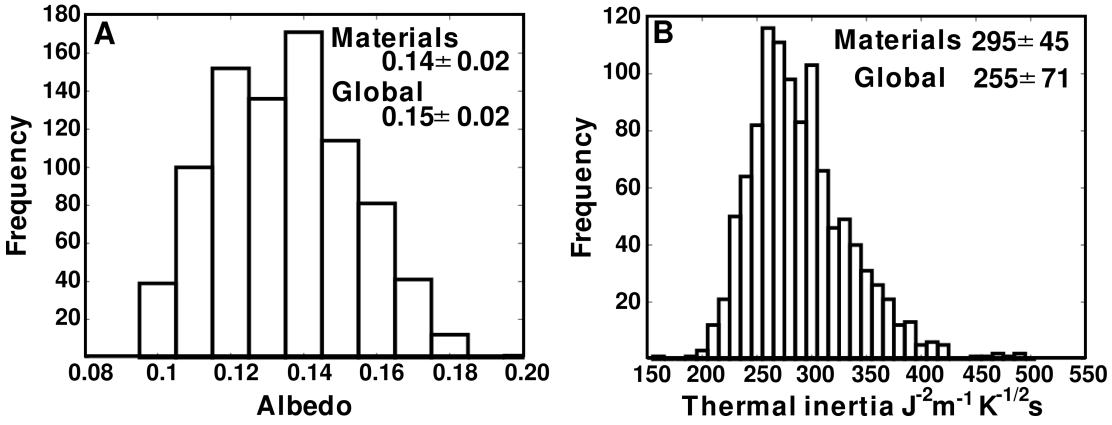

Figure 3.14. The values in each panel are the average and standard deviation for the proposed chloride-bearing materials (top) and the average and standard deviation for the low-albedo (<0.20) southern highlands (bottom). A) TES Single detector albedo values obtained from non-dusty seasons (L_s 180-330) for ten large proposed chloride-bearing materials. B) TES Single detector nighttime bolometer-derived thermal inertia values obtained from non-dusty seasons for the same ten large proposed chloride-bearing sites.

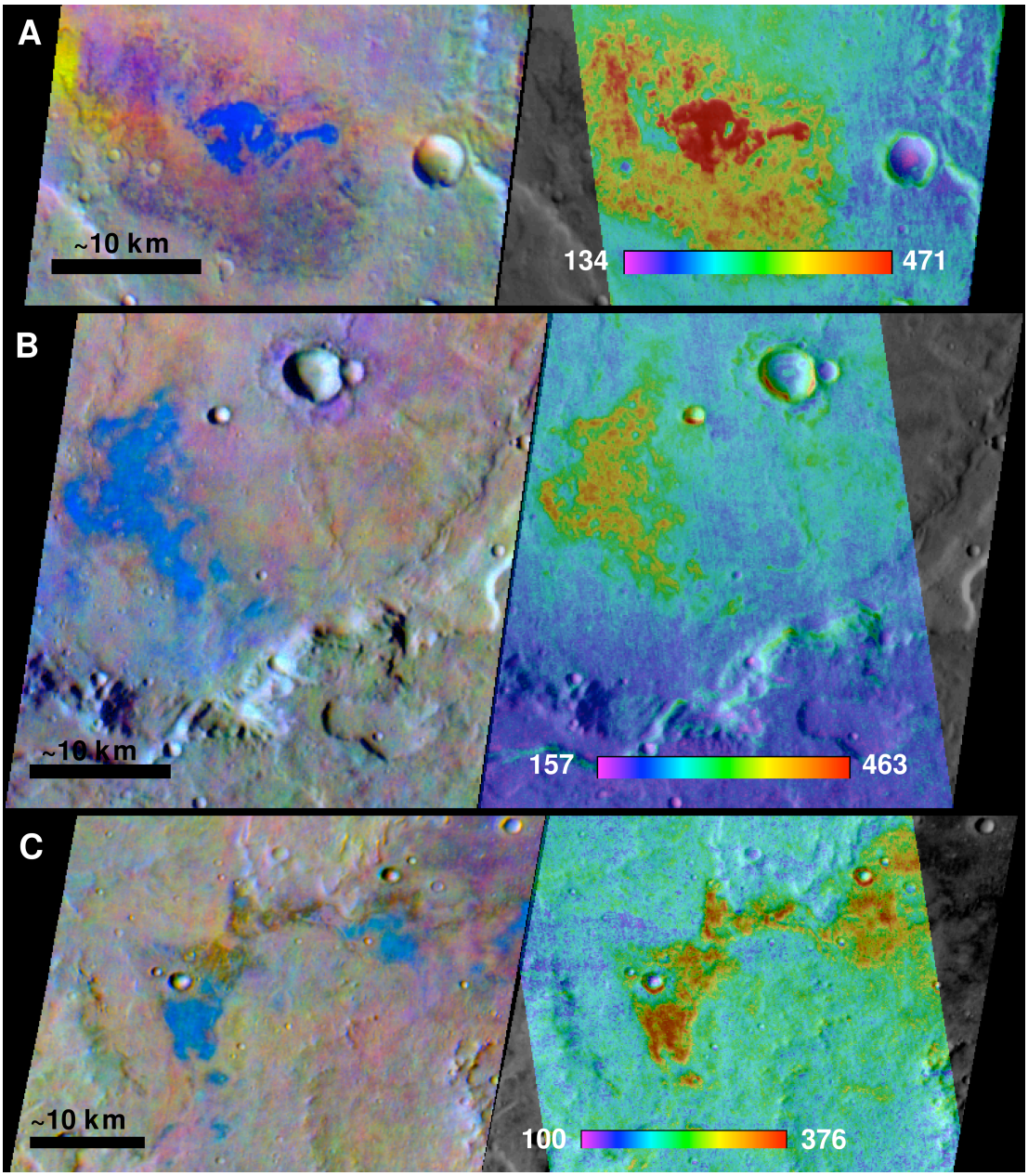

Figure 3.15. THEMIS DCS 8/7/5 radiance images (left) and corresponding THEMIS nighttime apparent thermal inertia images colorized and overlaid on band 9 brightness temperature images (right). The materials appear blue in the 8/7/5 daytime DCS stretch. A) I33185001 and I13687006 (~3.12ºS, ~351.55ºE. B) I16782002 and I106629006 (~27.25ºS, 180.46ºE). C) I33677002 and I11072004 (~32.25ºS, 190.52ºE).

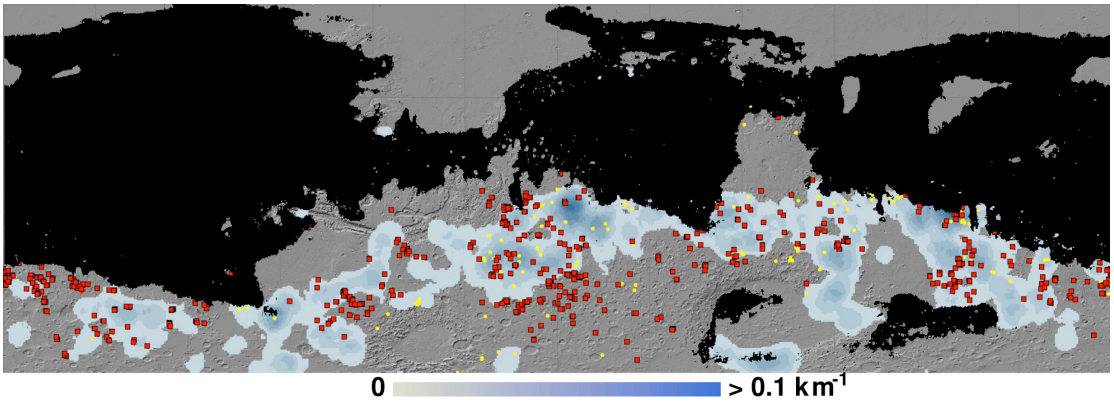

Figure 3.16. Valley network density map from *Hynek et al*. [2010 in press] in blue (dark blue indicates higher drainage density) with locations of valley network feed open basins from *Fassett and Head* [2008a] in yellow. The map is in simple cylindrical projection from 60º S to 60º N latitude and 180º W to 180º E and masked where the DCI index is less than ~0.94. Proposed chloride-bearing materials are shown as red boxes (enlarged for ease of viewing).

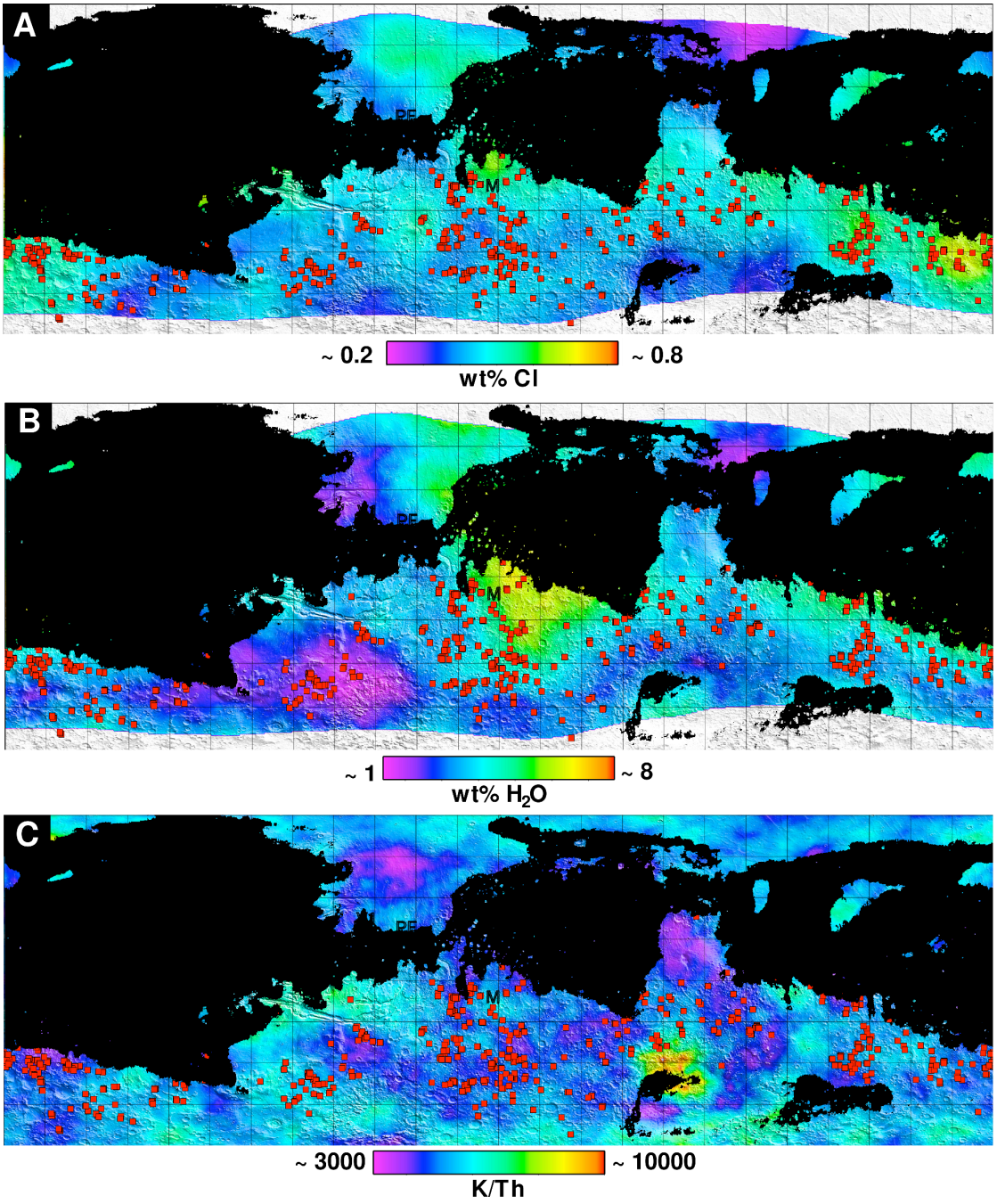

Figure 3.17. Global maps are in simple cylindrical projection from 60º S to 60º N latitude and 180º W to 180º E and maps are masked where the DCI index is less than ~0.94. Locations of proposed chloride-bearing materials are shown as red boxes (boxes are enlarged for ease of viewing). A) GRS Cl wt% [K*eller et al.*, 2006]. B) GRS H_2O wt% [*Boynton et al*., 2007]. C). K/Th map from *Taylor et al.*, [2006].

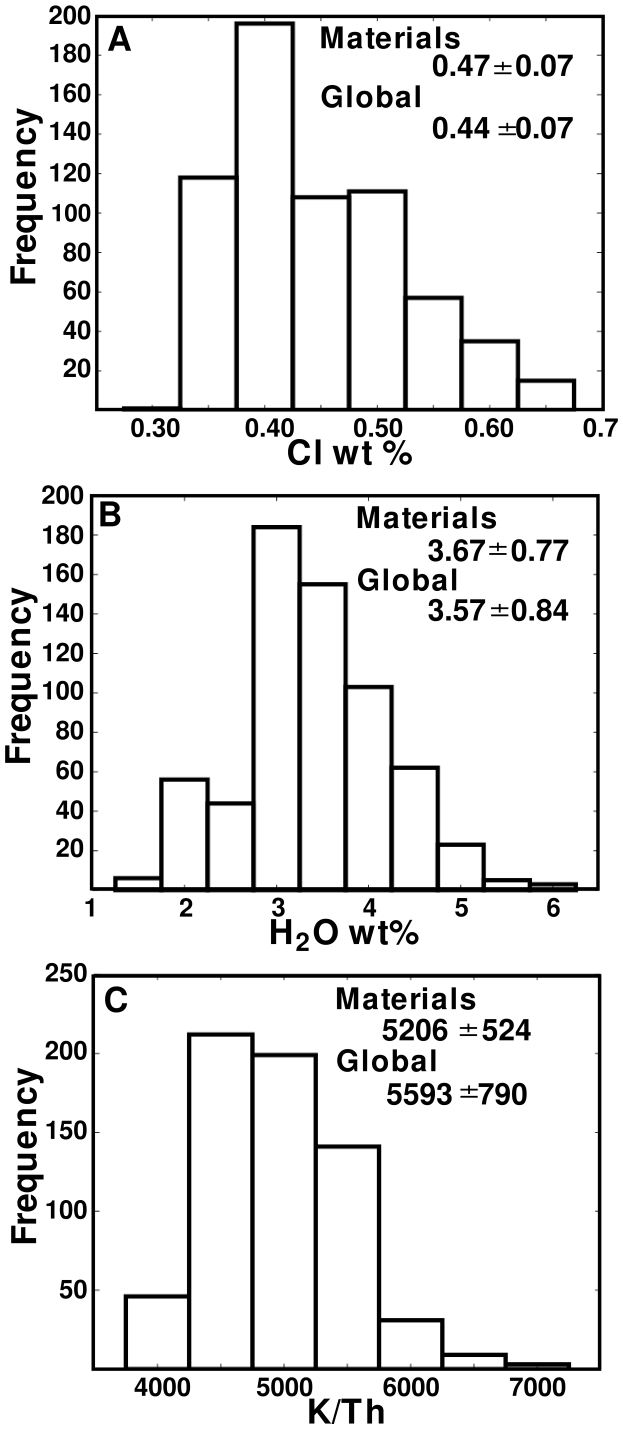

Figure 3.18. The values in each panel are the average and standard deviations for the proposed chloride-bearing materials (top) and the average and standard deviation for the low-albedo (<0.20) southern highlands (bottom) extracted from the gridded smoothed global maps. A) GRS Cl wt% from *Keller et al.*, [2006]. B) GRS H_2O wt% from *Boynton et al.*, [2007]. C) GRS K/Th from *Taylor et al*., [2006].

CHAPTER 4: A LABORATORY STUDY OF THE EFFECTS OF ROUGHNESS ON THE THERMAL INFRARED SPECTRA OF ROCK SURFACES

Abstract:

Previous studies have shown that surface roughness can change the contrast or obscure diagnostic spectral signatures of materials in the thermal infrared wavelength region. These studies attributed reduction in spectral contrast to blackbody cavity effects where multiple reflections reduce the number of photons measured at the sensor, resulting in shallowing of spectral features. However, not all rough surfaces have morphologies that create blackbody cavity effects. Here, we focus on investigating the effects of more geologically common surface roughness on the infrared spectra of a variety of natural rock samples. The surfaces we created can be approximated by half spherical pits that cause a reduction in spectral contrast through limited or low reflection cavities, analogous to surfaces created through aeolian abrasion processes. Our results indicate that: 1) our roughening process is highly repeatable across rock types, 2) rock types vary in the degree that they are susceptible to abrasion, 3) features in emissivity spectra do not change shape or position with increasing surface roughness, 4) reduction of spectral contrast is observed with increasing roughness across all rock groups until a threshold roughness (which varies across rock types) is achieved, whereupon further reductions do not occur or in some cases, spectral contrast begins to increase, 5) spectra from our roughened surfaces are well explained by few surface reflections, 6) we do not see complete obscuration of features in any of our roughened spectra, 7) surfaces created through our roughening process could be considered analogs to materials roughened by aeolian abrasion, a dominant process on the surface of Mars and 8) our study suggests that spectral contrast, strictly speaking, is not dependent upon surface roughness but upon the

morphology of the surface. We found that rough surfaces may display morphologies that are well modeled by low reflection cavities (LRCs), which reduce spectral contrast, but do not obscure spectral features.

1.0 Introduction

A wide range of natural geologic characteristics affect the interpretation of infrared spectra of rocks and minerals, including (but not limited to) major and minor elemental composition, particle size, coatings, and surface roughness. Each of these parameters may affect an infrared spectrum in such a way as to make a particular mineral or rock signature easier or harder to identify or quantify in the spectrum of an unknown material or surface. *Lane and Christensen* [1997] demonstrated that increasing surface roughness on solid carbonate samples reduces their spectral contrast. *Kirkland et al.* [2003] demonstrated that a sample of natural terrestrial calcrete, which is a solid, rocky type of carbonate formed by the interaction of soil and rainwater in an arid environment [*Gardner*, 1972], exhibits a sufficiently rough surface texture that its infrared spectral contrast is reduced relative to a solid crystal of calcite. *Kirkland et al.* [2003] also demonstrated that a sandblasted limestone exhibited a decrease in spectral contrast, which they related to volume scattering produced by the roughened surface. *Kirkland et al.* [2003] concluded that surface roughness effects might make the detection of carbonate in spectral data more difficult than in the case of pure crystalline calcite. Focusing purely on the physics of the observed effect (i.e., not geologic processes), they suggest that this surface character could also affect the spectral contrast (and thus, detectability) of silicate minerals, and that the subject should receive further study.

The objective of this work is to further characterize the effect of surface roughness on thermal infrared spectra of a suite of rock surfaces. Our study is not intended to determine what geologic process is responsible for creating surface

roughness variations; rather, it is intended to evaluate the physical/spectral response of geologic materials having variable surface roughness. By systematically roughening a range of natural geologic materials with different igneous, metamorphic and sedimentary compositions using abrasives of varying particle size we are able to study the effects of surface roughness on their infrared emissivity spectra.

2.0 Background

Thermal infrared emission spectroscopy is fundamentally based on vibrational spectroscopy. Vibrations occur within a crystal lattice and its component molecules at frequencies that are directly related to the crystal structural and elemental composition [e.g., *Wilson et al.,* 1955; *Farmer,* 1974]. When these vibrations cause a change in the charge distribution of a molecule, the result is a periodic change in the dipole moment [*Gaffey et al.,* 1993]. If this occurs, the molecule can interact with the electric component of incident radiation, which results in the absorption of photons [*Gaffey et al.,* 1993]. A molecule vibrating at a given frequency absorbs photons of that same frequency and the majority of molecular vibrations have frequencies in the infrared. Several factors affect the frequency, shape, intensity, and number of internal vibrational modes, including valences of the cations and anions, mass of the atoms, degree of covalency of the bond, bond length, and type (e.g., stretching or bending) and symmetry of the vibration modes [*Gaffey et al.,* 1993]. These variables are determined by the composition, location, and polymerization of the anions and cations within a crystal lattice. Because minerals are defined by their unique compositions and/or structures, virtually every mineral contains a unique set of

spectral features, creating a distinct spectrum in the thermal infrared. An extensive number of studies have used thermal infrared spectra to determine quantitative mineralogy and petrology in many studies [e.g., *Lyon,* 1965; *Vincent and Thompson*, 1972; *Farmer,* 1974; *Salisbury et al.,* 1987, 1991; *Salisbury and Walter*, 1989; *Salisbury*, 1993; *Christensen and Harrison*, 1993; *Feely and Christensen*, 1999; *Christensen et al.,* 2000a; *Hamilton and Christensen*, 2000; *Hamilton et al.*, 2001; *Koeppen and Hamilton*, 2008].

Spectral contrast can be reduced by physical attributes of the materials, such as particle size and porosity. Numerous previous researchers have discussed the complex effects of particle size and porosity on the infrared spectrum of particulate materials [e.g., *Vincent and Hunt*, 1968; *Aronson et al.,* 1969; *Conel* 1969; *Aronson and Emslie,* 1973; *Salisbury and Eastes,* 1985; *Salisbury and Wald,* 1992; *Moersch and Christensen,* 1995; *Mustard and Hays*, 1997]. In brief, *Vincent and Hunt* [1968] first described the two dominant ways light can be scattered by a material: surface and volume scattering. The surface scattering (or specular) component represents the surface-scattered Fresnel radiation, which results in emission minima at the very strong molecular vibration bands [*Hunt and Vincent,* 1968; *Conel*, 1969; *Hunt and Logan*, 1972; *Salisbury et al.,* 1987; *Salisbury and Wald*, 1992]. A strong band minimum in emission (and therefore a strong peak in reflectance from Kirchoff's law, E=1-R [*Nicodemus,* 1965]) is produced by Fresnel reflection from surface scattering because high opacity and strong absorption coefficients within the wavelength band produce a mirror-like characteristic and essentially little incident radiance is transmitted or absorbed and most is reflected [e.g., *Hunt and Vincent*, 1968; *Conel*

1969; *Hunt and Logan*, 1972; *Salisbury et al.,* 1987; *Salisbury and Wald,* 1992]. These emission minima are referred to as 'reststrahlen bands' and emission at these bands is due to 'first surface reflection' or 'surface scattering' because all returned radiation has been reflected from the surface of the material and none has passed through the material [*Gaffey et al*., 1993].

The volume scattering component consists of the radiation that has passed through the volume of grains before being backscattered to the observer, which can result in reflectance troughs (i.e., emission peaks) in areas of the spectrum where the absorption coefficient is low [*Aronson et al.,* 1966; 1967; *Vincent and Hunt*, 1968; *Conel,* 1969; *Hunt and Logan*, 1972; *Salisbury et al*., 1987; *Salisbury and Wald*, 1992). Volume scattering is expressed as troughs in reflectance or peaks in emission because more photons are absorbed in the band centers than in the less absorbing wing regions [*Salisbury et al*., 1992; *Gaffey et al.,* 1993]. The volume scattering process can result in an increase or decrease in spectral contrast of absorption bands as particle size is decreased, depending on the absorption coefficient as well as the relationship between the mean optical path length and the particle size [*Salisbury et al.,* 1992]. Bands decrease in spectral contrast with decreasing particle size when their absorption coefficients are relatively low, but some regions with the right range of absorption coefficients can increase in spectral contrast as particle sizes decreases [*Gaffey et al*., 1993].

Both band shape and strength vary with the relative contribution from surface and volume scattering. Surface scattering dominates the reststrahlen bands in large, optically thick particles or smooth surfaces [*Vincent and Hunt*, 1968]. However, as

particles are reduced in size (or surface asperities are introduced) and they become optically thin, volume scattering has a greater effect [*Aronson et al*., 1966; *Salisbury and Wald,* 1992]. As the contribution from volume scattering increases, the reststrahlen band shape changes, shifts towards higher wavenumber, loses spectral contrast, and finally inverts [*Vincent and Hunt*, 1968; *Salisbury and Wald*, 1992].

Surface roughness can also reduce spectral contrast by multiple reflections that reduce the number of photons measured at the sensor and result in a reduction in spectral contrast. Previous researchers have suggested that all surface roughness is similar to a blackbody cavity effect [*Kirkland et al.,* 2003]. Some physical properties that can cause variations in surface roughness and thereby induce multiple surface reflections include: grain texture, grooves, vesicles, gaps between rocks in a mount, interstices between grains, and pits and cracks in the rocks [*Kirkland et al.,* 2003]. Multiple reflection effects are observed for roughnesses of approximately one-fifth the measured wavelength [*Siegel and Howell*, 1968] to macro-roughnesses of such physical attributes as mounds of boulders [*Kirkland et al.,* 2003].

The increase in effective emissivity (ε_e) with the number of reflections (ξ) from a surface with true emissivity ε is given by:

$$\varepsilon_e = 1 - (1 - \varepsilon)^{(\xi + 1)} \quad (1)$$

[*Kirkland et al.,* 2003 and references therein]. Quantifying the total cavity effect is a complex problem because it is determined by the cavity shape, cavity surface area, entrance aperture area, the material's emissivity, and whether the material reflects in a diffuse or specular manner [*LaRocca*, 1978; *Bedford et al.,* 1985; *Kirkland et al.,* 2003]. However, the trend broadly manifests as an increase in emissivity and a

decrease in spectral contrast within the emissivity minima with increasing number of surface reflections. For example, *Lane and Christensen* [1997] and *Kirkland et al.* [2003] have demonstrated qualitatively the effect of surface roughness (i.e., reduced spectral contrast) on solid, natural carbonate samples, and other studies have observed this effect while determining vesicularity in basaltic rocks [e.g. *Ondrusek et al.,* 1993; *Ramsey and Fink,* 1999; *Carter et al*., 2009]. *Ondrusek et al*. [1993] found that both coarsely vesicular pumice and finely vesicular pumice have shallower spectral features than those observed in obsidian and this reduction in spectral contrast was attributed to an increasing contribution of blackbody energy due to increasing vesicularity. *Ramsey and Fink* [1999] found that the spectral contrast was reduced in a linear manner proportional to the number of interactions due to micron-scale roughness and they used this relationship to define a quantitative estimate of the percentage of surface vesicularity using a linear deconvolution algorithm. Despite these previous efforts, our study is the first to quantify the effects of a controlled range of surface roughness on the spectral contrast of a wide variety of solid samples.

3.0 Methods.

We obtained natural rock tile samples representing a range of igneous, metamorphic and sedimentary compositions (Figure 4.1). The cut or polished surfaces of the tile samples permit us to investigate the effects of surface roughness under controlled conditions with ideal starting surfaces. Our twelve tiles represent different rock compositions, and the specific tiles where chosen based on the relative compositional homogeneity of their visible appearance. Each tile was cut into at least

six separate samples (two groups, marble and basalt, have 10 samples). For this study, we will refer to individual tile pieces as 'samples', and all samples cut from the same rock tile as a 'group'.

We collected initial and roughened thermal infrared emissivity spectra on a ThermoElectron Nexus 470 FTIR interferometer spectrometer [*Hamilton and Lucey*, 2005]. The spectrometer has an internal, uncooled, deuterated tryglycine sulfate (DTGS) detector, which, in conjunction with the cesium iodide (CsI) beam splitter, permits measurements from ~2000 cm^{-1} (2.5 μm) to ~200 cm^{-1} (50 μm). The spectrometer setup is configured for emission measurements following the procedure outlined in Ruff et al. [1997]. A water-cooled environmental chamber controls the sample environment temperature [*Ruff et al.* 1997]. The emission configuration uses a conical blackbody at two temperatures for a calibration target [*Hamilton and Lucey,* 2005]. The spectrometer and sample environment are continuously purged during the measurement with scrubbed air to minimize atmospheric water vapor and CO_2, contributions to the measured spectrum.

A spot size of ~1 cm is used throughout our study, which is consistent with prior laboratory studies and sufficient to incorporate many randomly oriented grains within our samples [e.g., *Hamilton and Christensen*, 2000]. We marked the rock samples and sample stage to facilitate the repeatability of sample orientation and measurement location between initial and roughened measurements. All thermal infrared emissivity spectra are the average of 270 scans at a resolution of 4 cm^{-1} over the range of 2000 to 200 cm^{-1}. Measured radiance spectra were converted to emissivity using the two-temperature method discussed by *Christensen and Harrison* [1993] and *Ruff et al.*

[1997]. We used a spectrum of atmospheric water vapor to subtract out residual spectral features caused by low amounts of relative humidity (<~5 %) in the sample chamber from each measured spectrum [e.g., *Koeppen and Hamilton*, 2008]. We heated samples overnight at 100° C prior to spectral acquisition to provide a sufficient difference in thermal energy between the sample and the spectrometer for satisfactory signal to noise. To collect spectra of our particulate abrasives, we used an IR-black sample cup and settled the particles by gently tapping the cup on the table. The particulates were warmed in place to 80º C and allowed to reach equilibrium prior to sample acquisition.

We produce a wide range of surface roughnesses for a given sample by changing the particle size of the abrasive used in the roughening process, as outlined in the test matrix in Table 4.1. We applied one abrasive particle size to each sample. Because the result of abrading can be to either roughen or polish a surface depending upon the initial condition of the sample surface, we did not seek to pre-calculate desired surface roughnesses for our samples. Instead, our intent was to include conditions that may be unnatural, but would provide constraints on the extremes of the observed trends, and utilize abrasive conditions within a range that might naturally occur on Earth or Mars. We used aluminum oxide (Al_2O_3) (Mohs hardness of 9) and silicon carbide (SiC) (Mohs hardness of 9.5-10) abrasives over a range of available particle sizes (5 - 635 μm). We acquired infrared spectra of abrasive materials for reference and to characterize any potential contamination of the rock samples.

We acquired initial spectral and roughness measurements and designated the samples that would be roughened at each of the abrasive particle sizes (Table 4.1).

We roughened two of the groups, the marbles and basalts, with the full suite of available particle sizes, and we roughened the remainder of the groups with a subset of five abrasives (Table 4.1). We chose to only roughen the remainder of the samples with five abrasive particle sizes because we expected the resultant surface roughness variations to be sufficient for documenting any trends in spectral contrast changes. We kept the first sample in each group unmodified to act as a control sample.

We used a grinding wheel to roughen our samples, which reduced roughness directionality that could have been imposed by hand grinding. To minimize contamination from larger particle sizes within smaller particle size abrasives on the grinding wheel, we progressively roughened the samples from smaller- to larger-sized particulates. We thoroughly cleaned the grinding wheel between each sample to minimize compositional contamination between groups, and we removed the used abrasive and applied fresh abrasive before each successive sample was roughened. We attempted to subject all of our tile samples to the same time and pressure conditions by holding each sample and rotating continuously for ~20 seconds. We washed each sample under tap water and dried them with compressed air before visually inspecting the surface for homogeneity in surface roughness. We placed samples that did not appear homogeneous back on the wheel for another 10-20 seconds and re-inspected them. We used an ultrasonic bath to remove abrasive residue before obtaining emission and surface roughness measurements of the roughened samples.

We acquired high-resolution surface elevation measurements of initial and roughened surfaces using a Hommel-Etamic T500 precision surface roughness

measurement device (profilometer), which is manufactured by the Industrial Metrology Division of Jenoptik Group (http://www.jenoptik.com/EN_Industrielle_Messtechnik_Hommel-Etamic). The profilometer has a horizontal resolution of ~10 nm and can measure single line segments up to 15 mm. For our initial surface characterizations (prior to abrasion), we acquired profiles for three rock samples in each group to record initial conditions of the samples and document how roughnesses varied across samples within the same group (Table 4.1). We obtained two orthogonal linear profiles (at 0º and 90º) and another at 45º for initial and roughened surfaces. The area of the sample measured with the profilometer coincides with the ~1 cm spot size measured by the spectrometer for emission measurements.

There are a number of methods and parameters for characterizing roughness, but commonly the arithmetic average roughness (R_a) or the root mean square, R_q (RMS), are used [*Chauvy et al.,* 1998 and references therein]. However, these parameters do not convey information on the range of length scales over which different topographic features exist [*Chauvy et al*., 1998]. Therefore, we used the method described by *Chauvy et al.,* [1998] to characterize the surface roughness of our initial and abraded samples over a range of length scales. From a given set of measurements a roughness parameter, such as RMS deviation, is calculated for several interval lengths defined along a profile [*Chauvy et al.,* 1998]. The calculated parameter of interest is plotted on a log-log graph as a function of length scale. The method includes the following steps: (1) define an interval of length ε along the x-axis (starting from a small fraction of the entire surface), (2) perform a linear least squares fit on the data within the

interval ε and calculate the roughness, (3) move the interval point by point across the profile length and repeat step (2) for every interval section, (4) calculate the values of the average roughness and standard deviation for the multiple intervals, and (5) repeat steps (2)-(4) for increasing interval length [*Chauvy et al.,* 1998]. The length interval ε starts at the smallest size corresponding to 10 data points and increases logarithmically to the maximum size of the entire length of the profile [*Chauvy et al.,* 1998]. The parameter we used to characterize surface roughness is the RMS deviation, $R_{q\varepsilon}$, averaged over n_ε, the number of intervals of length ε and defined by Eq. (1):

$$R_{qe} = \frac{1}{n_\varepsilon}\sum_{i=1}^{n_\varepsilon}\sqrt{\frac{1}{p\varepsilon}\sum_{j=1}^{p_\varepsilon} z_j^2} \tag{2}$$

In this equation, z_j, is the *j*th height variation from the best fit line within the interval *i*, and p_ε is the number of points in the interval ε [*Chauvy et al.,* 1998].

Where the logarithm of $R_{q\varepsilon}$ varies linearly with logarithm of ε, the surface is described as a fractal or self-affine surface. Because fractals are scale invariant [*Mandelbro*t, 1982], they have been used to avoid the limitations of length scale dependence [*Stemp and Stemp*, 2003]. A self-affine surface is demonstrated by a power law relationship between horizontal length scales and statistical measurements of vertical roughness [*Mandelbrot,* 1982; *Shepard et al.,* 1995]. The slope of the log-log plot gives the Hurst exponent (*H*), which is a value characterizing the scaling properties of the topography over the range of horizontal scales [*Shepard et al*., 1995]. However, not all surfaces show a fractal behavior and specifically, *Chauvy et*

al. [1998] found that some mechanically polished, as well as rough and fine sandblasted titanium surfaces, did not exhibit a constant Hurst exponent.

4.0 Results

4.1 Repeatability and initial spectral characteristics

To investigate the variability in atmospheric conditions and variations inherent in the spectrometer we obtained emission spectra from a fine-grained, homogeneous marble (Mar1) (Figure 4.1, Marble**)** over 18 days. The standard deviation is remarkably low (< ~0.1 %), indicating variations in atmospheric conditions and slight variations in the spectrometer did not greatly affect reproducibility of spectral measurements (Figure 4.2A). In order to gauge the repeatability of our sample staging and the reproducibility of multiple measurements, we chose two additional rock samples that had slightly larger grain sizes and compositional variability, a basalt (Bas1) (Figure 4.1, Basalt) and a granodiorite (Gran1) (Figure 4.1, Granodiorite), and acquired spectra over the course of 8 days (Figure 4.2B and 2C). Over most of the wavenumber range the standard deviations average roughly 0.3%, which compare well to the reproducibility results from the fine-grained Mar1 sample. The standard deviations also compare well to the reproducibility results of *Ruff et al.* [1997]. Deviations in our reproducibility measurements likely occurred due to slight differences in the placement of the samples on the stage from one measurement to the next. Therefore, we used the highest standard deviations in our error analysis for intermediate to coarse-grained samples and the Mar1 standard deviations for the fine-grained samples throughout the remainder of our study.

To assess possible contamination of the roughened spectra from residual abrasive (SiC and Al_2O_3) particles, we measured the thermal infrared emissivity of our abrasive agents. Silicon carbide displays a relatively flat, high emissivity spectrum with the exception of a strong absorption at ~810 cm^{-1} (~12.4 μm) (Figure 4.3A). We collected data on packed Al_2O_3 particulates in an effort to reduce porosity effects due to their very small particle sizes (5 and 12 μm) [*Salisbury and Wald,* 1992]. The Al_2O_3 spectra show a typical roll-off in emissivity towards higher wavenumbers (> ~1070 cm^{-1}) and the observed 'peaks' resemble transparency features consistent with fine-grained particulates [*Vincent and Hunt*, 1968; *Conel*, 1969; *Salisbury and Walter,* 1989) (Figure 4.3B).

We acquired thermal infrared emissivity spectra of the initial surfaces of the samples to determine the spectral/compositional homogeneity of the groups (Figure 4.4). We verified rock composition by comparing our spectra to spectra of known composition and quality from *Feely and Christensen* [1999] and *Clark et al.* [2007]. The average spectrum and standard deviation (offset by 1.1) for each group are shown in Figure 4.4. From these initial measurements, it is apparent that there are slight compositional heterogeneities within the groups. Therefore, we compared only initial and roughened spectra from the same sample (i.e., we did not compare the initial spectrum of Bas1 to the roughened spectrum of Bas2), so that slight variations in composition between samples did not introduce errors into our analysis.

4.2 Surface roughness

We measured the initial surface roughnesses of three samples within each group to investigate the variations between samples within a group (Figure 4.5). Our objectives were to document the initial surface roughness because we anticipated that the abrasion technique could result in polishing instead of roughening some surfaces, resulting in an increased spectral emissivity contrast. As a preliminary estimate of surface roughness, we calculated the average roughness (R_a) (Figure 4.5) and standard deviation from the three separate profiles for each sample. It is apparent that most of the initial surfaces display very similar initial R_a values with respect to each other as well as within their individual groups. The phyllite and phyllite-schist display both higher R_a values as well as greater standard deviations. These R_a values are lower-end estimates for these samples because the initial surfaces displayed sufficiently rough surfaces to cause errors in the profilometer measurements, which is not designed to accommodate large elevation changes.

We show examples of the roughened surface profiles for two groups (Marble and Basalt) in Figure 4.6. The profiles are offset for ease of viewing and their R_a values are listed to the right of the plot. Ra and profiles shown are the average from the three separate profiles on each sample. Sample profiles are plotted in order of the size of abrasive used; the top profile is the control sample and the last sample is the sample abraded with the 635 μm SiC particles. The marble displays greater variation in surface elevation and has higher R_a values than the basalt. In the two profiles from the Marble surfaces created by the 423 and 635 μm abrasives, the topographic variations were large enough to exceed the limits of the profilometer in a few places. This erroneous data was manually removed and replaced with flat lines (Figure 4.6A).

To summarize the results of the roughening process, we calculated the R_a for each rock sample and plotted those values, in addition to the R_a for the initial surfaces, against their abrasive particle size for each group (Figure 4.7). It is apparent that seven of the groups were polished instead of roughened for at least the 5 μm abrasive, but the remainder of the groups appear to become rougher with the 5 μm abrasive and become progressively rougher with increasing abrasive particle sizes. The other trend we observed in this plot is that the groups display a fairly consistent trend of increasing R_a values with decreasing hardness, which is expected because softer rocks are more easily abraded than harder rocks. The phyllite and the phyllite-schist samples all display lower R_a values than their initial surfaces, indicating that all of the abraded surfaces are smoother than the original surfaces. It was evident from visible inspection that entire layers of material were removed from their surfaces, revealing surfaces that appeared visibly different in composition from those of the initial samples. The initial and roughened emissivity data from these samples also displayed evidence of significant compositional variations. Therefore, we removed these samples from the remainder of our study.

Because R_a may not accurately describe the variability in surface roughness over the different length scales of observation (Figure 4.6), we calculated R_{qe} (Equation 2) over lengths scales that varied from 30 to 10,000 μm for our samples (Figure 4.8). Though the absolute R_{qe} values vary between groups, the overall shape of the data compares well between groups, indicating our roughening process was highly repeatable. The surfaces that we created are not fractal over the entire length scale of observation because they do not vary linearly with length scale [*Mandelbrot*, 1982;

Shepard et al., 1995), although many of the initial surfaces are closer to displaying a fractal surface (i.e., a linear trend over at least an order of magnitude [*Stemp and Stemp*, 2003]). The shorter length scales (< ~100 μm) follow a roughly linear trend in the log-log plot, with a steeper slope and transition to a shallower slope at the longer interval lengths (>~100 μm) via a curved "shoulder." The shoulder defines the upper interval length-scale limit of the fractal nature of the sample due to the abrasive and the lower limit of the pre-abraded sample surface. Shoulder "points" are located by linearly fitting the last several data points on either end of the log-log plot and calculating the point on the curve where there is equal variance from both lines. The shoulder value, which we will refer to as R_{qes} for the remainder of our study, differentiates the two regimes of our surfaces. We use this value as an estimate of the surface roughness of the sample for spectral contrast analysis in *Section 4.3*.

4.3 Roughness Effects on TIR spectra of rock surfaces

An example initial surface spectrum and roughened surface (created from the largest particle size abrasive used for each group) spectrum for each group are plotted in Figure 4.9. Each spectrum is labeled with the sample's R_{qe} shoulder value (R_{qes}). For most of the groups there are observable reductions in spectral contrast between the initial and roughened surfaces (Figure 4.9). However, the magnitude of the spectral contrast reduction varies as a function of the group and wavenumber position of the spectral feature within the group. As mentioned previously, some of the softer rocks appear to have been smoothed by the finest abrasives, so a deepening of spectral contrast is expected (e.g., Figure 4.9G). We carefully inspected all of the

initial and roughened spectra for changes in feature shapes, but we did not observe variations that would indicate that surface roughness was affecting the shape of the feature in addition to its spectral contrast. Furthermore, we carefully inspected each set of spectra (e.g., initial and roughened) for evidence of contribution of SiC or Al_2O_3 into the roughened spectra, but we did not find evidence of contamination from the abrasives.

To further investigate the reduction in spectral contrast, we chose four wavenumber positions for each group that corresponds to distinct minimum features. These wavenumber positions are summarized in Table 4.2 for each group and shown as vertical lines in Figure 4.9. At each position we subtracted the emissivity value of the initial spectrum from the emissivity value of the roughened spectrum to calculate the change, or delta (Δ), in emissivity (E). If a reduction or shallowing occurred, the sign is positive and if a deepening of the feature occurred, the sign is negative. These ΔE values for each wavenumber position are plotted against the samples' R_{qes} and standard deviation values in Figure 4.10. The errors for the emissivities are given by the highest standard deviations from the repeatability measurements and are shown as a gray box. If the ΔE values plotted within this range, their change is suspect. Because our groups have different grain sizes, we used standard deviations for each group from the repeatability measurements of a material with similar grain sizes. For example, we applied the Mar1 standard deviations to the Marble, Shale, Limestone1, and Limestone2 samples, the Bas1 standard deviations were applied to the Basalt samples, and the Gran1 standard deviations were applied to the rest of the intermediate to larger grained igneous groups. Using the standard deviations from the

repeatability measurements allows us to gauge whether or not the reduction (or in some cases increase) in spectral contrast is above the error in our method. To discuss the percent shallowing or deepening of spectral contrast at each wavenumber position, we normalized the ΔE to the emissivity of the initial sample and multiplied by 100 (%ΔE). These results are shown in Figure 4.11, and similarly to Figure 4.10, a decrease in spectral contrast is shown by a positive percentage, and an increase in spectral contrast is shown by a negative percentage. We will discuss our results in detail by categorizing the groups into their respective geologic formation types, igneous, metamorphic, and sedimentary, below.

4.3.1 Igneous compositions

The mafic igneous compositions investigated here include a gabbro (Figure 4.9A) and a basalt sample (Figure 4.9B). Both groups display shallowing and most of the reductions are above the standard deviations (Figure 4.10A and 4.10B); however the amount of reduction is greater for the gabbro than the basalt group (Figure 4.11A and 4.11B). The gabbro group indicates a reduction of ~20%, but the overall contrast reduction is less for the basalt (< ~14 %), despite subjecting this group to additional roughening with larger particle size abrasives. Furthermore, we do not observe any linear trends in the ΔE or % ΔE values with respect to their surface roughness for either the gabbro or basalt data. Shallowing is observed, but the amount of shallowing does not increase linearly with increasing R_{qes} values. Instead, the spectral contrast appears to be initially reduced with an increase of R_{qes}, but the amount of contrast reduction stays approximately the same with increasing R_{qes} values. The basalt data,

which includes samples roughened with larger particle size abrasives, shows that the degree of shallowing increases until an R_{qes} value between 1 and 2 μm, whereupon the amount of shallowing remains approximately the same, or may even slightly increase in spectral contrast again with additional surface roughness.

Although the data of the felsic igneous groups (Figure 4.10C-4.10F) display some scatter, we observe broadly similar trends to those observed in the mafic igneous compositions. Specifically, there appears to be an immediate decrease in spectral contrast, which attains a maximum reduction at a certain value usually in the 1 to 2 μm range, and then either remains flat, indicating no additional reduction in spectral contrast, or becomes reduced, which suggests that increasing surface roughness has less of an effect on the spectral contrast at or above a certain roughness. The majority of ΔE values plot well outside the standard deviations (Figure 4.10C, 4.10E, 4.10F), which indicates real changes in spectral contrast. The felsics, with the exception of the granodiorite, show similar reductions in spectral contrast at similar wavenumber positions (Figures 4.11C, 4.11E, and 4.11F), with a maximum between ~15 to 24% reduction in spectral contrast. The reductions in spectral contrast for the granodiorite (Figure 4.11D) are not as great as those observed in the rest of the felsic groups. Additionally, many of the changes show a decrease in emissivity and/or increase in spectral contrast, or plot within the uncertainty (Figure 4.10D). Therefore, we are left with very little evidence for shallowing or deepening within this group. We will discuss possible causes for the lack of observed trends in the *Section 5.3*.

4.3.2 Sedimentary and metamorphic compositions

Because we removed the phyllite and phyllitic-schist (described in *Section 4.2*), we only were able to incorporate one metamorphic rock type, the marble (Figure 4.1). However, because of its compositional similarity to the two limestone samples, we discuss them together below. First, the initial and roughened spectra of the shale (Figure 4.9G) show that spectral contrast reduction as well as deepening occurred. The ΔE values of the fine grained and visibly, as well as spectrally, homogeneous shale also show a complex trend of scattered data (Figure 4.10G and Figure 4.11G). Additionally, many of the ΔE values plot within the range of uncertainty (Figure 4.10G). Investigating the R_{qe} vs. length scale plot of the shale data in Figure 4.8G partially explains the complex nature of the scattered data. From Figure 4.8G it is apparent that the initial surface of the shale was rougher than the surfaces produced by the 5-, 12-, and 51-μm abrasives, explaining why some of the dominant features display shallowing, with lower R_{qes} values.

The marble used in our study is one of our best samples for assessing the effects of surface roughness on spectral contrast due to its fine-grained and compositionally homogeneous nature (Figure **4.**9H). Most ΔE values for the marble, limestone1, and limestone2 samples indicate that the features shallow with increasing R_{qes} values (Figure 4.10H, 4.10I, and 4.10J) and most reductions are above the uncertainty. In general the ΔE and %ΔE values (Figure 4.11H, 4.11I, and 4.11J) for all of the wavenumber positions compare well between the limestone1 and limestone2 groups, which is expected because the initial spectra compare well between groups (Figure 4.4). It is apparent that most of the features across the wavenumber positions decrease in spectral contrast until an R_{qes} value between 3 and 4 μm, and do not shallow further

with rougher surfaces (Figure 4.10H, 4.10I, 4.10J and Figure 4.11H, 4.11I, and 4.11J). In fact, above R_{qes} values of ~5μm for the marble and ~2.5 μm for the limestone1 sample, the reductions in spectral contrast are not as great or spectral contrast is increased (Figure 4.11H and 4.11I). The groups show the greatest reduction in spectral contrast at the lower wavenumbers (maximum of ~30%) at R_{qes} values that vary between groups (~3-4μm for the marble and limestone2, and ~2.5 μm for the limestone1), and higher wavenumber features show less spectral contrast reduction than the lower wavenumber features (~10-15%) at lower R_{qes} values (~2-3 μm for the marble and limestone1). Thus, similar to the igneous compositions, these trends seem to imply that over the range and morphologies of roughnesses we studied, rougher surfaces may not continue to affect spectral contrast after a certain roughness is induced and this roughness may be partially controlled by the wavenumber position of the feature.

4.3.3 Grain size

Because our groups display a wide range of grain sizes we investigated the role of grain size in producing variable surface roughnesses as well as in reduction (or enhancement) of spectral contrast. We placed our groups into two categories based on their visible appearance, fine-grained (basalt, marble, shale, and limestones) and intermediate to coarse-grained (granodiorite, alkalic granite, aplite, monzonite, and gabbro). The range of qualitative trends we observed in the R_{qes} vs. ΔE plots vary, but can be placed into one of five categories:

1) "Scattered," indicating the data did not display any relationships,

2) “Constant,” indicating that reduction or increase in spectral contrast was constant across all R_{qes} values,

3) “Increase,” indicating that the reduction or increase in spectral contrast became greater with increasing R_{qes} values,

4) “Increase/Constant,” indicating that the data showed a maximum reduction in spectral contrast at some R_{qes} value and then did not display further reduction with increasing R_{qes} values, and

5) “Increase/Decrease,” indicating that the data showed a maximum reduction in spectral contrast at some R_{qes} value and then decreased in magnitude with increasing Rqes values.

We investigated these qualitative trends, wavenumber position of peak, the region that shows the dominant absorptions in the initial emissivity data, the ~R_{qes} value of the peak reduction, maximum percent shallowing, enhancement in contrast (i.e., deepening), the initial surface roughness (lower, mid-range, or higher than roughened surfaces), and wavenumber region most affected (i.e., higher, lower, intermediate).

Most of the fine-grained materials showed a peak/decrease or peak/consistent trend in their reduction of spectral contrast with increasing R_{qes} values (Table 4.3). Although the peak in spectral contrast reduction appears to occur at different wavenumber positions throughout the fine-grained materials and at least three correspond to the largest spectral features observed in the initial emissivity data. It appears that the calcite dominated limestones and marble have a peak in spectral contrast reduction (~30%) at R_{qes} values between ~2.3 and 4 μm, and the basalt

displays a peak reduction (~14%) at ~2μm. The shale data is difficult to interpret due to its scatter and higher initial surface roughness. The marble and limestone1 also show a deepening of spectral features at higher wavenumber positions at the roughest surfaces (highest attained R_{qes} values) (Figure 4.11H and 4.11I), although because the values are near the range of uncertainty (Figure 4.10H and 4.10I), it is not clear if this is a real trend.

Similar to the fine-grained samples, most intermediate- to coarse-grained materials display a peak/decrease or peak/consistent trend (Table 4.4). Most of the materials show a maximum decrease in spectral contrast at lower R_{qes} values than do the finer grained materials (between 0.5 -1.5 μm compared to ~2.3 - 4 μm respectively). None of the intermediate grained rocks display a deepening of spectral features at the highest R_{qes} values, as displayed in some of the data from the fine-grained samples. As with the fine-grained samples, the features most affected by roughness appear to also be the largest absorption features in the initial emissivity data. The exception to the observed trend is the granodiorite. The data appear scattered, but there may be a trend of continued reduction of spectral contrast with increasing surface roughness. It does not display R_{qes} values that would indicate it had a rougher initial surface, similar to the shale. Therefore it is possible that our chosen wavenumber positions do not accurately describe the changes in the spectral features or that compositional heterogeneity and slight offsets in sample placement on the stage have significantly altered the roughened spectra.

5.0 Discussion

5.1 Causes of spectral contrast changes

As described in *Section 2.0,* spectral contrast can be affected by two dominant processes; (1) surface properties that cause multiple surface reflections or photon absorption in opaque materials [e.g., *Kirkland et al.,* 2002, 2003; *Ondrusek et al.,* 2003; *Ramsey and Fink*, 1999; *Carter et al.,* 2009], and (2) particle size and texture on a scale that causes volume absorption and surface scattering [e.g., *Williams*, 1961; *Lyon*, 1964; *Aronson et al.,* 1969; *Hunt and Vincent*, 1968; *Vincent and Hunt,* 1968; *Conel*, 1969; *Hunt and Logan,* 1972; *Aronson and Emslie,* 1973; *Hunt,* 1976; *Salisbury and Eastes,* 1985; *Salisbury et al.,* 1987; *Salisbury and Wald,* 1992; *Hapke,* 1993b; *Moersch and Christensen*, 1995; *Mustard and Hays*, 1997]. We will discuss these processes and how they may explain the trends we observe in our data in the following sections.

5.1.1 Reflections

The first process, multiple surface reflections, has previously been described as the result of surface roughness [e.g., *Kirkland et al.,* 2003]. However, there is a critical difference between surface roughnesses that result in many reflections, and possibly trapping photons, versus rough surfaces that result in only a few reflections. Surfaces that contain asperities that simulate blackbody qualities (i.e., blackbody cavities), such as vesicles in pumice and lava flows or dissolution voids in carbonates, can be described by geometric shapes that consist of a void (spherical or not) with an entrance (aperture) that may be much smaller than the diameter of the cavity. The effect of a blackbody cavity increases as the ratio of the cavity depth to entrance

width increases. Within this type of cavity, which we will call a high reflection cavity or HRC, photons undergo multiple reflections and may become trapped (i.e., absorbed). As the photon path becomes increasingly convoluted and there are numerous reflections (as demonstrated for pumice [e.g., *Ramsey and Fink,* 1999; *Carter et al*., 2009]), the resultant emitted energy will contain very shallow absorption bands that are well approximated by the linear addition of the non-vesicular material and a blackbody. For these reasons, HRCs, such as those described above, are commonly used as close experimental approximations to theoretical blackbodies [e.g., *Bedford et al.,* 1985; *Ruff et al.,* 1997; *Christensen et al.,* 2001a].

However, natural surfaces display a wide variety of roughnesses and morphologies, which are not all well described as HRCs. These morphologies, which we will call low reflection cavities or LRCs, could be described as a geometric shape that displays an aperture that is greater than or approximately equal to the depth of the cavity. In these surface types, one to a few reflections may occur, but the photons do not have the possibility of becoming photometrically trapped (i.e., absorbed). Additionally, it is probable that for LRCs, increasing surface roughness will not result in additional reflections and further reductions in spectral contrast (unless the ratio of the depth to the aperture also increases).

There are a couple factors that need to be considered when investigating the problem of the interaction of light with a surface. The first is the wavelength of light that interacts with the surface. The Rayleigh criterion states that a surface is optically smooth if the following equation is met:

$$H \leq \frac{\lambda}{8\cos\theta_{inc}} \quad (3)$$

Where H is the height of the topographic feature, θ_{inc} is the angle of incidence, and λ is the wavelength of light [*Hapke*, 1993a]. Therefore, surface asperities and irregularities that are smaller than the wavelength will not affect the photon and the surface will appear to be smooth. We calculate the necessary height of the topographic feature required to interact with the wavelength (plotted as wavenumber) in Figure 4.12. The roughnesses below the curve would appear as optically smooth. Because $H \approx 2\ R_a$, most of our roughened surfaces plot above the curve (shown as grey area in Figure 4.12) and therefore would not appear optically smooth in the thermal infrared. The second limit deals with the areas that are being illuminated. Essentially, the asperities or features that are larger than the spot of illumination do not affect the interaction of the light with the surface [*Harloff and Arnold,* 2001]. None of our surface roughnesses are larger than our spot size (~1 cm); therefore this limit does not apply to our study.

Our observations generally show that samples display reduced spectral contrast with increasing roughness until a certain R_{qes} value. Once this surface roughness is attained, spectral contrast is not further reduced or the emissivities begin to progressively decrease and less of a reduction is observed. Using our roughened and initial spectra, we can model the number of reflections that occur on the roughened surface, if we assume that the initial spectrum is the true emissivity. Equation (1) defined in *Section 2.0,* describes the reduction in spectral contrast with multiple reflections. We can solve for ξ by rearranging the terms below:

$$\xi = \frac{\log(1-\varepsilon_r)}{\log(1-\varepsilon_i)} - 1 \quad (4)$$

If the abrasion process is producing LRCs it is possible that the number of reflections will no longer increase despite additional increases in surface roughness. We show the results of our calculations in Figure 4.13. We plot the average percent of reflections against the R_{qes} values for each group. If a sample displays a 20% average reflection, it indicates that if 100 photons interact with the surface, ~20 of those photons will undergo one reflection. For the groups that had rougher initial surfaces (e.g., the shale, Figure 4.13B), or those that had higher spectral variability between initial and roughened measurements (e.g., the granodiorite in Figure 4.13A) this equation breaks down because the initial emissivity is not the true emissivity and negative reflections are calculated. The groups show that the percentage of reflections increase as the R_{qes} values increase, but the majority of the groups show that the percentage of reflections attain a maximum upon which no further increase in reflections occur despite increasing surface roughness. For the samples that do not appear to attain this maximum (e.g., gabbro and aplite Figure 4.12A), it is likely further roughening of the samples would show this effect. The two best examples of this effect are the basalt (Figure 4.12A) and marble samples (Figure 4.12B), which were roughened with the entire suite of abrasives, enabling us to consider a larger range of roughnesses.

Increasing the abundance of HRCs within a sample or observation footprint should cause the emissivity to shallow as the proportion of HRCs to sample increases. With enough HRCs, it is possible that spectral features could be completely obscured

and they would appear as a blackbody spectrum. However, HRCs such as vesicles in lava flows or dissolution voids in carbonates may be less common geologically (discussed in Section 5.2). It is evident from our data that despite increasing surface roughness (over the surface roughness and morphologies created through out abrasion process), the reduction in spectral contrast is not increasing.

5.1.2 Volume and surface scattering

Reductions in spectral contrast can also occur by surface scattering and volume scattering. Most of the investigations of these two effects have concentrated on particulate samples [e.g., *Williams*, 1961; *Lyon*, 1964; *Aronson et al.,* 1969; *Hunt and Vincent,* 1968; *Vincent and Hunt,* 1968; *Conel,* 1969; *Hunt and Logan*, 1972; *Hapke*, 1993b; *Aronson and Emslie*, 1973; *Hunt*, 1976; *Salisbury and Eastes*, 1985; *Salisbury et al.,* 1987; *Salisbury and Wald,* 1992; *Moersch and Christensen*, 1995; *Mustard and Hays,* 1997]. Thermal infrared spectral features measured by reflection or emission spectroscopy are the result of both the absorption coefficient and the refractive index. Whether the measured radiance is dominated by surface or volume scattering ultimately depends on the complex index of refraction, defined by the optical constants n and k [e.g., *Vincent and Hunt*, 1968; *Hunt and Vincent*, 1968; *Conel*, 1969; *Salisbury and Wald,* 1992; *Moersch and Christensen*, 1995; *Mustard and Hays*, 1997]. Volume scattering refers to the optical process that occurs when k is small ($<<$ 1.0) and n is greater than 1 [*Mustard and Hays*, 1997]. Volume scattering becomes prominent as the dominant particle size approaches the wavelength of observation (generally less than ~65μm in the thermal infrared). These constraints are met in fine

particulates when light is refracted into particle interiors and is then scattered or refracted back out. Spectra that are dominated by volume scattering are generally reduced in spectral contrast in the reststrahlen bands and display an increase in spectral contrast in the transparency regions (interband regions) where the absorption coefficient is very low, the refractive index is moderate, and photons interact with a large number of interfaces and cannot easily escape [*Gaffey et al.,* 1993]. Additionally, surfaces that are dominated by volume scattering also typically display changes in the overall shape of the spectral feature and the maximum is shifted to slightly higher wavenumbers [*Salisbury and Wald,* 1992].

Kirkland et al. [2003] attributed changes between the spectra of a fresh limestone hand sample and a surface that was cut with a saw, ground with a grinding wheel, and then grit-blasted with a coarse Al_2O_3 abrasive to volume scattering. Specifically, the grit-blasted surface spectrum shows slightly lower continuum emissivity, reduced spectral contrast, and an altered spectral shape in the 6.5 and 11.2 μm band shapes [*Kirkland et al*., 2003]. The altered band shape consists of a better developed shoulder displaying a relatively small 'wing' or doublet, within the dominant absorption features. The sample was cleaned in an ultrasonic cleaner and XRD measurements indicated that the grit-blasting did not cause any alteration to the aragonite [*Kirkland et al.,* 2003], thus compositional variability as the reason for the spectral differences was not a possibility. *Kirkland et al.* [2003] interpreted the presence of this feature shape change (as well as overall reduction in spectral contrast and higher emissivity continuum) to volume scattering and concluded that grit-blasting caused micro-fracturing of the surface.

It is difficult to directly compare our results to the results of *Kirkland et al.* [2003] because they did not indicate the size of the abrasives used, which could have yielded information on the approximate R_a or R_{qes} values attained for a limestone sample by comparison to our own, nor did they investigate quantitatively the morphologies and roughnesses produced by their abrasion process. We have thoroughly and carefully inspected our roughened spectra for variations, such as spectral shape change, shifts in absorption feature positions, or increase in transparency features in interband regions that would indicate that our spectra are dominated by volume scattering. We have found no evidence of volume scattering in our study, however our results do not preclude that the grit-blasted surface spectrum from *Kirkland et al.* [2003] was the result of volume scattering. It is possible that this difference reflects the variations in the roughening processes used in the two studies. The exact method of grit-blasting was not discussed by *Kirkland et al.* [2003], but typical procedures for grit-blasting, or sand-blasting, involve accelerating an abrasive media through a blasting nozzle by means of compressed air. Therefore, grit-blasting is commonly accomplished under a significantly higher applied force than hand/wheel grinding. It is possible that the presumably soft aragonite- limestone used by *Kirkland et al.* [2003] was micro-fractured through the grit-blasting procedure, but our samples, which were roughened under significantly lower applied forces, did not result in micro-fracturing of the surface. It is possible that micro-fracturing causes volume scattering, but because our roughening process did not micro-fracture the surface, there is no evidence to conclude our roughened spectra are altered due to volume scattering.

As discussed in *Section 2.0*, surface scattering, or 'specular scattering' [*Vincent and Hunt*, 1968], represents the surface scattered Fresnel radiation that results in emission minima (or reflectance peaks) at very strong molecular vibration bands. Reststrahlen bands occur when k is large (> 1.0) such that very little light passes through grain boundaries. Thus, scattering and absorption are dominated by first surface reflection and multiple scattering. For surfaces of coarse particulates and solids, light is reflected without penetration into the substrate and therefore they exhibit strong reststrahlen bands. As particle size decreases such that the size is less than the wavelength of light, the particle as a whole interacts with the wavelength of light [*Mustard and Hays*, 1997].

Observations indicate that decreasing the mean particle size of a sample (> ~65 μm), results in a generally/approximately uniform decrease in spectral contrast, with no change in the positions of the primary absorptions [e.g., *Lyon,* 1965; *Hunt and Vincent*, 1968; *Salisbury and Wald,* 1992; *Moersch and Christensen*, 1995]. The reductions in spectral contrast appear to vary somewhat with rock type. For example, *Hamilton* [1999] demonstrated that the reduction in spectral contrast between the spectrum of a basaltic rock and the spectrum of the same rock crushed to particulate sizes of 710-1000 μm was ~67%, and granitic rock exhibited a decrease of ~40% in the particulate sample [*Ruff,* 1998]. For comparison, the reductions in spectral contrast in our study range from ~14 % for a basalt, to between 15-20% for felsic igneous materials, and ~25-30% for limestones. The reductions in spectral contrast observed between particulates and solid samples have been attributed to pore spaces between grains acting as blackbody cavities (HRCs), which as described above, result

in multiple reflections that manifest as a reduction of spectral contrast by adding a fixed amount of unit emissivity (e.g., a blackbody) to the spectrum [*Salisbury and Eastes,* 1985]. However, other studies have found that the reduction in spectral contrast is due directly to particle size and indirectly (although critically) to porosity [*Salisbury and Wald*, 1992].

Our samples are flat slabs of rock and not particulates, thus it is difficult to draw direct comparisons to previous work. However, our samples show a wide range of grain sizes and textures, which could influence how a resultant surface roughness may affect the spectral contrast. However, we investigated the spectral contrast effects as a function of general grain size (i.e., fine and intermediate to coarse) and found no obvious trends. Therefore, over the range of morphologies and roughnesses produced by our abrasion processes, a reduction in the efficiency of surface scattering may be influencing the reduction in spectral contrast at rougher surfaces, but we find no evidence that suggests volume scattering has played a role in reducing the spectral contrast of our samples.

5.2 Applicability to natural surface roughnesses

The roughening process we utilized produced similar R_{qe} vs. epsilon profiles for all the groups, indicating that the method was highly repeatable and produced similar surfaces for all rock types, although absolute elevations varied between groups (Figure 4.8). The profiles in Figure 4.8 display a curved shape, where R_{qe} values increase with increasing observation length scales. However, at longer observation length scale values, and the particular length scale varies between groups, the profiles

appear to remain fairly consistent and do not increase with increasing observation length scale. The profile shapes compare well to the fine and coarse particle sandblasted titanium surfaces of *Chauvy et al.,* [1998]. These profile shapes are expected for polished and flat surfaces that undergo an abrasion process. As a polished surface is subjected to abrasion by fine particles the calculated R_{qe} will vary the most at the small length scales and remain relatively unchanging at length scales much greater than the surface pits caused by abrasion. This causes a regime change in the R_{qe} vs. length scale slope from very strong dependence on length scale (steep slope) to a weaker dependence on length scale (shallower slope) via a "shoulder region," where the transition or shoulder between the regimes is diagnostic of the abrasive size applied to the surface. The surface of sample measured at length scales larger than ~ abrasive size, remain dominated by original topography of samples, which is flat at long length scales of observation.

Many natural surfaces (e.g., lava flows, weathered surfaces) are fractal in nature [*Mandelbrot*, 1982; *Shepard et al*., 1995; *Morris et al.,* 2008]. For a surface to be considered fractal, the data on a log-log plot must be linear over a measurement of length scale of at least an order of magnitude [*Stemp and Stemp,* 2003]. At smaller length scales of observation our surfaces are fractal in nature and dominated by abrasive sizes applied, but at longer length-scales of observation the surfaces are also fractal but primarily reflect the properties of the macroscopic flat, initial polished sample.

Surface roughness is important for a wide range of geological studies. For example, surface roughness characterization of fractured materials [e.g., *Brown and*

Shultz, 1985; *Schmittbuhl et al.,* 1993; *Bouchard and Bouchard,* 1994; *Dagier et al.,* 1996; *Amitrano and Schmittbuhl,* 2002] is important because the mechanical and hydraulic behaviors of discontinuities in rocks, such as joints and faults, depends strongly on the topography of the contacting surfaces and the degree of correlations between them [*Brown and Shultz*, 1985]. Another area of research where the surface roughness plays an important role is in weathering and water-mineral reaction rates [e.g., *Anbeek,* 1992; *Hodson*, 1999; *Brantely and Mellott*, 2000; *White and Brantely,* 2003]. Surface roughness increases the available surface area for chemical reactions and increasing the surface area increases the rates of dissolution [*Anbeek,* 1992; *White and Brantely*, 2003]. However because most previous studies used a variety of different roughness parameters, direct comparison to our study is difficult.

One process that our roughening method may mimic is that of rock alteration through aeolian abrasion. Aeolian abrasion has played a substantial role in shaping the surface of Mars and given the in situ documentation of dust storms, dust devils, and the movement of sand across the surface, continues to do so at present [e.g., *Greeley et al.,* 2002, 2005, 2006a, 2006b; *Fenton et al.,* 2007; *Sullivan et al*., 2008). On a regional scale, the ability of wind to move sand-sized particles on Mars is documented by the occurrence of abundant dunes, sand-sheets, and yardangs [*Greeley et al.,* 1992; *Malin and Edgett,* 2000]. Additionally, eroded rocks showing evidence of ventifacts have been observed at all the Martian landing sites [e.g., *Bridges et al.,* 1999; *Sullivan et al.,* 2005, 2008; *Greeley et al*., 2008]. Ventifacts are rocks that have undergone erosion for long periods of time (decades or more on Earth), by windblown sediments and typically display distinctive morphologies, such as facets,

grooves, elongated pits, and flutes [*Bridges et al.,* 2004]. The sizes of particles able to be transported by wind on Earth and Mars include materials that move by creep (>2000 μm), sand sized particles moved by saltation (~60 to 2000 μm), and dust sized particles moved by suspension (< 60 μm) [*Greeley and Iverson,* 1985; *Greeley et al.,* 2000, 2002]. Our abrasives range from ~5 to 623 μm making them representative of the sizes of dust and sand- blown particles on Mars. The abrasives we used here are harder (~9 -10 on Mohs scale) and different in composition than the particles on Mars, however the roughening process utilized here, as well as sandblasting, may nonetheless create similar surfaces. We conclude that our R_{qe} values, which are appropriate up to the shoulder points, describe what could be expected under relatively short duration times of natural rock surface abrasion by aeolian processes.

5.3 Suggestions for additional work and improved studies

There are a number of additional tasks that would augment our work and aid in future investigations. These are detailed below.

By increasing the size range of abrasives used we may be able to confirm that the reduction in spectral contrast does in fact remain consistent or decreases with increasing surface roughness for the surface morphologies created through our abrasion process. Currently, this trend is suggested for many of the samples, but additional data would strengthen our conclusion. For our study, this task could be accomplished by roughening the remainder of samples with the 317, 423, and 635 μm SiC abrasives, which were only used on the basalt and marble samples. Furthermore, it also may be helpful to use an abrasive with a different composition, or employ the

use of grit-blasting with sand particles to better compare our results to those of *Kirkland et al.* [2003], as well as create surface morphologies that may vary from those created here.

Furthermore, using a single sample within each group for repeated abrasion and spectral analysis could reduce the complicating factors of compositional variability between samples within a group. By comparing only the spectra of initial to roughened surfaces of the same sample, this effect was limited, but by choosing an average wavenumber position where the samples displayed spectral variability (i.e., slight shifts in position), we may have slightly reduced the magnitude of the spectral reduction (e.g., our granodiorite data).

In order to fully characterize the surfaces created through any grinding process, it would be beneficial to have a high resolution, 3-D map of the surface. Investigating the geometries of the voids, pits, grooves, and other surface morphologies are important for understanding how the different surfaces may be interacting with and reflecting photons. Such a map could be similar to the scanning electron microscope (SEM) sterology used by *Carter et al.* [2009] to study surface roughness and vesicularity effects on infrared emission spectra, where a pair of SEM images was acquired at a separation angle and a digital elevation model was generated. Alternatively, there are other nondestructive methods such as optical profilometers that may be more useful to our study because they do not require applying an electrically conductive coating (as scanning electron microscopy requires) to the sample for analysis (which could complicate the investigation if a sample were to be repeatedly roughened and re-analyzed).

6.0 Conclusions

Geologic processes produce a wide range of textures and surfaces. The surfaces produced by our roughening process may be analogous to surfaces eroded by aeolian abrasion. However, many geologic surfaces are products of numerous formation and alteration processes and it is therefore likely that they are made up of a variety of textures, morphologies and roughness that vary depending on the scale of observation. Spectra from such complex surfaces may be well described by LRCs, similar to those produced here, in combination with HRCs. However, it is also possible that some surfaces could be described by moderately reflecting surfaces that are between the two end member cases. Our study is an initial investigation into the effects of surface roughness, but additional detailed studies utilizing a range of abrasive sizes, techniques, and minerals and materials will significantly aid in the unraveling the complex interactions between surface composition, surface roughness, and emissivity spectra. Our initial detailed laboratory study of the effects of surface roughness on the thermal infrared spectra of a range of rock surfaces has shown the following over the range of roughnesses and morphologies created from our abrasion process:

1) Our roughening process resulted in highly repeatable surfaces between all rock classes, although absolute R_{qe} values varied due to the hardness of the materials. This is consistent with the fact that different lithologies vary in the degree to which they are susceptible to abrasion.

2) Our roughened rock samples are fractal in nature in two regimes. At small length scales (< ~100 μm) of observation, the surfaces reflect the abrasives used and at longer length scales (> ~100 μm) of observations the surfaces reflect the characteristics of the smooth, polished original surfaces.

3) Features in roughened spectra do not change shape or position with increasing surface roughness.

4) Features shallow with increasing roughness across all rock groups until a certain roughness is achieved. After that roughness is attained, further reductions do not occur, or in some cases, spectral contrast begins to increase.

5) Spectra from our roughened surfaces are explained by low surface reflections, which we characterize as low reflection cavities (LRCs).

6) We do not see complete obscuration of features in any of our roughened spectra.

7) The surfaces created through our roughening process could be considered analogs to materials roughened by aeolian abrasion, a dominant process on the surface of Mars.

8) Our study suggests that spectral contrast, strictly speaking, is not dependent upon surface roughness but upon the morphology of the surface. We found that rough surfaces may display morphologies that are well modeled by low reflection cavities (LRCs), as investigated here, which would reduce spectral contrast, but not obscure spectral features.

Acknowledgments:

We would like to thank Dr. Christopher Dreyer at the Colorado School of Mines for allowing us to use the Hommel precision measurement instrument in his laboratory. John Skok graciously allowed us to prepare and roughened our samples in his Sample Prep Room at the Colorado School of Mines and provided essential assistance and knowledge in helping us develop our roughening process. We thank Tony Jeffreys for cutting our ~30 initial natural rock tile samples into our small ~2x2" squares. Keith Nowicki and Meryl McDowell provided helpful reviews on our initial manuscript.

TABLES

Table 4.1. Rock samples

µm	Gab	Ba	Alk	Gr	Mon	Apl	Sha	Mar	Lim	Lim	Sch	Phy
0	X	X	X	X	X	X	X	X	X	X	X	X
5	X	X	X	X	X	X	X	X	X	X	X	X
12	X	X	X	X	X	X	X	X	X	X	X	X
51	X	X	X	X	X	X	X	X	X	X	X	X
79		X						X				
115	X	X	X	X	X	X	X	X	X	X	X	X
212	X	X	X	X	X	X	X	X	X	X	X	X
317	X	X	X	X	X	X	X	X	X	X	X	X
423		X						X				
635		X						X				

Table 4.2. Wavenumber positions

Label	**1**	**2**	**3**	**4**
Gab	1038	644	594	119
Bas	1101	1004	541	376
Alk	1080	781	479	376
Gran	1159	800	643	539
Apl	1159	780	595	376
Monz	1085	763	600	375
Sha	1532	1097	474	311
Mar	1548	898	372	311
Lim1	1528	1411	880	316
Lim2	1531	1412	879	315

Table 4.3: Fine-grained materials

Sample	*Sha*	*Lim2*	*Lim1*	*Mar*	*Bas*
Trends	scattered	increase/ decrease	increase/ decrease	increase/ decrease	increase/ decrease
Max contrast (%)	5	30	29	29	13
cm^{-1} position	474	315	316	372	1004
Absorp. cm^{-1}	~1610 - 1360	~400 - 280	~400 - 280	~1620 - 1340	~1250 - 810
Rqes (µm)	~2.5	~4	~2.3	~4	~2
+ contrast (%)	~11		~3	~4	
Initial Rqe	mid/high	low/mid	mid	mid	low
cm^{-1} affected	low	low	low	low	mid

Table 4.4: Intermediate- to coarse-grained materials

Sample	*Gab*	*Gran*	*Apl*	*Monz*	*Alk*
Trends	increase/ constant	increase	increase/ constant	increase/ decrease	increase/ decrease
Max contrast	19	5	19	24	18
cm^{-1} position	1038	539	1159	1085	1080
Absorp. cm^{-1}	~1230 - 800	~1260 - 815	~1270 - 820	~1260 - 820	~1270 - 820
Rqes (µm)	~1	~3.5	~0.5	~1	~1.5
+ contrast (%)		~4			
Initial Rqes	low	low	low	low	low
cm^{-1} affected	high	low	high	high	high

FIGURES

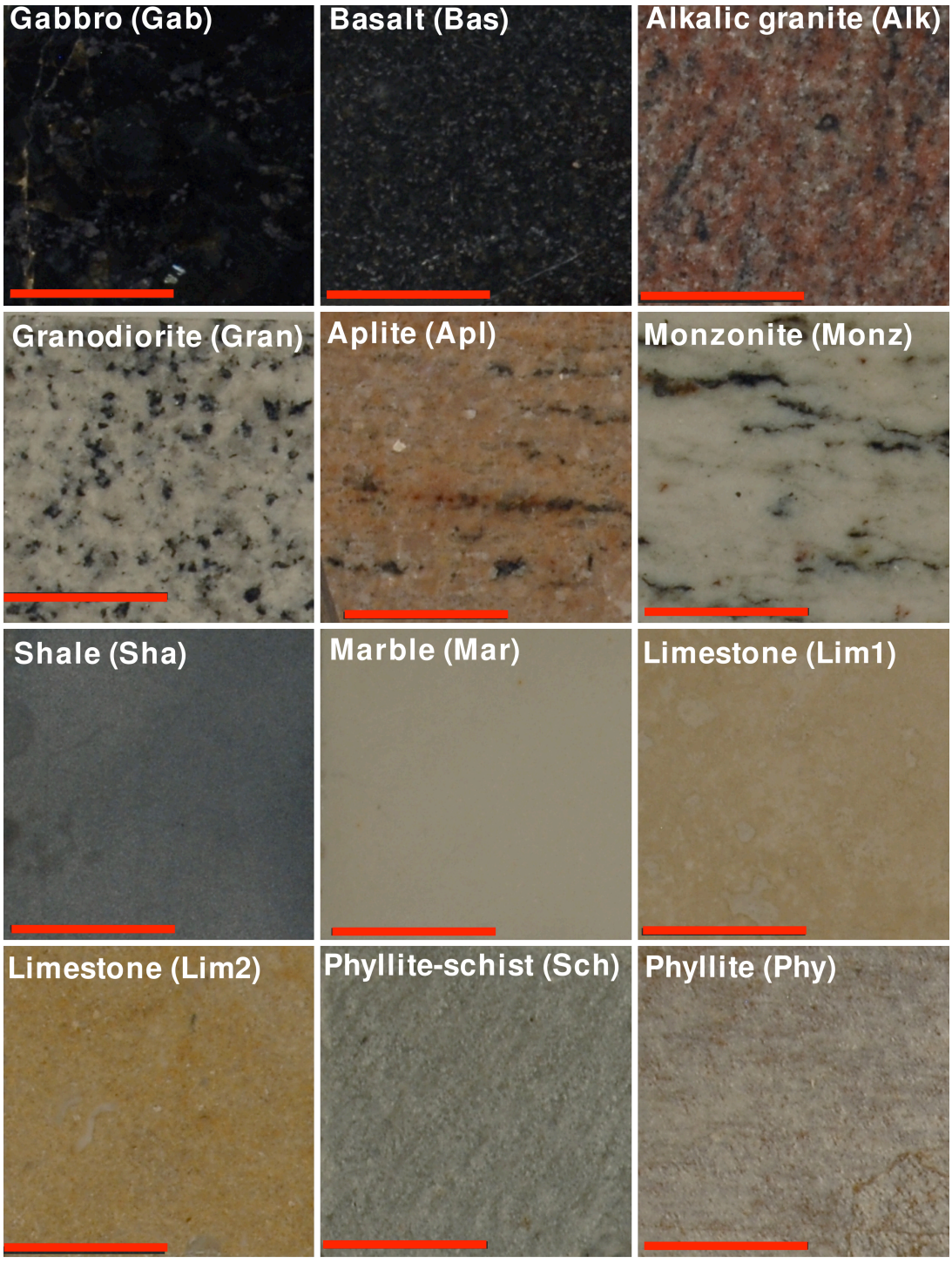

Figure 4.1: Examples of the twelve suites of rock samples chosen for our study. The red scale bar indicates ~19 mm.

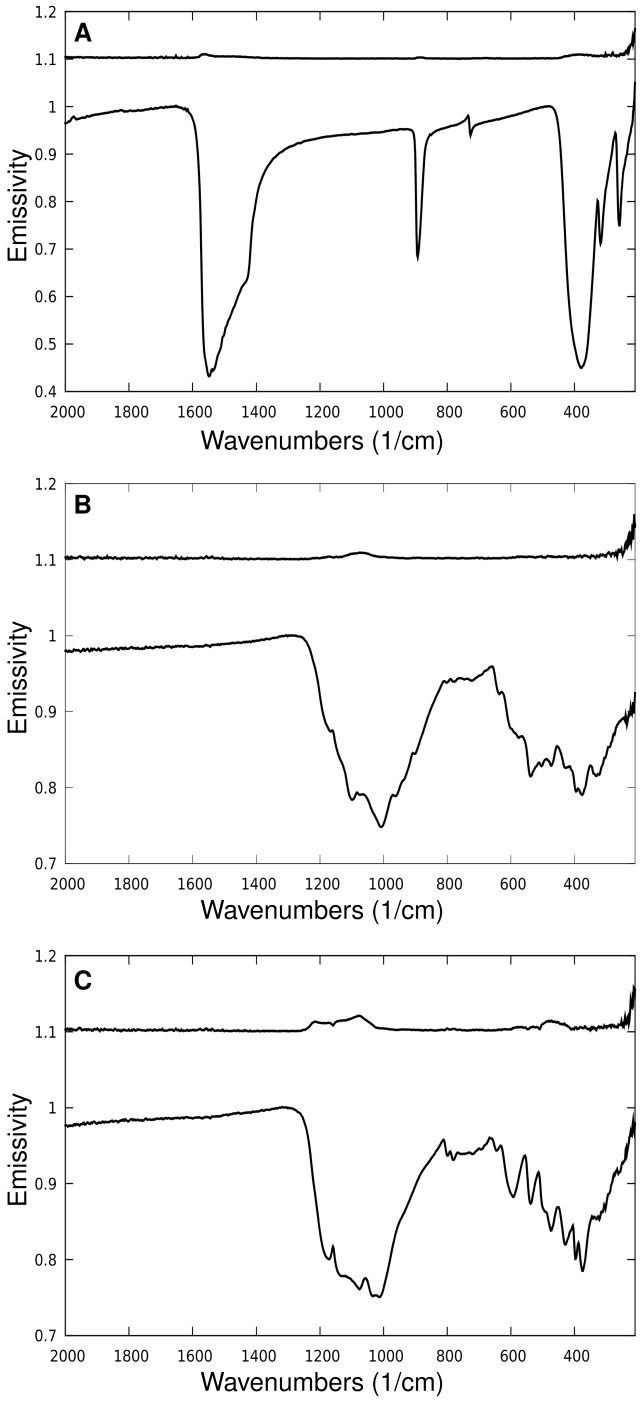

Figure 4.2. Averages of spectra collected over 18 days for the marble, and 8 days for the basalt and granodiorite. Standard deviations are offset and plotted above the averages. A) Repeatability measurements for the fine grained marble control (Mar1). B) Repeatability measurements for the fine grained basalt (Bas1). C) Repeatability measurements for the intermediate grained granodiorite (Gran1).

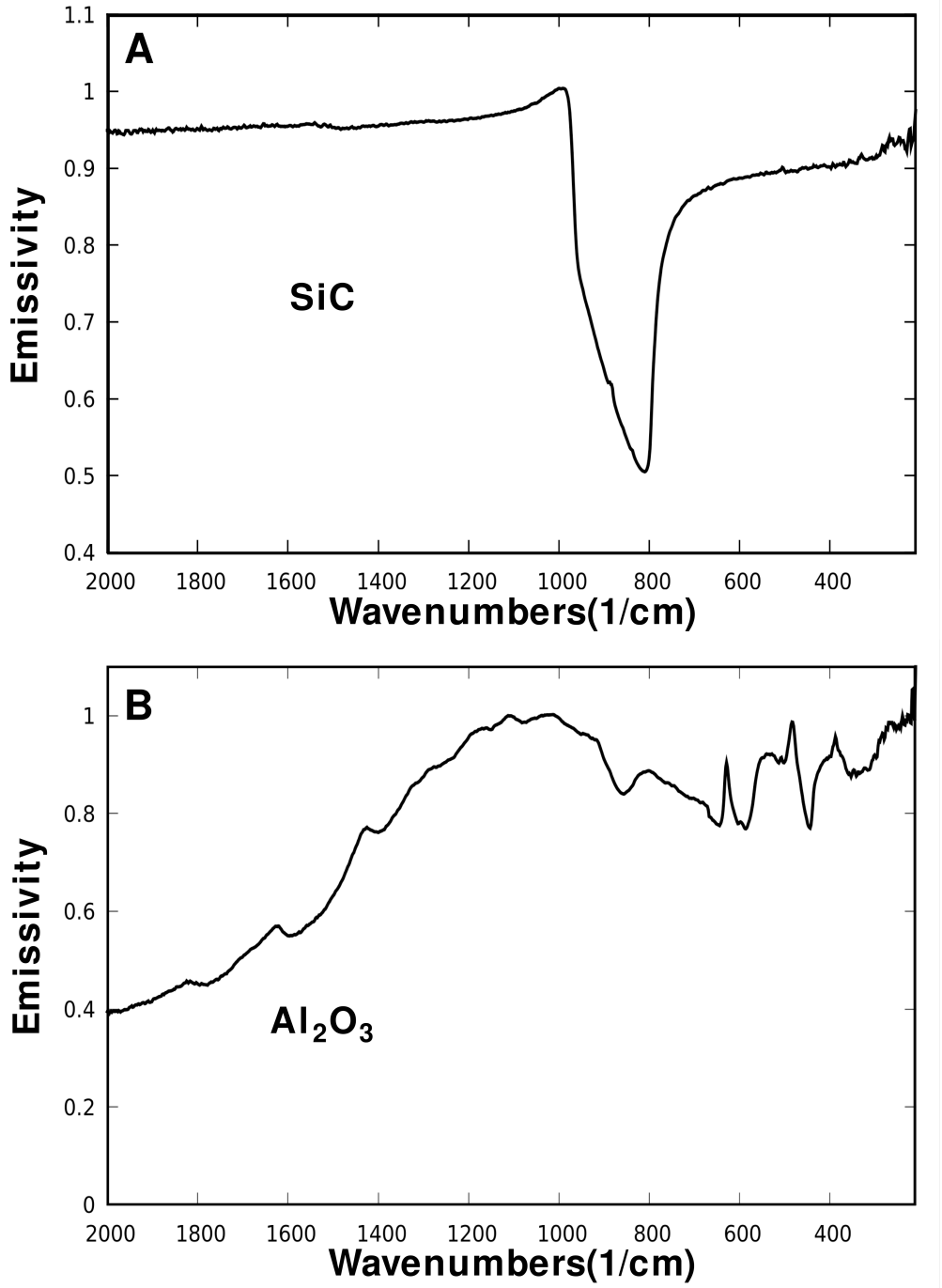

Figure 4.3. Spectra of the abrasives used in our study. A) Silicon carbide (SiC) displays a deep absorption feature between ~760 and ~980 cm^{-1}, with the lowest part of the trough located at ~815 cm^{-1}, but are relatively featureless otherwise. B) Aluminum oxide (Al_2O_3) spectra of 12 μm packed particle sizes.

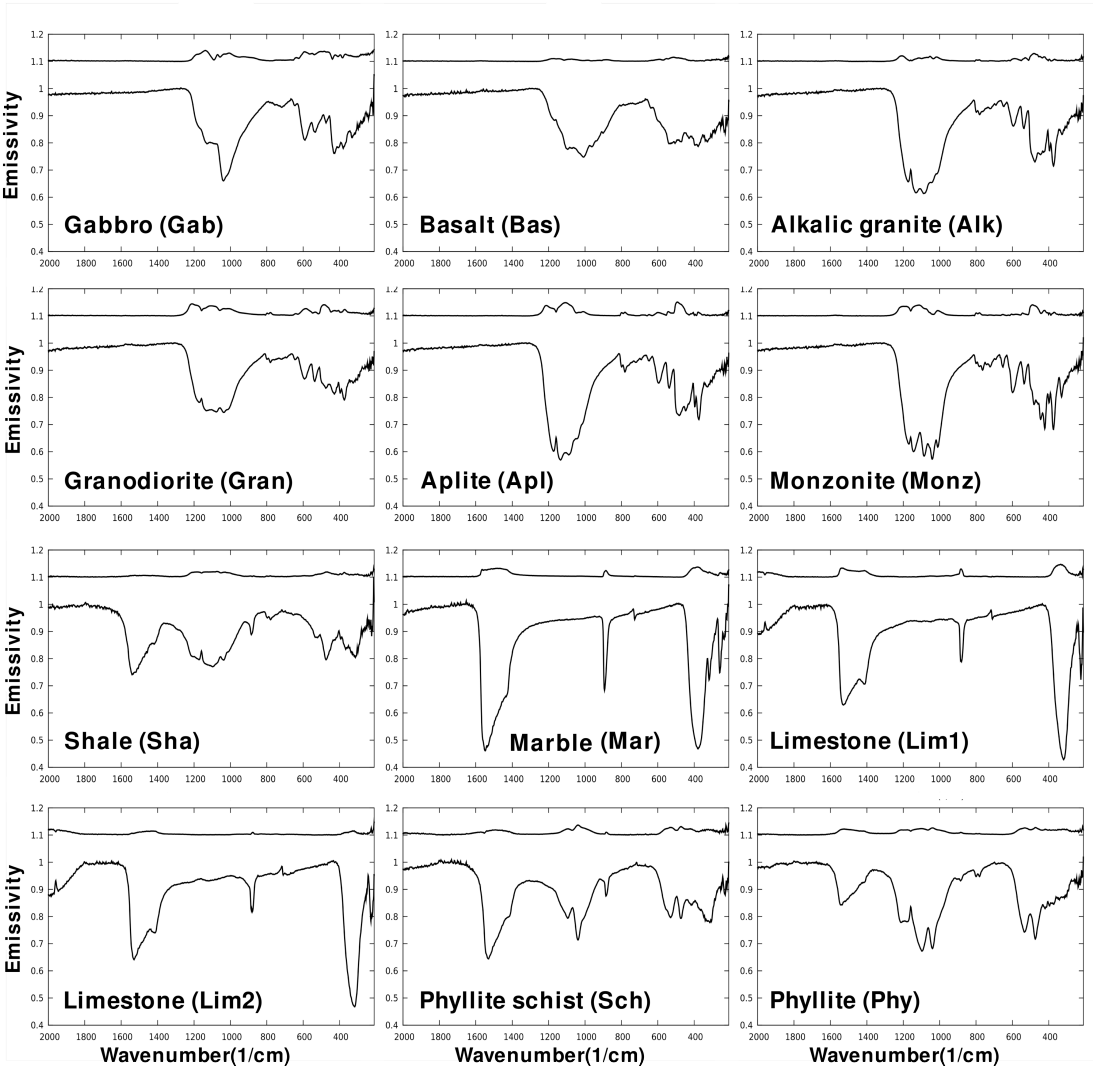

Figure 4.4: Average spectra for each group with standard deviations offset and plotted above the average spectrum.

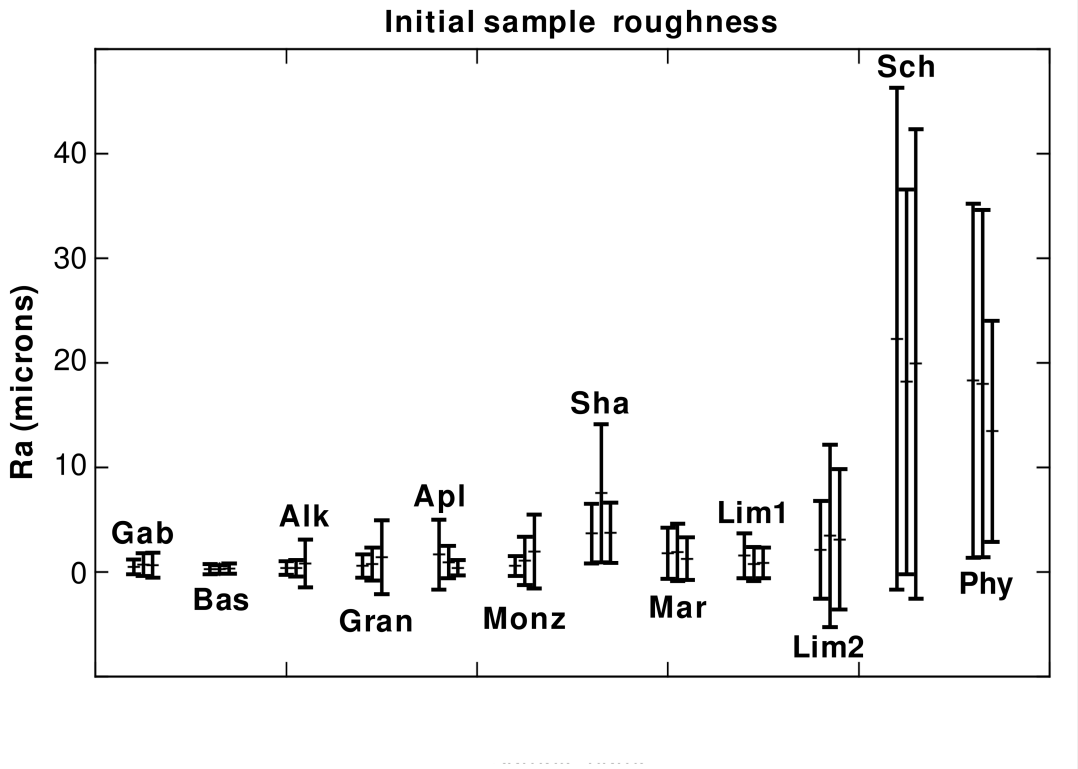

Figure 4.5. We collected initial R_a values for three samples within each group to investigate unroughened initial surfaces as well as the surface roughness variability within each group.

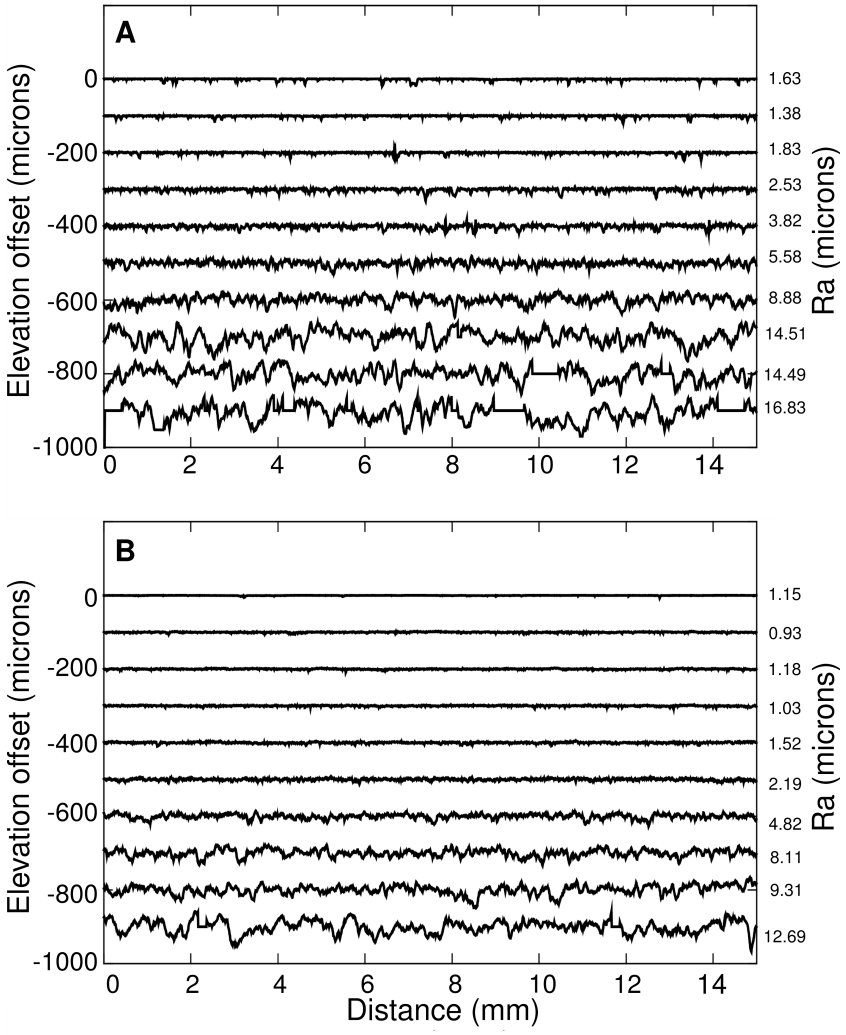

Figure 4.6. The profiles move successively through the abrasive particle sizes utilizes (e.g., 5, 12, 51, 79, 114, 212, 317, 423 and 635 μm) from the top to the bottom. At right are the average roughness values (R_a) derived from each profile. A) Marble samples show fairly consistent increase in elevation and roughness from the finest to the largest abrasive used. B) Basalt samples also show a fairly consistent increase in surface roughness from the finest to largest abrasive size used.

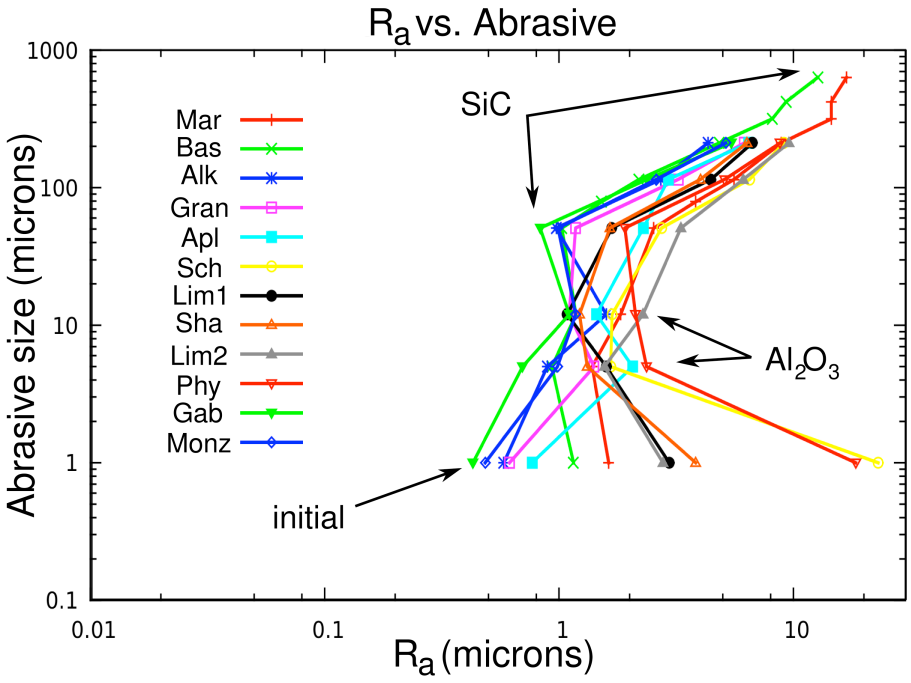

Figure 4.7. The R_a values for each sample within the various groups are plotted against the abrasive size used to create the roughened surface.

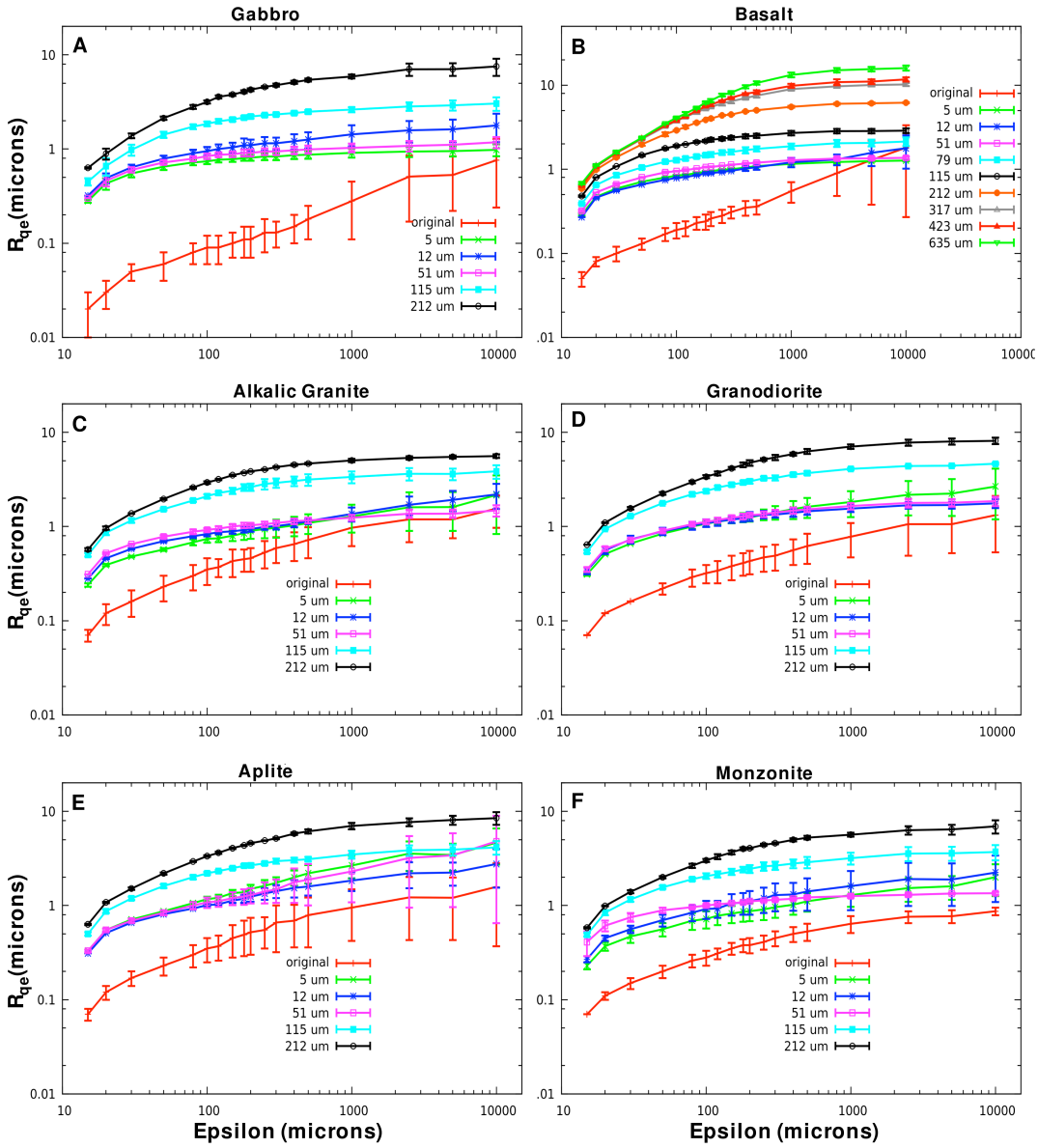

Figure 4.8. Log-log plots of R_{qe} (μm) vs. Epsilon (μm) for our roughened samples. Initial surfaces are plotted in red. A) Gabbro. B) Basalt. C) Alkalic granite. D) Granodiorite. E) Aplite. F) Monzonite. G) Shale. H) Marble. I) Limestone1. J) Limestone2.

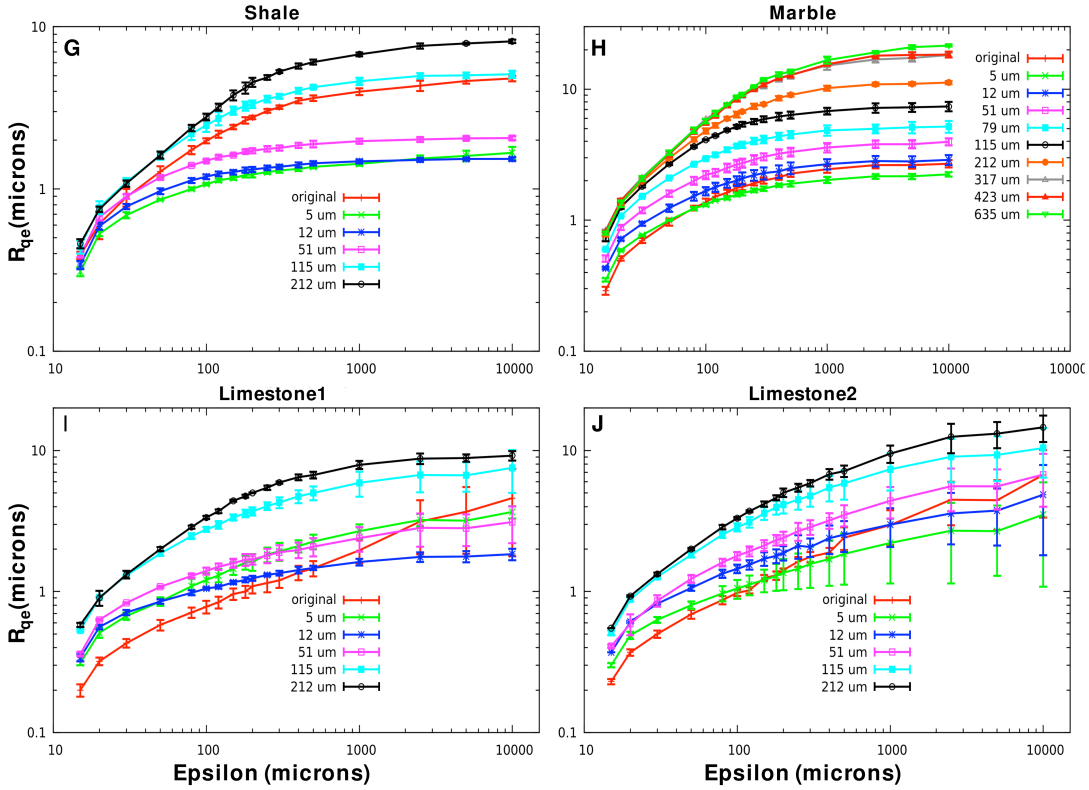

Figure 4.8. (continued)

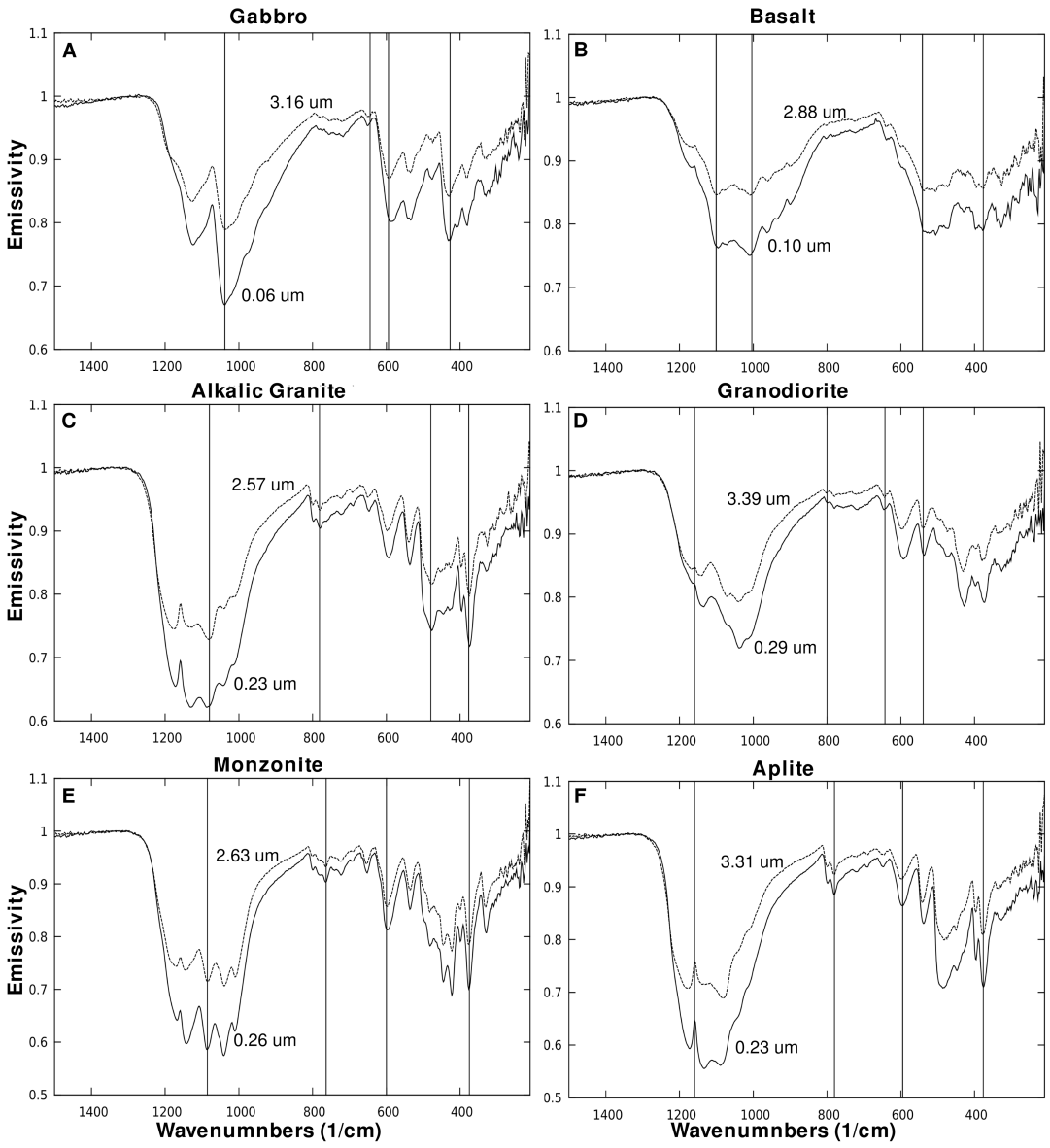

Figure 4.9. Example emissivity spectra of initial (smooth lines) and roughened (dotted lines) surfaces from each group. Wavenumber positions used to measure delta emissivity values between initial and roughened surfaces are shown in black. The R_{qes} values are also given above the spectra of the roughened surfaces and below the spectra of the initial surfaces. A) Gabbro. B) Basalt. C) Alkalic granite. D) Granodiorite. E) Aplite. F) Monzonite. G) Shale. H) Marble. I) Limestone1. J) Limestone2.

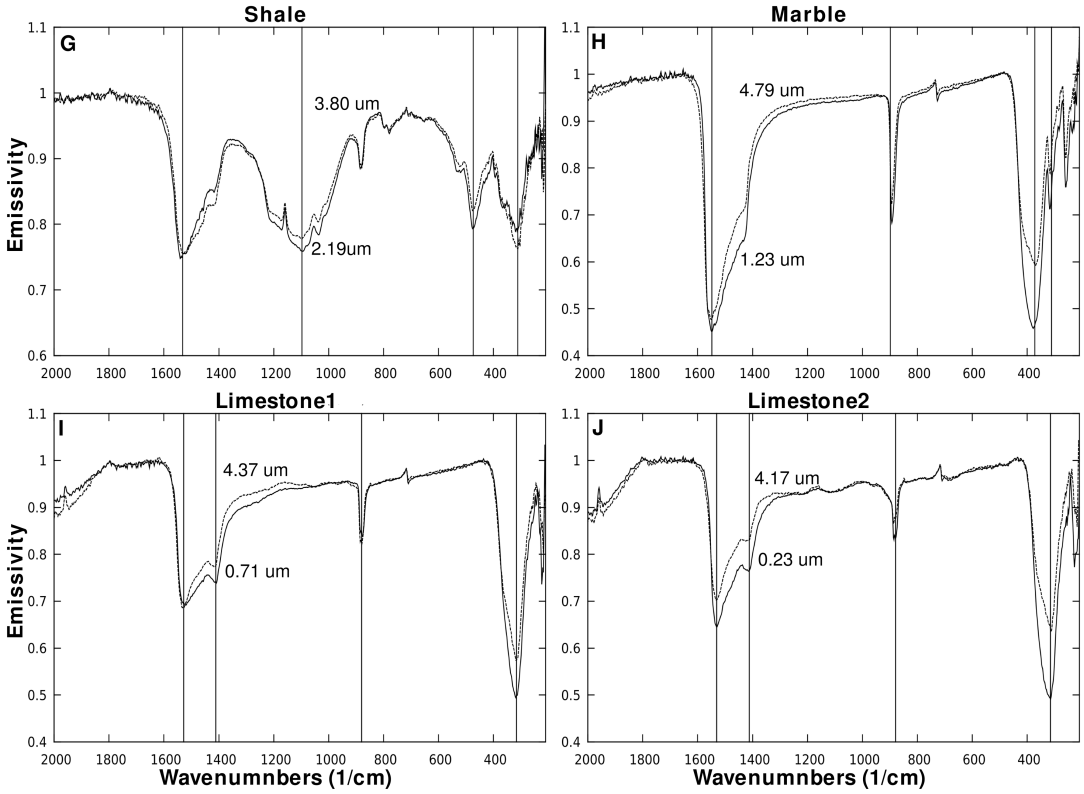

Figure 4.9. (continued)

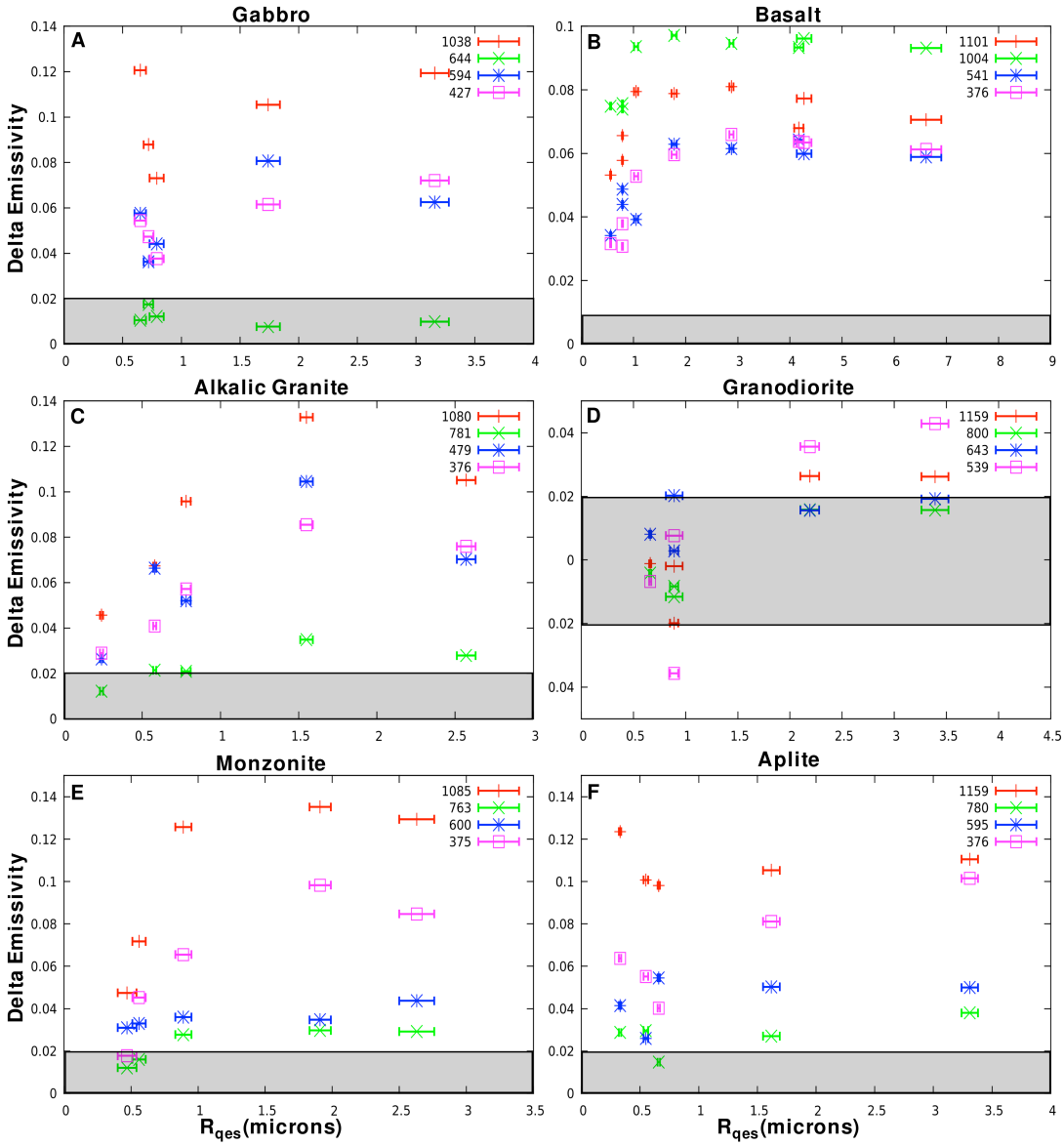

Figure 4.10. Delta emissivity values are plotted against the R_{qes} values for each sample. Positive values indicate a decrease in spectral contrast and negative numbers represent an increase in spectral contrast. Uncertainties derived from repeatability measurements are plotted as gray boxes. A) Gabbro. B) Basalt. C) Alkalic granite. D) Granodiorite. E) Aplite. F) Monzonite. G) Shale. H) Marble. I) Limestone1. J) Limestone2.

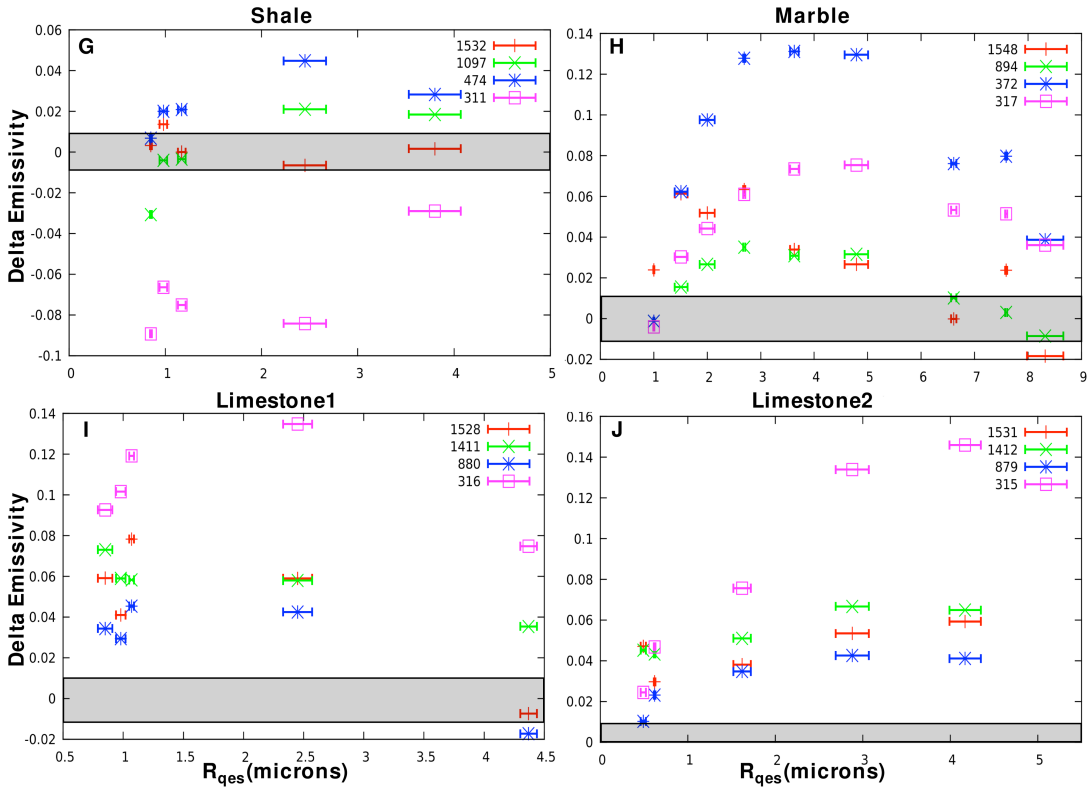

Figure 4.10. (continued)

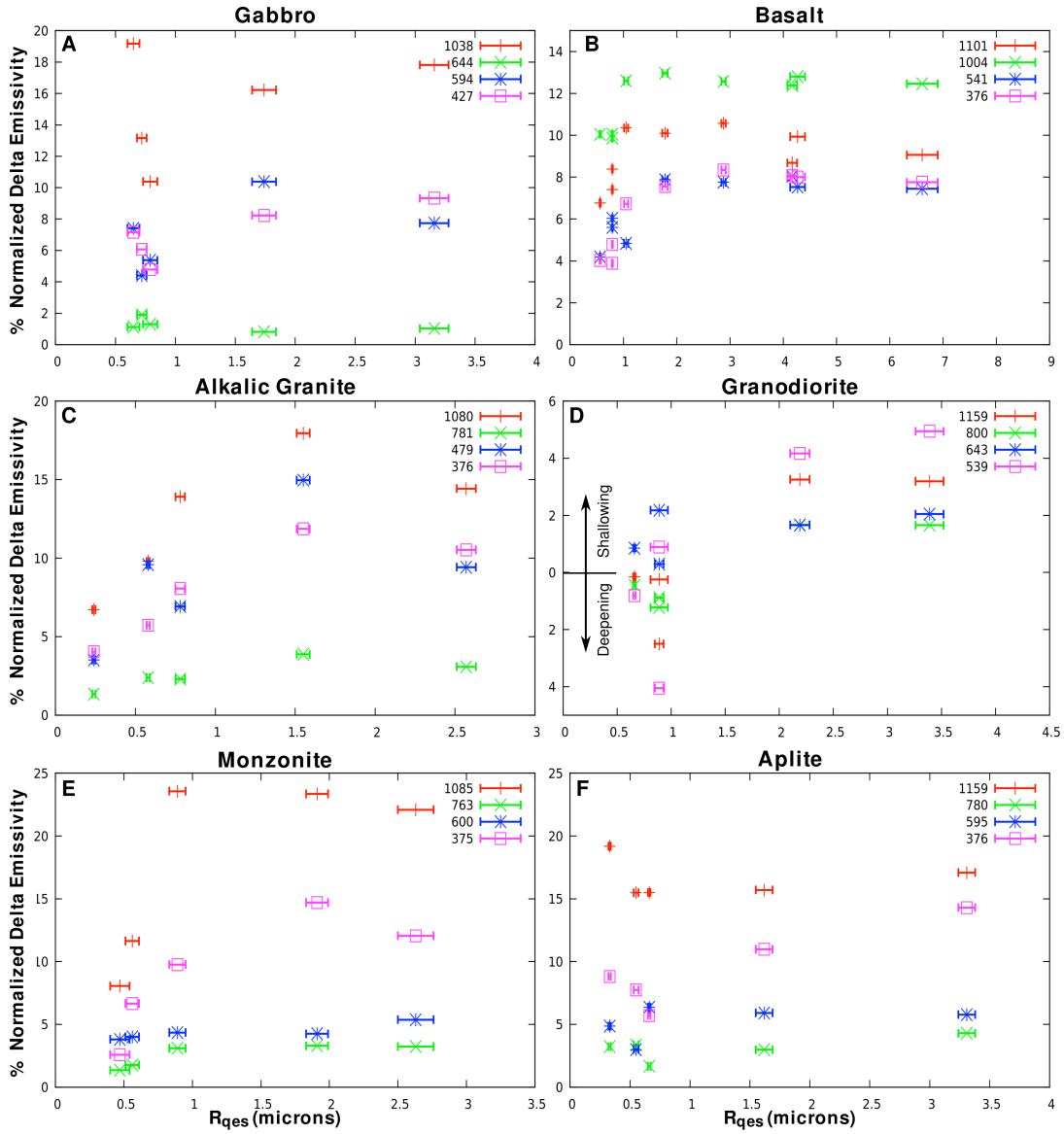

Figure 4.11. Percentages of normalized delta emissivity increase (negative numbers) or decrease (positive numbers) for each wavenumber position is shown plotted again the R_{qes} values for each rock group. A) Gabbro. B) Basalt. C) Alkalic granite. D) Granodiorite. E) Aplite. F) Monzonite. G) Shale. H) Marble. I) Limestone 1. J) Limestone 2.

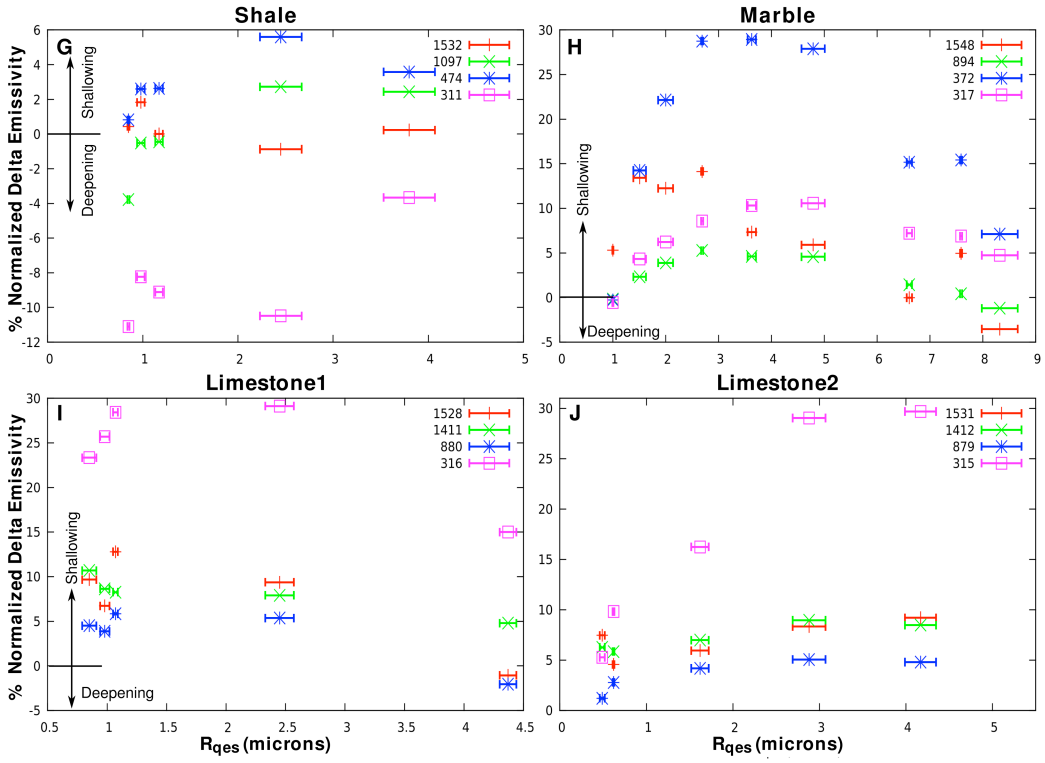

Figure 4.11. (continued)

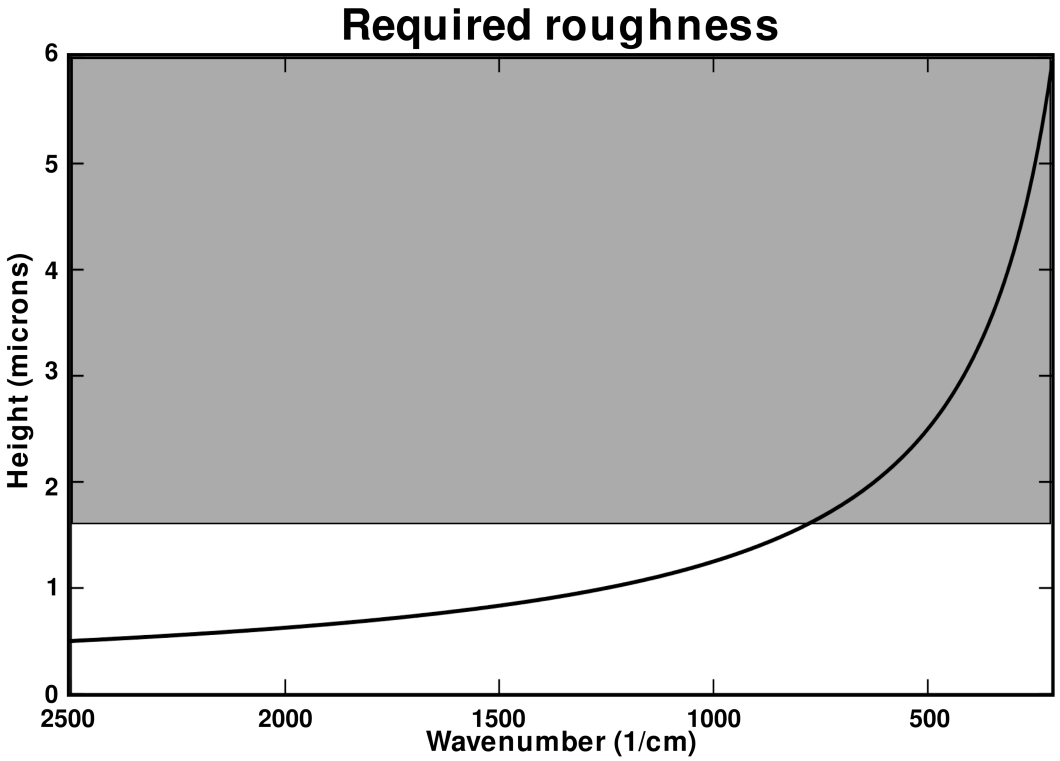

Figure 4.12. Using the equation from *Hapke* [1993a] we estimated the approximate height of the topographic feature necessary to affect photons in various wavenumber regions. The approximate heights of topographic features produced by our roughening process are shown in the grey area.

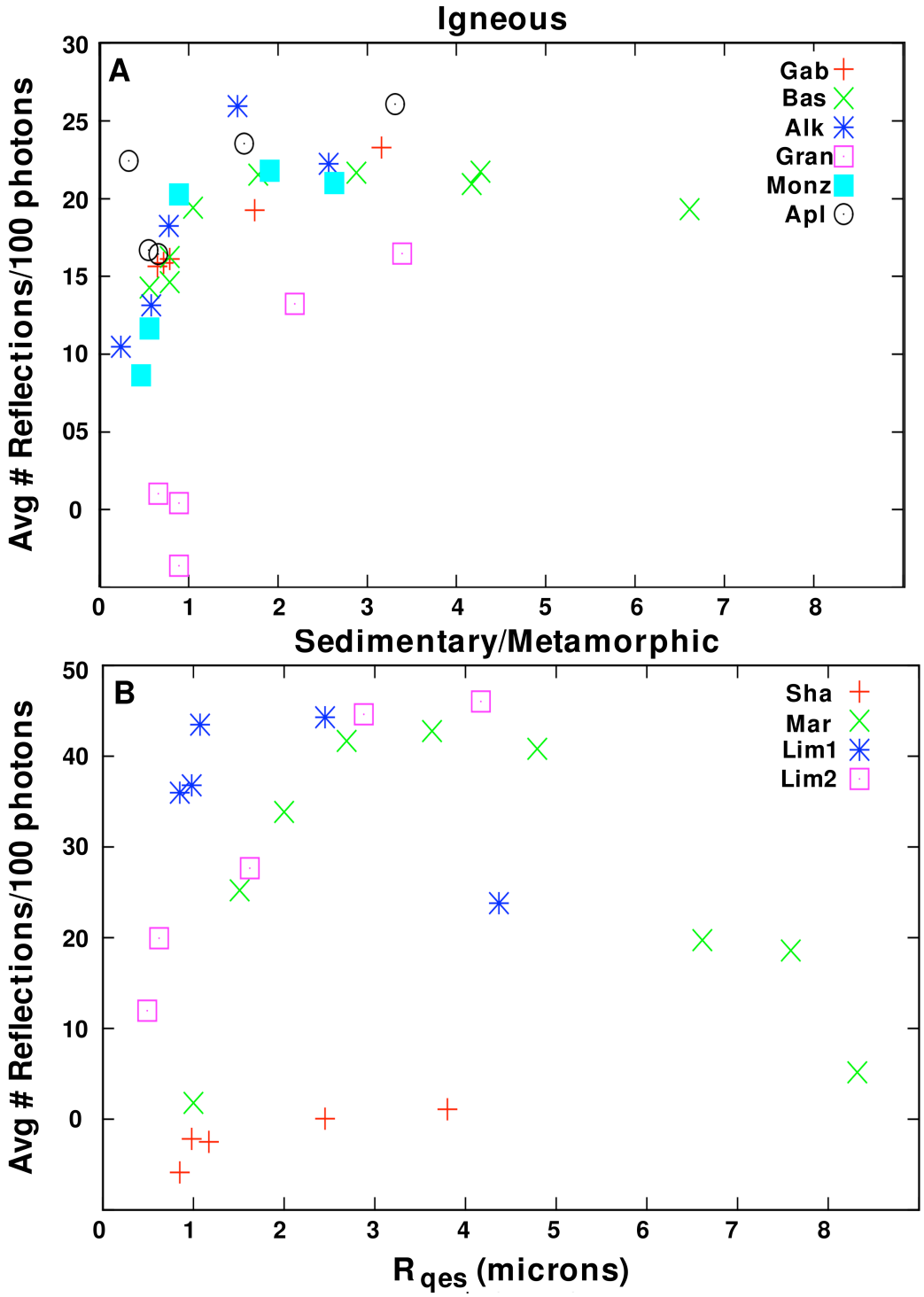

Figure 4.13. We calculated the average number of reflections per 100 photons using equation (5). A) Igneous compositions, Gab, Bas, Alk, Gran, Monz, Apl. B) Sedimentary and metamorphic compositions, Sha, Mar, Lim1, and Lim2.

REFERENCES

Abramov, O. and D. A. Kring (2005), Impact-induced hydrothermal activity on early Mars, *Journal of Geophysical Research,* 11, E12S09, doi:10.1029/2005JE002453.

Adams, J. B. and T. B. McCord (1969), Mars: Interpretation of spectral reflectivity of light and dark regions, *Journal of Geophysical Research*, 74, 20, 4851-4856.

Adams, J. B., J. E. Conel, J. A. Dunne, F. Fanale, G. B. Holstron, and A. A. Loomis (1986), Strategy for scientific exploration of the terrestrial planets*, Reviews of Geophysics,* 7, 3, p. 623-631.

Amitrano, D. and J. Schmittbuhl (2002), Fracture roughness and gouge distribution of granite shear band, *Journal of Geophysical Researc*h, 107, B12, 2375, doi:10.1029/2002JB001761.

Anbeek, C. (1992), Surface roughness of minerals and implications for dissolution studies, *Geochimica et Cosmochimica Acta*, 56, 1461- 1469.

Andrews-Hanna, J. C., M. T. Zuber, and W. B. Banerdt (2008), The Borealis basin and the origin of the martian crustal dichotomy, *Nature*, *453*, 1212-1216, doi:10.1038/nature07011.

Andrews-Hanna, J.C., M.T. Zuber, R.E. Arvidson, and S.M. Wiseman (2010), Early Mars hydrology: Meridiani playa deposits and the sedimentary record of Arabia Terra, *Journal of Geophysical Research*, doi:10.1029/2009JE003485.

Aronson, J. R. and A. G. Emslie (1973), Spectral reflectance and emittance of particulate materials. 2: Application and results, *Applied Optics*, 12, 11, p. 2573-2584.

Aronson, J. R., A. G. Emslie, and H. G. McLinden (1966), Infrared spectra from fine particulate surfaces, *Science*, 152, 3720, p. 345-346.

Aronson, J. R., A. G. Emslie, R. V. Allen, and H. G. McLinden (1967), Studies of the middle- and far-infrared spectra of mineral surfaces for application in remote compositional mapping of the Moon and planets, *Journal of Geophysical Research*, 72, 2, p. 687-703.

Aronson, J. R., A. G. Emslie, T. P. Rooney, I. Coleman, and G. Horlick (1969), Spectral emittance and reflectance of powders, *Applied Optic*s, 8, 8, p. 1639-1644.

Baird, A. K., P. Toulmin III, B. C. Clark, H. J. Rose, Jr., K. Keil, R. P. Christian, and J. L. Gooding (1976), Mineralogic and petrologic implications of Viking geochemical results from Mars: Interim Report, *Science*,194, 1288-1293.

Baldridge, A. M., J. D. Farmer, and J. E. Moersch (2004), Mars remote-sensing analog studies in the Badwater Basin, Death Valley, California, *Journal of Geophysical Research,* 109, E12006, doi:10.1029/2004JE002315.

Baldridge, A. M., S. J. Hook, J. K. Crowley, G. M. Marion, J. S. Kargel, J. L. Michalski, B. J. Thomson, C. R. de Souza Filho, N. T. Bridges, and A. J. Brown (2009), Contemporaneous deposition of phyllosilicates and sulfates: Using Australian acidic saline lake deposits to describe geochemical variability on Mars, *Geophysical Research Letters, 36,* L19201, doi:10.1029/2009GL040069.

Bandfield, J. L. (2002), Global mineral distributions on Mars, *Journal of Geophysical Research*, *107*, E6, doi:10.1029/2001JE001510.

Bandfield, J. L. (2006), Extended surface exposures of granitoid compositions in Syrtis Major, Mars, *Geophysical Research Letters*, 33, L06230, doi:10.1029/2005GL025.

Bandfield, J. B. (2007), High-resolution subsurface water-ice distributions on Mars, *Nature* 447, 64-67, doi:10.1028/nature05781.

Bandfield, J. B. (2008), High-silica deposits of an aqueous origin in western Hellas Basin, Mars, *Geophysical Research Lette*rs, 35, L12205, doi:10.1029/2008GL033807.

Bandfield, J. L. (2009), Effects of surface roughness and graybody emissivity on martian thermal infrared spectra, *Icarus*, *202,* 414-428*,* doi:10.1016/j.icarus.2009.03.031.

Bandfield, J. L. and M. D. Smith (2003), Multiple emission angle surface-atmosphere separations of Thermal Emission Spectrometer data, *Icarus*, 161, 47-65.

Bandfield, J. L., V. E. Hamilton, and P. R. Christensen (2000), A global view of Martian surface compositions from MGS-TES, *Science, 287*, 1626-1630, doi:10.1126/science.287.5458.1626.

Bandfield, J.L., P. R. Christensen, and M. D. Smith (2000), Spectral data set factor analysis and end-member recovery: Application to analysis of Martian atmospheric particulates, *Journal of Geophysical Research*, 105, E4, 9573-9587.

Bandfield, J. L., T. D. Glotch, and P. R. Christensen (2003), Spectroscopic identification of carbonate minerals in the Martian dust, *Science*, 301, 5636, 1084-1087.

Bandfield, J. L., Rogers, A. D., Smith, M. D., and Christensen, P. R. (2004), Atmospheric correction and surface spectral unit mapping using Thermal Emission Imaging System data, *Journal of Geophysical Research*, 109, E10008.

Bandfield, J. L., V. E. Hamilton, P. R. Christensen, and H. Y. McSween, Jr. (2004), Identification of quartzofeldspathic materials on Mars, *Journal of Geophysical Research*, 109, E10009, doi:10.1029/2004JE002290.

Barbieri, R., N. Stivaletta, L. Marinangeli, and G. G. Ori (2006), Microbial signatures in sabkha evaporite deposits of Chott el Gharsa (Tunisia) and their astrobiological implications, *Planetary and Space Science, 54*, 726-736, doi:10.1016/j.pss.2006.04.003

Bedford, R. E., C. K. Ma., Z. Chu, Y. Sun, and S. Chen (1985), Emissivities of diffuse cavities. 4: Isothermal and nonisothermal cylindro-inner-cones, *Applied Optics*, 24, 18, p. 2971- 2980.

Bibring, J-P., Y. Langevin, A. Gendrin, B. Gondet, F. Poulet, M. Berthe, A. Soufflot, R. Arvidson, N. Mangold, J. Mustard, P. Drossart, and the OMEGA team (2005), Mars surface diversity as revealed by the OMEGA/Mars Express Observations, *Science*, 307, 1576, doi:10.1126/science.1108806.

Bibring, J.-P., Y. Langevin, J. F. Mustard, F. Poulet, R. Arvidson, A. Gendrin, B. Gondet, N. Mangold, P. Pinet, F. Forget, and the OMEGA team (2006), Global mineralogical and aqueous Mars history derived from OMEGA/ Mars Express data, *Science, 312*, 400-404, doi:10.1126/science.1122659.

Bibring, J-P., R. E. Arvidson, A. Gendrin, B. Gondet, Y. Langevin, S. Le Mouelic, N. Mangold, R. V. Morris, J. F. Mustard, F. Poulet, C. Quantin, and C. Sotin (2007), Coupled ferric oxides and sulfates on the Martian surface, *Science*, 317, 1206, doi:10.1126/science.1144174.

Bishop, J. L., E. Z. Noe Dobrea, N. K. McKeown, M. Parente, B. L. Ehlmann, J. R. Michalski, R. E. Milliken, F. Poulet, G. A. Swayze, J. F. Mustard, S. L. Murchie, and J.-P. Bibring (2008), Phyllosilicate diversity and past aqueous activity revealed at Mawrth Vallis, Mars, *Science,* 321, 830, doi:10.1126/science.1159699.

Bishop, J. L., M. Parente, C. M. Weitz, E. Z. Noe Dobrea, L. H. Roach, S. L. Murchie, P. C. McGuire, N. K. McKeown, C. M. Rossi, A. J. Brown, W. M.

Calvin, R. Milliken, and J. F. Mustard (2009), Mineralogy of Juventae Chasma: Sulfates in the light-toned mounds, mafic minerals in the bedrock, and hydrated silica and hydroxylated ferric sulfate on the plateau, *Journal of Geophysical Research,*114, E00D09, doi:10.1029/2009JE003352.

Bleacher, J. E., R. Greeley, D. A. Williams, S. R. Cave, and G. Neukum (2007), Trends in effusive style at the Tharsis Montes, Mars, and implications for the development of the Tharsis province, *Journal of Geophysical Research, 112*, E09005, doi:10.1029/2006JE002873.

Boggs, S. Jr. (2001), Carbonate and Evaporite Environments, in *Principles of Sedimentology and Stratigraphy*, 3rd Ed., edited by P. Lynch, pp.417-448, Prentice-Hall, Upper Saddle River, New Jersey.

Bouchard, E. and J.-P. Bouchaud (1994), Fracture surfaces: Apparent roughness, relevant length scales, and fracture toughness, *Physical Review*, 50, 23.

Boynton, W. V., W. C. Feldman, S. W. Squyres, T. H. Prettyman, J. Brückner, L. G. Evans, R. C. Reedy, R. Starr, J. R. Arnold, D. M. Drake, P. A. J. Englert, A. E. Metzger, I. Mitrofanov, J. I. Trombka, C. d'Uston, H. Wänke, O. Gasnault, D. K. Hamara, D. M. Janes, R. L. Macialis, S. Maurice, I. Mikheeva, G. J. Taylor, R. Tokar, and C. Shinohara (2002), Distribution of hydrogen in the near surface of Mars: Evidence for subsurface ice deposits, *Science*, 297, 81, doi:10.1126/science.1073722.

Boynton, W. V., W. C. Feldman, I. G. Mitrofanov, L. G. Evans, R. C. Reedy, S. W. Squyres, R. Starr, J. I. Trombka, C. D'Uston, J. R. Arnold, P. A. J. Englert, A. E. Metzger, H. Wänke, J. Brückner, C. M. Drake, C. Shinohara, C. Fellows, D. K. Hamara, K. Harshman, K. Kerry, C. Turner, M. Ward, H. Barthe, K. R. Fuller, S. A. Storms, G. W. Thornton, J. L. Longmire, M. L. Litvak, and A. K. Ton'chev (2004), The Mars Odyssey Gamma-Ray Spectrometer Instrument Suite, *Space Science Reviews, 110(*1-2), 37-87, doi:10.1023/B:SPAC.0000021007.76126.15.

Boynton, W. V., G. J. Taylor, L. G. Evans, R. C. Reedy, R. Starr, D. M. Janes, K. E. Kerry, D. M. Drake, K. J. Kim, R. M. S. Williams, M. K. Crombie, J. M. Dohm, V. Baker, A. E. Metzger, S. Karunatillake, J. M. Keller, H. E. Newsom, J. R. Arnold, J. Brückner, P. A. J. Englert, O. Gasnault, A. L. Sprague, I. Mitrofanov, S. W. Squyres, J. I. Trombka, L. d'Uston, H Wänke, and D. K. Hamara (2007), Concentration of H, Si, Cl, K, and Th in the low- and mid-latitude regions of Mars, Journal of Geophysical Research, 112, E12S99, doi:10.1029/2007JE002887.

Boynton, W. V., G. J. Taylor, S. Karunatillake, R. C. Reedy, and J. M. Keller (2008), Elemental abundances determined via the Mars Odyssey GRS, in *The Martian*

Surface: Composition, Mineralogy, and Physical Properties, Edited by Jim Bell, p. 105-124, Cambridge University Press, New York.

Brantley, S. L. and N. P. Mellott (2000), Surface area and porosity of primary silicate minerals, *American Mineralogist*, 85, 1767-178

Brass, G. W. (1980), Stability of brines on Mars, *Icarus* 42, 1, 20-28.

Bridges, J. C. and M. M. Grady (1999), A halite-sinderite-anhydrite-chlorapatite assemblage in Nakhla: Mineralogical evidence for evaporites on Mars, *Meteoritics and Planetary Science*, 34, 407-416.

Bridges, J. C and M. M.Grady (2000), Evaporite mineral assemblages in the nakhlite (martian) meteorites, *Earth and Planetary Science Letters*, 176, 267-279.

Bridges, N. T., R. Greeley, A. F. C. Haldermann, K. E. Herkenhoff, M. Kraft, T. J. Parker, and A. W. Ward (1999), Ventifacts at the Pathfinder landing site, *Journal of Geophysical Research*, 104, E4, 8595-9615.

Bridges, N. T., J. E. Laity, R. Greeley, J. Phoreman, and E. E. Eddlemon (2004), Insights on rock abrasion and ventifact formation from laboratory and field analog studies with applications to Mars, *Planetary and Space Science*, 52, 199-213.

Brown, S. R. and C. H. Scholz (1985), Broad bandwidth study of the topography of natural rock surfaces, *Journal of Geophysical Research*, 90, B14, 12,575-12,582.

Brückner, J., G. Dreibus, R. Rieder, and H. Wänke (2003), Refined data of Alpha Proton X-ray Spectrometer analyses of soils and rocks at the Mares Pathfinder site: Implications for surface chemistry, *Journal of Geophysical Research*, 108, E12, doi:10.1029/2003JE002060.

Burns, R. G. and D. S. Fisher (1990), Evolution of Sulfide Mineralization on Mars, *Journal of Geophysical Research,* 95, B9, 14169-14173.

Burns, R. G. and D. S. Fisher (1993), Rates of Oxidative Weathering on the Surface of Mars, *Journal of Geophysical Research, 98,* E2, 3365-3372.

Carr, M. H. (1973), Volcanism on Mars, *Journal of Geophysical Research, 78*, 4049-4082.

Carter, A. J., M. S. Ramsey, A. J. Durant, I. P. Skilling, and A. Wolfe (2009), Micron-scale roughness of volcanic surfaces from thermal infrared

spectroscopy and scanning electron microscopy, *Journal of Geophysical Research*, 114, B02213, doi:10.1029/2008JB005632.

Chauvy, P. F., C. Madore, and D. Landolt (1998), Variable length scale analysis of surface topography: characterization of titanium surfaces for biomedical applications, *Surface and Coatings Technology*, 110, 48- 56.

Christensen, P. R., Calibration Report for the Thermal Emission Spectrometer (TES) for the Mars Global Surveyor Mission, Mars Global Surveyor Project (Jet Propulsion Laboratory, Pasadena, CA, 1999).

Christensen, P. R. and S. T. Harrison (1993), Thermal infrared emission spectroscopy of natural surfaces: Application to desert varnish coatings on rocks, *Journal of Geophysical Research*, 98, B11, 19819- 19834.

Christensen, P. R., J. L. Bandfield, M. D. Smith, V. E. Hamilton, and R. N. Clark (2000a), Identification of a basaltic component on the Martian surface from Thermal Emission Spectrometer data, *Journal of Geophysical Research, 105*, 9609-9621, doi:10.1029/1999JE001127.

Christensen, P. R., Bandfield, J. L., Clark, R. N., Edgett, K. S., Hamilton, V. E., Hoefen, T., Kieffer, H. H., Kuzmin, R. O., Lane, M. D., Malin, M. C., Morris, R. V., Pearl, J. C., Pearson, R., Roush, T. L., Ruff, S. W., and Smith, M. D. (2000b), Detection of crystalline hematite mineralization on Mars by the Thermal Emission Spectrometer: Evidence for near-surface water, *Journal of Geophysical Research*, 105(E4), 9623-9642.

Christensen, P. R., Bandfield, J. L., Hamilton, V. E., Howard, D. A., Lane, M. D., Piatek, J. L., Ruff, S. W., and Stefanov, W. L. (2000c), A thermal emission spectral library of rock-forming minerals, *Journal of Geophysical Research*, 105(E4), 9735-9739.

Christensen, P. R., J. L. Bandfield, V. E. Hamilton, S. W. Ruff, H. H. Kieffer, T. N. Titus, M. C. Malin, R. V. Morris, M. D. Lane, R. L. Clark, B. M. Jakosky, M. T. Mellon, J. C. Pearl, B. J. Conrath, M. D. Smith, R. T. Clancy, R. O. Kuzmin, T. Roush, G. L. Mehall, N. Gorelick, K. Bender, K. Murray, S. Dason, E. Greene, S. Silverman, and M. Greenfield (2001a), Mars Global Surveyor Thermal Emission Spectrometer experiment: Investigation description and surface science results, *Journal of Geophysical Research*, 106, E10, 238230- 23871.

Christensen, P. R., R. V. Morris, M. D. Lane, J. L. Bandfield, and M. C. Malin (2001b), Global mapping of Martian hematite mineral deposits: Remnants of water-driven processes on early Mars, *Journal of Geophysical Researc*h, 106, E10, 23873-23885.

Christensen, P. R., Jakosky, H. H., Kieffer, H. H., Malin, M. C., McSween, H. Y, Nealson, K., Mehall, G. L., Silverman, S. H., Ferry, S., Caplinger, M., and Ravine, M. (2004), The Thermal Emission Imaging Systems (THEMIS) for the Mars 2001 Odyssey Mission, *Space Science Reviews*, 110, 85-130.

Christensen, P. R., H. Y. McSween Jr., J. L. Bandfield, S. W. Ruff, A. D. Rogers, V. E. Hamilton, N. Gorelick, M. B. Wyatt, B. M. Jakosky, H. H. Kieffer, M. C. Malin, and J. E. Moersch (2005), Evidence for magmatic evolution and diversity on Mars from infrared observations, *Nature*, 436, 504-509, doi:10.1028/nature03639.

Clark, B. C. and D.C. VanHart (1981), The salts of Mars, *Icarus*, 45, 370-378.

Clark, B. C., A. K. Baird, H. J. Rose, Jr., P. Toulmin III, K. Keil, A. J. Castro, W. C. Kelliher, C. D. Rowe, and P. H. Evans (1976), Inorganic analyses of Martian surface samples at the Viking landing sites, *Science*, 194, 1283-1288.

Clark, B. C., R. V. Morris, S. M. McLennan, R. Gellert, B. Jolliff, A. H. Knoll, S. W. Squyres, T. K. Lowenstein, D. W. Ming, N. J. Tosca, A. Yen, P. R. Christensen, S. Gorevan, J. Brückner, W. Calvin, G. Dreibus, W. Farrand, G. Klingelhoefer, H. Wänke, J. Zipfel, J. F. Bell III, J. Grotzinger, H. Y. McSween, R. Rieder (2005), Chemistry and mineralogy of outcrops at Meridiani Planum, *Earth and Planetary Science Letters, 240*, 73-94, doi:10.1016/j.epsl.09.040.

Clark, R. N., G. A. Swayze, R. Wise, E. Livo, T. Hoefen, R. Kokaly, and S. J. Sutley (2007), USGS digital spectral library splib06a, *U. S. Geological Survey, Digital Data Series 231.*

Conel, J. R. (1969), Infrared emissivities of silicates: Experimental results and a cloudy atmosphere model of spectral emission from condensed particulate mediums, *Journal of Geophysical Research*, 74, 6, p. 1614-1643.

Connerney, J. E. P., M. H. Acuña, N. F. Ness, G. Kletetschka, D. L. Mitchell, R. P. Lin, and H. Reme (2005), Tectonic implications for Mars crustal magnetism, *Proceedings of the National Academies of Science, 102*, 14970-14975, doi:10.1073/pnas.0507469102.

Craddock, R. A. and A. D. Howard (2002), The case for rainfall on a warm, wet early Mars, *Journal of Geophysical Research, 107*(E11), doi:10.1029/2001JE001505.

Daguier, P., S. Henaux, E. Bouchaud, and F. Creuzet (1996), Quantitative analysis of a fracture surface by atomic force microscopy, *Physical Review*, 53, 6, 5637-5642.

Deer, W. A., R. A. Howie, and J. Zussman (1992), *An introduction to the Rock-Forming Minerals*, 2nd Ed., 696 pp. Longman, London.

Delamere, W. A., L. L. Tornabene, A. S. McEwen, K. Becker, J. W. Bergstrom, N. T. Bridges, E.M. Eliason, D. Gallagher, K. E. Herkenhoff, L. Keszthelyi, S. Mattson, G. K. McArthur, M. T. Mellon, M. Milazzo, P. S. Russell (2009), Color imaging of Mars by the High Resolution Imaging Science Experiment (HiRISE), *Icarus, 205, 38-52*,doi:10.1016/j.icarus.2009.03.012.

DiAchille, G. and B. M. Hynek (2010), Ancient ocean on Mars supported by global distribution of deltas and valleys, *Nature Geoscience, 3*, 459-463, doi:10.1028/ngeo891.

Eastes, J. W. (1989), Spectral properties of halite-rich mineral mixtures: Implications for middle infrared remote sensing of highly saline environments, *Remote Sensing of the Environment*, 27, 289-304.

Edwards, C. S., P. R. Christensen, and V. E. Hamilton (2008), Evidence for extensive olivine-rich bedrock outcrops in Ganges and Eos chasmas, Mars, *Journal of Geophysical Research,* 113, E11003, doi:10.1029/2008JE003091.

Edwards, C. S., J. L. Bandfield, P. R. Christensen, and R. L. Fergason (2009), Global distribution of bedrock exposures on Mars using THEMIS high-resolution thermal inertia, *Journal of Geophysical Research, 114*, E11001, doi:10.1029/2009JE003363.

Edwards, C. S. et al. (2010) THEMIS daytime and nighttime mosaics: Part 2, Results from Global and Regional mosaics, *in preparation*.

Ehlmann, B. L., J. F. Mustard, S. L. Murchie, F. Poulet, J. L. Bishop, A. J. Brown, W. M. Calvin, R. N. Clark, D. J. Des Marais, R. E. Milliken, L. H. Roach, T. L. Roush, G. A. Swayze, and J. J. Wray (2008), Orbital identification of carbonate-bearing rocks on Mars, *Science,* 322, 1828, doi:10.1126/science.1164759.

Ehlmann, B. L., J. H. Mustard, G. A. Swayze, R. N. Clark, J. L. Bishop, F. Poulet, D. J. Des Marais, L. H. Roach, R. E. Milliken, J. J. Wray, O. Barnouin-Jha, and S. L. Murchie (2009), Identification of hydrated silicate minerals on Mars using MRO-CRISM: Geologic context near Nili Fossae and implications for aqueous alteration, *Journal of Geophysical Research, 114*, E00D08, doi:10.1029/2009JE003339.

Eugster, H. P. and L. A. Hardie (1978), Saline lakes In: *Lakes: Chemistry, Geology, Physics,* Edited by A. Lerman, 237-293, Springer, New York.

Fairen, A. G., J. Ruiz, and F. Anguita (2002), An Origin for the Linear Magnetic Anomalies on Mars through Accretion of Terrains: Implications for Dynamo Timing, *Icarus, 160*, 220-223, doi:10.1006/icar.2002.6942.

Farmer, J. D., and Des Marais, D. J. (1999), Exploring for a record of ancient Martian life, *Journal of Geophysical Research*, 104, E11, 26977-26995.

Farmer, V. C. (1974), *The Infrared Spectra of Mineral*s, 539 p., Mineralogical Society of London.

Farrand, W. H., T. D. Glotch, J. W. Rice, Jr., J. A. Hurowitz, and G. A. Swayze (2009), Discovery of jarosite within the Mawrth Vallis region of Mars: Implications for the geologic history of the region, *Icarus, 204*, 478-488, doi:10.1016/j.icarus.2009.07.014.

Fassett, C. I. and J. W. Head III (2008a), Valley network-fed, open-basin lakes on Mars: Distribution and implications for Noachian surface and subsurface hydrology, *Icarus, 198*, 37-56, doi: 10.1016/j.icarus.2008.06.016.

Fassett, C.I and J. W. Head III (2008b), The timing of martian valley network activity: Constraints from buffered crater counting, *Icarus, 195*, 61-89, doi:10.1016/j.icarus.2007.12.009

Feely, K. C. and P. R. Christensen (1999), Quantitative compositional analysis using thermal emission spectroscopy: Application to igneous and metamorphic rocks, *Journal of Geophysical Research*, 104, 24, 24195-24210.

Fenton, L. K., P. E. Geissler, and R. M. Haberle (2007), Global warming and climate forcing by recent albedo changes on Mars, *Nature*, 446, 646-649.

Fergason, R. L., P. R. Christensen, and H. H. Kieffer (2006), High-resolution thermal inertia derived from the Thermal Emission Imaging System (THEMIS): Thermal model and applications, *Journal of Geophysical Research, 111*, E12004, doi:10.1029/2006JE002735.

Fish, S. A., T. J. Shepherd, T. J. McGenity, and W. D. Grant (2002), Recovery of 16S ribosomal RNA gene fragments from ancient halite, *Nature, 417*, 432-436.

Foley, C. N., T. Economou, and R. N. Clayton (2003), Final chemical results from the Mars Pathfinder alpha proton X-ray spectrometer, *Journal of Geophysical Researc*h, 108, E12, doi:10.1029/2002JE002019.

Fournier, R. O. (1989), Geochemistry and dynamics of the Yellowstone National Park hydrothermal system, *Annual Reviews of Earth and Planetary Sciences, 17*, 13-53, doi:10046/annurev.ea.17.050189.000305.

Fredrickson, J. K., D. P. Chandler, and T. C. Onstolt (1997), Potential for preservation of halobacteria and their micromolecular constituents in brine inclusions from bedded salt deposits, *SPIE Proceedings, 3111*, 318-329.

Frey, H. V., J. H. Roark, K. M. Shockey, E. L. Frey, and S. E.H. Sakamoto (2002), Ancient lowlands on Mars, *Geophysical Research Letters.*, 29, 10, doi:10.1029/2001GL013832.

Gaffey, S. J., L. A. McFadden, D. Nash, and C. M. Pieters (1993), Ultraviolet, visible, and near-infrared reflectance spectroscopy: Laboratory spectra of geologic materials, In *Remote Geochemical Analysis: Elemental and Mineralogical Composition*, Ed. C. M. Pieters and P. A. Englert, pp. 43-77, Cambridge University Press, Cambridge.

Gardner, L. R. (1972), Origin of the Mormon Mesa Caliche, Clark County, Nevada, *Geological Society of America Bulletin*, 83, p. 143-156, doi:10.1130/0016-7606.

Gellert, R., R. Rieder, R. C. Anderson, J. Brückner, B. C. Clark, G. Dreibus, T. Economou, G. Klingelhöfer, G. W. Lugmair, D. W. Ming, S. W. Squyres, C. d'Uston, H. Wänke, A. Yen, J. Zipfel (2004), Chemistry of Rocks and Soils in Gusev Crater from the Alpha Particle X-ray Spectrometer, *Science, 305*, 829-832, doi:10.1126/science.1099913.

Gendrin, A., N. Mangold, J.-P. Bibring, Y. Langevin, B. Gondet, F. Poulet, G. Bonello, C. Quantin,J. Mustard, R. Arvidson, and S. LeMouélic (2005), Sulfates in Martian layered terrains:The OMEGA/Mars Express view, *Science*, 307, 1587, doi:10.1126/science.1109087.

Getahun, A., M. H. Reed, R. Symonds (1996), Mount St. Augustine volcano fumarole wall rock alteration: mineralogy, zoning, composition and numerical models of its formation process, *Journal of Volcanology and Geothermal Research., 71*, 73-107.

Gillespie, A.R. (1992), Spectral mixture analysis of multispectral thermal infrared images, *Remote Sensing of the Environment*, 42, 2, 137-145.

Gillespie, A. R. et al. (1986), Color enhancement of highly correlated images: I. Decorrelation and HSI contrast stretches, *Remote Sensing of the Environment, 20*, 209-235, doi:10.1016/0034-4257(86)90044-1.

Gillespie, A., S. Rokugawa, T. Matsunaga, J. S. Cothern, S. Hook and A. B. Kahle (1998), A temperature and emissivity separation algorithm for Advanced Spaceborne Thermal Emission and Reflection Radiometer (ASTER) images, *IEEE Transactions on Geoscience and Remote Sensing*, 36, 4, 1113-1125.

Glotch, T. D. and J. L. Bandfield (2006), Determination and interpretation of surface atmospheric Miniature Thermal Emission Spectrometer spectral end-members at the Meridiani Planum landing site, *Journal of Geophysical Research*, 111, E12S06, doi:10.1029/2005JE002671.

Glotch, T.D., R. V. Morris, P. R. Christensen, and T. G. Sharp (2004), Effect of precursor mineralogy on the thermal infrared emission spectra of hematite: Application to Martian hematite mineralization, *Journal of Geophysical Research*, 109, E07003, doi:10.1029/2003JE002224.

Goff, F. and C. J. Jank (2000), Geothermal Systems, in *Encyclopedia of Volcanoes* (Ed. H. Sigurdsson), 817-834, Academic Press, An Imprint of Elsevier, San Diego, CA.

Goodall, T. M. et al. (2000), Surface and subsurface sedimentary structures produced by salt crusts, *Sedimentology, 47*, 99-118.

Gooding, J. L. (1992), Soil mineralogy and chemistry on Mars: possible clues from salts and clays in SNC meteorites, *Icarus*, 99, 28-41.

Gooding, J. L., K. E. Aggrey and D. W. Muenow (1990), Volatile compounds in shergottite and nakhlite meteorites, *Meteoritic*s, 25, 281-289.

Gooding, J. L., S. L. Wentworth, and M. E. Zolensky (1991), Aqueous alteration of the Nakhla meteorite, *Meteoritics*, 26, 135-143.

Gorelick, N. S., M. Weiss-Malik, B. Steinberg, and S. Anwar (2003), JMARS: A multimission data fusion application, *Lunar and Planetary. Science Conference, XXXIV*, Abstract #2057.

Greeley, R. and J. D. Iversen (1985), *Wind as a Geological Process on Earth, Mars, Venus, and Titan*, 333 p. Cambridge Univ. Press, New York.

Greeley, R. and J. E. Guest (1987), Geologic map of the eastern equatorial region of Mars, scale1:15,000,000, *U.S. Geological Survey Miscellaneous Investigations Series Map, I-1802-B.*

Greeley, R., N. Lancaster, S. Lee, and P. Thomas (1992), Martian aeolian processes, sediments, and features, In *Mars*, edited by H. H. Kieffer, B. M. Jakosky, C. W. Snyder, and M. S. Matthews, University of Arizona Press, Tucson, 730-766.

Greeley, R., M. D. Kraft, R. O. Kuzmin, and N. T. Bridges (2000), Mars Pathfinder landing site: Evidence for a chance in wind regime from lander and orbiter data, *Journal of Geophysical Research*, 105, E1, 1829-1840.

Greeley, R. N. T. Bridges, R. O. Kuzmin, and J. E. Laity (2002), Terrestrial analogs to wind-related features at the Viking and Pathfinder landing sites on Mars, *Journal of Geophysical Research*, 107, E1, 5005, doi:10.1029/2000JE001481.

Greeley, R. N., R. Arvidson, J. F. Bell III, P. Christensen, D. Foley, A. Haldermann, R. O. Kuzmin, G. Landis, L. D. V. Neakrase, G. Neukum, S. W. Squyres, R. Sullivan, S. D. Thompson, P. L. Whelley, and D. Williams (2005), Martian variable features: new insight from the Mars Express Orbiter and the Mars Exploration Rover Spirit, *Journal of Geophysical Research*, 110, E06002, doi:10.1029/2005JE002403.

Greeley, R., P. L. Whelley, R. E. Arvidson, N. A. Cabrol, D. J. Foley, B. J. Franklin, P. Geissler, M. P. Golombek, R. O. Kuzmin, G. A. Landis, M. T. Lemmon, L. D. V. Neakrase, S. W. Squyres, and S. D.Thompson (2006a), Active dust devils in Gusev crater, Mars: Observations from the Mars Exploration Rover Spirit, *Journal of Geophysical Research*, 111, E12S09, doi:10.1029/2006JE002743.

Greeley, R., R. E. Arvidson, P. W. Barlett, D. Blaney, N. A. Cabrol, P. R. Christensen, R. L. Fergason, M. P. Golombek, G. A. Landis, M. T. Lemmon, S. M. McLennan, J. N. Maki, T. Michaels, J. E. Moersch, L. D. V. Neakrase, S. C. R. Rafkin, L. Richter, S. W. Squyres, P. A. de Souza Jr., R. J. Sullivan, S. D. Thompson, and P. L. Whelley (2006b), Gusev crater: Wind-related features and processes observed by the Mars Exploration Rover Spirit, *Journal of Geophysical Research*, 111, E02S09, doi:10.1029/2005JE002491.

Greeley, R., P. L. Whelley, L. D. V. Neakrase, R. E. Arvidson, N. T. Bridges, N. A. Cabrol, P. R. Christensen, K. Di, D. J. Foley, M. P. Golombek, K. Herkenhoff, A. Knudson, R. O. Kuzmin, R. Li, T. Michaels, S. W. Squyres, R. Sullivan, and S. D. Thompson (2008), Columbia Hills, Mars: Aeolian features seen from the ground and orbit, *Journal of Geophysical Research*, 113, E06S06, doi:10.1029/2007JE002971.

Griffith, J. D., S. Willcox, D. W. Powers, R. Nelson, and B. K. Baxter (2008), Discovery of Abundant Cellulose Microfibers Encased in 250 Ma Permian

Halite: A Macromolecular Target in the Search for Life on Other Planets, *Astrobiology, 8*, 2, doi:10.1089/ast. 2007.0196.

Grotzinger, J. P., R. E. Arvidson, J. F. Bell III, W. Calvin, B. C. Clark, D. A. Fike, M. Golombek, R. Greeley, A. Haldemann, K. E. Herkenhoff, B. L. Jolliff, A. H. Knoll, M. Malin, S. M. McLennan, T. Parker, L. Soderblom, J. N. Sohl-Dickstein, S. W. Squyres, N. J. Tosca, W. A.Watters (2005), Stratigraphy and sedimentology of a dry to wet eolian depositional system, Burns formation, Meridiani Planum, Mars, *Earth and Planetary Science Letters, 240*, 11-72, doi:10.1016/j. epsl.2005.09.039.

Hamilton, V. E. (1999), The effect of particle size on rock spectra in the thermal infrared: Implications for TES data analysis, *Lunar and Planetary Science Conferenc*e, XXX, abstract #2001.

Hamilton, V. E. and P. R. Christensen (2000), Determination of modal mineralogy of mafic and ultramafic igneous rocks using thermal emission spectroscopy, *Journal of Geophysical Research*, 105, p. 9717-9734.

Hamilton, V. E. and P. R. Christensen (2005), Evidence for extensive, olivine-rich bedrock on Mars, *Geology, 33*, 6, 433-436, doi:10.1130/G21258.1

Hamilton, V. E, M. B. Wyatt, H. Y. McSween Jr., and P. R. Christensen (2001), Analysis of terrestrial and martian volcanic compositions using thermal emission spectroscopy: II Application to martian surface spectra from MGS TES, *Journal of Geophysical Research*, 106, 14,733- 14,747.

Hamilton, V. E., P. R. Christensen, H. Y. McSween Jr., and J. L. Bandfield (2003), Searching for the source regions of the martian meteorites using MGS TES; Integrating martian meteorites into the global distribution of igneous materials on Mars, *Meteoritics and Planetary Science*, 38, 6, 871-885.

Hamilton, V. E., R. V. Morris, J. E. Gruener, and S. A. Mertzman (2008), Visible, near-infrared, and middle infrared spectroscopy of altered basaltic tephras: Spectral signatures of phyllosilicates, sulfates, and other aqueous alteration products with application to the mineralogy of Columbia Hills of Gusev, Mars, *Journal of Geophysical Research*, 113, E12S43, doi:10.1029/2007JE003049.

Hapke, B. (1993a) *Theory of Reflectance and Emittance Spectroscopy*, pp. 373-374, Cambridge University Press, New York

Hapke, B. (1993b), Combined Theory of Reflectance and Emittance Spectroscopy, in *Remote Geochemical Analysis: Elemental and Mineralogical Composition*,

edited by C. M. Pieters and P. A. J. Englert, Cambridge University Press, Cambridge.

Harloff, J. and G. Arnold (2001), Near-infrared reflectance spectroscopy of bulk analog materials for planetary crust, *Planetary Space Science*, 49, 191-211.

Harrison, K. P., and R. E. Grimm (2005), Groundwater-controlled valley networks and the decline of the surface runoff on early Mars, *Journal of Geophysical Research, 110*, E12S16, doi:10.1029/2005JE002455.

Hartmann, W. K. and G. Neukum (2001), Cratering chronology and the evolution of Mars, *Space Science Reviews, 96*, 165-194.

Haskin, L. A., A. Wang, B. L. Jolliff, H. Y. McSween, B. C. Clark, C. J. Des Marais, S. M. McLennan, N. J. Tosca, J. A. Hurowitz, J. D. Farmer, A. Yen, S. W. Squyres, R. E. Arvidson, G. Klingelhöfer, C. Schröder, P. A. deSouza Jr., D. W. Ming, R. Gellert, J. Zipfel, J. Brückner. J. F. Bell III, K. Herkenhoff, P. R. Christensen, S. Ruff, B. Blaney, S. Gorevan, N.A. Cabrol, L. Crumpler, J. Grant, and L. Soderblom (2005), Water alteration of rocks and soils on Mars at the Spirit rover site in Gusev Crater, *Nature, 436*, 66-69, doi:10.1038/nature03640.

Hodson, M. E. (1999), Micropore surface area variation with grain size in unweathered alkali feldspars: Implications for surface roughness and dissolution studies, *Geochimica et Cosmochimica Acta*, 62, 21/22, 3429-3435.

Hoefen, M. T., R. N. Clark, J. L. Bandfield, M. D. Smith, J. C. Pearl, and P. R. Christensen (2003) Discovery of olivine in the Nili Fossae region of Mars, *Science*, 302, 627, doi:10.1126/science.1089647

Hoke, M. R. T. and B. M. Hynek (2009), Roaming zones of precipitation on ancient Mars as recorded in valley networks, *Journal of Geophysical Research, 114*, E08002, doi:10.1029/2008JE003247.

Howard, A. D., J. M. Moore, and R. P. Irwin III (2005), An intense terminal epoch of widespread fluvial activity on Mars: 1. Valley network incision and associated deposits, *Journal of Geophysical Research, 110*, E12S14, doi:10.1029/2005JE002459.

Huppert, H. E., R. S. J. Sparks, J. S. Turner, and N. T. Arndt (1984), Emplacement and cooling of komatiite lavas, *Nature, 309*, 19-22.

Hunt, G. R. (1976) Infrared spectral behavior of fine particulate solids, *Journal of Physical Chemistry,* 80, 1195-1198.

Hunt, G. R. and R. K. Vincent (1968), The behavior of spectral features in the infrared emission from particulate surfaces of various grain sizes, *Journal of Geophysical Researc*h, 73, 18, p. 6039-6046.

Hunt, G. K. and L. M. Logan (1972), Variation of single particle mid-infrared emission spectrum with particle size, *Applied Optics*, 11, 1, p. 142-147.

Huval, J. H. and R. H. Vreeland (1991), Taxonomy of halophilic bacteria from underground saline waters and salt formations, in *General and Applied Aspects of Halophilic Bacteria*, edited by F. Rodriguez-Valera, pp. 53-60, Plenum, New York.

Hynek, B. M., M. R. T. Hoke, and M. Beach (2010), Updated Global Map of Martian Valley Networks and Implications for Climate and Hydrologic Processes, *Journal of Geophysical Research,* doi:10.1029/2009JE003542, in press.

Irwin, R. P., III, A. D. Howard, R. A. Craddock, and J. M. Moore (2005), An intense terminal epoch of widespread fluvial activity on Mars. 2. Increased runoff and paleolake development, *Journal of Geophysical Research, 110*, E12S15, doi:10.1029/2005JE002460.

Ivanov, B. A. (2001), Mars/Moon Crater Rate Ratio Estimates, *Space Science Reviews*, *96*(1-4), 87-104, doi:10/1023/A.1011941121102

Jakosky, B. M., B. G. Henderson, and M. T. Mellon (1995), Chaotic obliquity and the nature of the Martian climate, *Journal of Geophysical Research, 100*, 1579-1584, doi:10.1029/94JE02801.

Javor, B. (1989), *Hypersaline Environments*, 334 pp., Springer-Verlag, New York.

Jensen, H. B. and T. D. Glotch (2010), Near infrared spectral analysis of mixtures of halite and labradorite for application to putative chloride deposits observed by CRISM, *Lunar and Planetary Science Conference, 41st*, Abstract #1436.

Keller, J. M., W. V. Boynton, S. Karunatillake, V. R. Baker, J. M. Dohm, L. G. Evans, M. J. Finch, B. C. Hahn, D. K. Hamara, D. M. Janes, K. E. Kerry, H. E. Newsom, R. C. Reedy, A. L. Sprague, S. W. Squyres, R. D. Starr, G. J. Taylor, and R. M. S Williams (2006), Equatorial and midlatitude distribution of chlorine measured by Mars Odyssey GRS, *Journal of Geophysical Research, 111*, E03S08, doi:10.1029/2006JE002679.

Keszthelyi, L. P., W. L. Jaeger, C. M. Dundas, S. Martínez-Alonso, A. S. McEwen, M. P. Milazzo (2010), Hydrovolcanic features on Mars: Preliminary observations from the first Mars year of HiRISE imaging, *Icarus, 205*, 211-229, doi:10.1016/j. icarus.2009.08.020.

Kieffer, H. H., S. C. Chase Jr., E. Miner, G. Münch, and G. Neugebauer (1973), Preliminary report on infrared radiometric measurements from the Mariner 9 spacecraft, *Journal of Geophysical Research, 78*(20), 4291- 4312.

Kieffer, H. H., Z. Martin, A. R. Peterfreund, B. M. Jakosky, E. D. Miner, and F. D. Palluconi (1977), Thermal and albedo mapping of Mars during the Viking primary mission, *Journal of Geophysical Research, 82*(28), 4249-4291.

Kirkland, L. E., K. C. Herr, P. M. Adams (2003), Infrared stealthy surfaces: Why TES and THEMIS may miss some substantial mineral deposits on Mars and implications for remote sensing of planetary surfaces, *Journal of Geophysical Research*, 108, E12, 5137, doi:10.1029/2003JE002105.

Klein, C., and C. S. Hurlburt Jr. (1985), *Manual of Mineralogy, After James D. Dana*, 21 st ed., 681 pp. John Wiley, New York.

Knauth, P.L. and D. M. Burt (2002), Eutectic brines on Mars: Origin and possible relation to young seepage features, *Icarus* 158, 267-271, doi:10.1006/icar.2002.6866.

Knoll, A. H., B. L. Jolliff, W. H. Farrand, J. F. Bell III, B. C. Clark, R. Gellert, M. P. Golombek, J. P. Grotzinger, K. E. Herkenhoff, J. R. Johnson, S. M. McLennan, R. Morris, S. W. Squyres, R. Sullivan, N. J. Tosca, A. Yen, and Z. Learner (2007), Veneers, rinds, and fracture fills: Relatively late alteration of sedimentary rocks at Meridiani Planum, Mars, *Journal of Geophysical Research,* 113, E06S16, doi:10.1029/2007JE002949.

Koeppen, W. C. and V. E. Hamilton (2008), Global distribution, composition, and abundance of olivine on the surface of Mars from thermal infrared data, *Journal of Geophysical Research*, 113, E05001, doi:10.1029/2007JE002984.

Knauth, L. P., D. M. Burt, and K. H. Wohletz (2005), Impact origin of sediments at the Opportunity landing site on Mars, *Nature, 438*, 1123-1128, doi:10.1038/nature04383.

Knoll, A. H., B. L. Jolliff, W. H. Farrand, J. F. Bell III, B. C. Clark, R. Gellert, M. P. Golombek, J. P. Grotzinger, K. E. Herkenhoff, J. R. Johnson, S. M. McLennan, R. Morris, S. W. Squyres, R. Sullivan, N. J. Tosca, A.. Yen, and Z. Learner (2008), Veneers, rinds, and fracture fills: Relatively late alteration of sedimentary rocks at Meridiani Planum, Mars, *Journal of Geophysical Research.,* 113, E06S16, doi:10.1029/2007JE002949.

Lane, M. D (2007), Midinfrared emission spectroscopy of sulfate and sulfate-bearing minerals, *American Mineralogist*, 92, 1-18.

Lane, M. D. and P. R. Christensen (1997), Thermal infrared emission spectroscopy of anhydrous carbonates, *Journal of Geophysical Researc*h, 102, E11, 25581-25592.

Lane, M.D. and P. R. Christensen (1998), Thermal infrared emission spectroscopy of salt minerals predicted for Mars, *Icarus* 135, 528-536.

LaRocca, A. J. (1978), Artificial sources, in *The Infrared Handbook*, edited by W. Wolfe and G. Zissis, Ch. 2, p. 2-1 to 2-97, ERIM Press, Ann Arbor, Mich.

Leverington, D. W. and T. A. Maxwell (2004), An igneous origin for features of a candidate crater-lake system in western Memnonia, Mars, *Journal of Geophysical Research, 109*, E06006, doi:10.1029/2004JE002237.

Lichtenberg, K. A., R. E. Arvidson, R. V. Morris, S. L. Murchie, J. L. Bishop, D. Fernandes Remolar, T. D. Glotch, E. Noe Dobrea, J. F. Mustard, J. Andrews-Hanna, and L. H. Roach (2010), Stratigraphy of hydrated sulfates in the sedimentary deposits of Aram Chaos, Mars, *Journal of Geophysical Research,* 115, E00D17, doi:10.1029/2009JE003353.

Lowenstein, T. K., J. Li, C. Brown, S. M. Roberts, T. Ku, S. Luo, and W. Yang (1999), 200 k.y. paleoclimate record from Death Valley salt core, *Geology, 27*, 3-6, doi:10.1130/0091-7613(1999)027

Lyon, R. J. P. (1964) Evaluation of Infrared Spectraphotometry for Compositional Analysis of Lunar and Planetary Soils, Part II, Rough and Powdered Surfaces. NASA Report CR-100.

Lyon, R. J. P. (1965), Analysis of rocks spectra by infrared emission (8-25μm), *Economic Geology*, 60, 715 -736.

Malin, M. C., G. E. Danielson, A. P. Ingersoll, H. Masursky, J. Veverka, M. A. Ravine, and T. A. Soulanille (1992), Mars Observer Camera, *Journal of Geophysical Research, 97*, E5, 7699-7718, doi:10.1029/92JE00340

Malin, M. C. and K. S. Edgett (2000) Sedimentary Rocks of Early Mars, *Science, 290*, 1927-1937, doi:10.1126/science.290.5498.1927

Malin, M. C. and K. S. Edgett (2001), 2001 Global Surveyor Mars Orbiter Camera: Interplanetary cruise through primary mission, *Journal of Geophysical Research*, 106, 23429-23570.

Malin, M. C., J. F. Bell III, B. A. Cantor, M. A. Capliner, W. M. Calvin, R. T. Clancey, K. S. Edgett, L. Edwards, R. M. Haberle, P. B. James, S. W. Lee,

M. A. Ravine, P. C. Thomas, and M. J. Wolff (2007), Context Camera Investigation on board the Mars Reconnaissance Orbiter, *Journal of Geophysical Research*, 112, E05S04, doi:10.1029/2006JE002808.

Mandelbrot, B. B. (1982), *The Fractal Geometry of Nature*, W. H. Freeman, New York.

Marion, G. M., D. C. Catling, J. S. Kargel (2009), Br/Cl partitioning in chloride minerals in the Burns formation on Mars, *Icarus, 200*, 436-445, doi:10.1016/j. icarus.2008.12.004.

McEwen, A. S., E. M. Eliason, J. W. Bergstrom, N. T. Bridges, C. J. Hansen, W. A. Delamere, J. A. Grant, V. C. Gulick, K. E. Herkenhoff, L. Keszthelyi, R. L. Kirk, M. T. Mellon, S. W. Squyres, N. Thomas, and C. M. Weitz (2007), Mars Reconnaissance Orbiter's High Resolution Imaging Science Experiment (HiRISE), *Journal of Geophysical Research, 112*, E05S02, doi: 10.1029/2005JE002605.

McGenity, T. J, R. T. Gemmell, W. D. Grant, and H. Stan-Lotter (2000), Origins of halophilic microorganisms in ancient salt deposits, *Environmental Microbiology,2*(3), 243-250.

McLennan, S. M., J. F. Bell III, W. M. Calvin, P. R. Christensen, B. C. Clark, P. A. deSouza, J. Farmer, W. H. Farrand, D. A. Fike, R. Gellert, A. Ghosh, T. D. Glotch, J. P. Grotzinger, B. Hahn, K. E. Herkenhoff, J. A. Hurowitz, J. R. Johnson, S. S. Johnson, B. Jolliff, G. Klingelhöfer, A. H. Knoll, Z. Learner, M. C. Malin, H. Y. McSween Jr., J. Pocock, S. W. Ruff, L. A. Soderblom, S. W. Squyres, N. J. Tosca, W.A.Watters, M.B.Wyatt, A.Yen (2005), Provenance and diagenesis of the evaporite-bearing Burns formation, Meridiani Planum, Mars, *Earth and Planetary Science Letters, 240*, 95-121, doi:10.1016/j.epsl.2005.09.041.

Mellon, M. T., B. M. Jakosky, H. H. Kieffer, and P. R. Christensen (2000), High-resolution thermal inertia mapping from the Mars Global Surveyor Thermal Emission Spectrometer, *Icarus, 148*, 437-455.

Melosh, H. J. (1989) *Impact Cratering: A Geologic Process*. Oxford University Press, New York, 245 p.

Melosh, H. J. and A. M. Vickery (1989), Impact erosion of the primordial martian atmosphere, *Nature, 338*, 487-489.

Michalski, J. R., M. D. Kraft, T. G. Sharp, L. B. Williams, and P. R. Christensen (2006), Emission spectroscopy of clay minerals and evidence for poorly crystalline alunimosilicates on Mars fromThermal Emisison Spectrometer

data, *Journal of Geophysical Research*, 111, E03004, doi:10.1029/2005/JE002438.

Milliken, R.E., G. A. Swayze, R. E. Arvidson, J. L. Bishop, R. N. Clark, B. L. Ehlmann, R.O. Green, J. P. Grotzinger, R. V. Morris, S. L. Murchie, J. F. Mustard, and C. Weitz (2008), Opaline silica in young deposits on Mars, *Geology, 36*, 11, 847-850, doi:10.1130/G24967A.1

Milliken, R. E., K. S. Edgett, G. Swayze, R. N. Clark, B. J. Thomson, R. Anderson, J. F. Bell III (2009), Clay and sulfate-bearing rocks in a stratigraphic sequence in Gale Crater, *Lunar and Planetary Science Conference, XL*, Abstract #1479.

Ming, D. W., D. W. Mittlefehldt, R. V. Morris, D. C. Golden, R. Gellert, A. Yen, B. C. Clark, S. W. Squyres, W. H. Farrand, S. W. Ruff, R. E. Arvidson, G. Klingelhöfer, H. Y. McSween, D. S. Rodionov, C. Schröder, P. A. de Souza Jr., and A. Wang (2006), Geochemical and mineralogical indicators for aqueous processes in the Columbia Hills of Gusev crater, Mars, *Journal of Geophysical Research*, 111, E02S12, doi:10.1029/2005JE002560

Mouginis-Mark, P. L., L. Wilson, and M. T. Zuber (1992), The physical volcanology of Mars, in *Mars*, edited by H. H. Kieffer et al., pp. 424-452, Univ. of Ariz. Press, Tucson.

Moersch, J. E. and P. R. Christensen (1995), Thermal emission from particulate surfaces: A comparison of scattering models with measured spectra, *Journal of Geophysical Research*, 100, p. 7,465- 7,477.

Morris, A. M., F. S. Anderson, P. J. Mouginis-Mark, A. F. C. Haldermann, B. A. Brook, and J. Foster (2008), Roughness of Hawaiian volcanic terrains, *Journal of Geophysical Research*, 113, E12007, doi:10.1029/2008JE003079.

Murchie, S. L., R. Arvidson, P. Bedini, K. Beisser, J.-P. Bibring, J. Bishop, J. Boldt, P. Cavender, T. Choo, R. T. Clancy, E. H. Darlington, D. Des Marais, R. Espiritu, D. Fort, R. Green, E. Guinness, J. Hayes, C. Hash, K. Heffernan, J. Hemmler, G. Heyler, D. Humm, J. Hutcheson, N. Izenberg, R. Lee, J. Lees, D. Lohr, E. Malaret, T. Martin, J. A. McGovern, P. McGuire, R. Morris, J. Mustard, S. Pelkey, E. Rhodes, M. Robinson, T. Roush, E. Schaefer, G. Seagrave, F. Seelos, P. Silverglate, S. Slavney, M. Smith, W.-J. Shyong, K. Stronbehn, H. Taylor, P. Thompson, B. Tossman, M. Wirzburger, and M. Wolff (2006), Compact Reconnaissance Imaging Spectrometer for Mars (CRIMS) on Mars Reconnaissance Orbiter (MRO), *Journal of Geophysical Research*, 112, E05S03, doi:10.1029/2006JE002682.

Murchie, S. L., J. F. Mustard, B. L. Ehlmann, R. L. Milliken, J. L. Bishop, N. K. McKeown, E. Z. Noe Dobrea, F. P. Seelos, D. L. Buczkowski, S.M.

Wiseman, R. E. Arvidson, J. J. Wray, G. Swayze, R. N. Clark, D. J. Des Marais, A. S. McEwen, and J.-P. Bibring (2009), A synthesis of Martian aqueous mineralogy after 1 Mars year of observations from the Mars Reconnaissance Orbiter, *Journal of Geophysical Research, 114*, E00D06, doi:10.1029/2009JE003342.

Mustard, J. F. and J. E. Hays (1997), Effects of hyperfine particles on reflectance spectra from 0.3 to 25 μm, *Icarus*, 125, p. 145-163.

Mustard, J. F., F. Poulet, J. W. Head, N. Mangold, J.-P. Bibring, S. M. Pelkey, C. I. Fassett, Y. Langevin, and G. Neukum (2007), Mineralogy of the Nili Fossae region with OMEGA/ Mars Express data: 1. Ancient impact melt in the Isidis Basin and implications for the transition from the Noachian to Hesperian, *Journal of Geophysical Research, 112*, E08S03, doi:10.1029/2006JE002834.

Mustard, J. F., S. L. Murchie, S. M. Pelkey, B. L. Ehlmann, R. E. Milliken, J. A. Grant, J.-P. Bibring, F. Poulet, J. Bishop, E. Noe Dobrea, L. Roach, F. Seelos, R. E. Arvidson, S. Wiseman, R. Green, C. Hash, D. Humm, E. Malaret, J. A. McGovern, K. Seelos, T. Clancy, R. Clark, D. Des Marais, N. Izenberg, A. Knudson, Y. Langevin, T. Martin, P. McGuire, R. Morris, M. Robinson, T. Roush, M. Smith, G. Swayze, H. Taylor, T. Titus, and M. Wolff (2008), Hydrated silicate minerals on Mars observed by the Mars Reconnaissance Orbiter CRISM instrument, *Nature*, *454,* 305-309, doi:10.1038/nature07097.

Newsom, H. E., J. J. Hagerty, and F. Goff (1999), Mixed hydrothermal fluids and the origin of the Martian soil, *Journal of Geophysical Research, 104*, E4, 8717-8728.

Nicodemus, N. E. (1965), Directional reflectance and emissivity of an opaque surface, *Applied Optics*, 25, 2427-2433.

Norton, C. F. and W. D. Grant (1988), Survival of halobacteria within fluid inclusions in salt crystals, *Journal of General Microbiology, 134*, 1365-1373.

Norton, C. F., T. J. McGenity, and W. D. Grant (1993), Archaeal halophiles (halobacteria) from two British salt mines. *Journal of General Microbiolgy, 139*, 1077-1081.

Ondrusek, J., P. R. Christensen, and J. H. Fink (1993), Mapping the distribution of vesicular textures on silicic lavas using the Thermal Infrared Multispectral Scanner, *Journal of Geophysical Research*, 98, B9, p.15,903-15,908.

Osterloo, M. M., V. E. Hamilton, J. L. Bandfield, T. D. Glotch, A. M. Baldridge, P. R. Christensen, L. L. Tornabene, and F. S. Anderson (2008), Chloride-bearing

materials in the southern highlands of Mars, *Science*, *319*, 1651, doi:10.1126/science.1150690.

Palluconi, F.D. and H. H. Kieffer (1981), Thermal inertia mapping of Mars from 60º S to 60º N, *Icarus* 45, 415-426.

Piqueux, S. and P. R. Christensen (2009), A model of thermal conductivity for planetary soils: 2. Theory for cemented soils, *Journal of Geophysical Research, 114*, E09006, doi:10.1029/2008JE003309.

Poulet, F., J. -P. Bibring, J. F. Mustard, A. Gendrin, N. Mangold, Y. Langevin, R. E. Arvidson, B. Gondet, C. Gomez, and the OMEGA Team (2005), Phyllosilicates on Mars and implications for early martian climate, *Nature*, 438, 623-627, doi:10.1028/nature04274.

Presley, M. A. and P. R. Christensen (1997), Thermal conductivity measurements of particulate materials 2. Results, *Journal of Geophysical Research, 102*, E3, 6551-6566.

Putzig, N. E., M. T. Mellon, K. A. Kretke, and R. E. Arvidson (2005), Global thermal inertia and surface properties of Mars from the MGS mapping mission, *Icarus, 173*, 325-341, doi:101016/j.icarus.2004.08.017.

Putzig, N. E. and M. T. Mellon (2007), Apparent thermal inertia and surface heterogeneity of Mars, *Icarus, 191*, 68-94, doi:10.1016/j.icarus.2007.05.013.

Ramsey, M. S. and P. R. Christensen (1998), Mineral abundance determination: Quantitative deconvolution of thermal emission spectra, *Journal of Geophysical Research*, 103, B1, p. 577-596.

Ramsey, M. S. and J. H. Fink (1999), Estimating silicic lava vesicularity with thermal remote sensing: A new technique for volcanic mapping and monitoring, *Bulletin of Volcanology*, 61, 32-39.

Rao, M. N., S. R. Sutton, D. S. McKay, and G. Dreibyus (2005), Clues to Martian brines based on halogens in salts from nakhlites and MER samples, *Journal of Geophysical Research,* 110,E12S06, doi:10.1029/2005JE002470.

Rieder, R., T. Economou, H. Wänke, A. Turkevich, J. Crisp, J. Brückner, G. Dreibus, and H. Y. McSween, Jr., (1997), The chemical composition of Martian soil and rocks returned by the Mobile Alpha Proton X-ray Spectrometer: Preliminary results from the x-ray mode, *Science*, 278, 1771, doi:10.1126/science.278.5344.1771.

Rieder, R., R. Gellert, R. C. Anderson, J. Brückner, B. C. Clark, G. Dreibus, T. Economou, G. Klingelhöfer, G. W. Lugmair, D. W. Ming, S. W. Squyres, D. d'Uston, H. Wänke, A. Yen, J. Zipfel (2004), Chemistry of Rocks and Soils at Meridiani Planum from the Alpha Particle X-ray Spectrometer, *Science, 306*, 1746-1749, doi:10.1126/science.1104358.

Roach, L. H., J. F. Mustard, S. L. Murchie, J.-P. Bibring, F. Forget, K. W. Lewis, O. Aharonson, M. Vincendon, and J. L. Bishop (2009), Testing evidence of recent hydration state change in sulfates on Mars, Journal of Geophysical Research, 114, E00D02, doi:10.1029/2008JE003245.

Robbins, S. J. and B. M. Hynek (2010) Progress towards a new global catalog of martian craters and layered ejecta properties, complete to 1.5 km, *Lunar and Planetary Science Conference, XLI*, Abstract #2257.

Roedder, E. (1984), The fluids in salts, *American Mineralogist, 69*, 413-439.

Rogers, A. D. and P. R. Christensen (2007), Surface mineralogy of Martian low-albedo regions from MGS-TES data: Implications for upper crustal evolution and surface alteration, *Journal of Geophysical Research, 112*, E01003, doi:10.1029/2006JE002727.

Rogers, A. D., P. R. Christensen, and J. L. Bandfield (2005), Compositional heterogeneity of the ancient Martian crust: Analysis of Ares Vallis bedrock with THEMIS and TES data, *Journal of Geophysical Research*, 110, E05010, doi:10.1029/2005JE002399.

Rogers, A. D. J. L. Bandfield, and P. R. Christensen (2007), Global spectral classification of Martian low-albedo regions with Mars Global Surveyor Thermal Emission Spectrometer (MGS-TES) data, *Journal of Geophysical Research, 112*,E02004, doi:10.1029/2006JE002726.

Rothschild, L. J. and R. L. Mancinelli (2001), Life in extreme environments, *Nature, 409,* 1092-1101.

Ruff, S. W. (1998), Quantitative thermal infrared emission spectroscopy applied to granitoid petrology, Ph. D. dissertation, 234 pp. Ariz. State Univ., Tempe, 1998.

Ruff, S. W. and Christensen, P. R. (2002), Bright and dark regions on Mars: Particle size and mineralogical characteristics based on Thermal Emission Spectrometer data, *Journal of Geophysical Research*, 107, 5119, doi:10.1029/2001JE001580.

Ruff, S. W., Christensen, P. R., Barbera, P. W., and Anderson, D. L. (1997), Quantitative thermal emission spectroscopy of minerals: A laboratory technique for measurement and calibration, *Journal of Geophysical Research*, 102, 14,899- 14,913.

Salisbury, J. W. (1993), Mid-infrared spectroscopy: Laboratory data, in *Remote Geochemical Analysis: Elemental and Mineralogical Composition*, edited by C. Pieters and P. Englert, Ch. 4, Cambridge University Press, Cambridge.

Salisbury, J. W. and J. W. Eastes (1985), The effect of particle size and porosity on spectral contrast in the mid-infrared, *Icarus*, 64, p. 586-588.

Salisbury, J. W. and L. S. Walter (1989), Thermal infrared (2.5-13.5μm) spectroscopic remote sensing of igneous rock types on particulate planetary surfaces, *Journal of Geophysical Research*, 94 (B7), 9192- 9202.

Salisbury, J. W. and A. Wald (1992), The role of volume scattering in reducing spectral contrast of reststrahlen bands in spectra of powdered minerals, *Icarus*, 96, 121-128.

Salisbury, J. W., B. Hapke, and J. W. Eastes (1987), Usefulness of weak bands in midinfrared remote sensing of particulate planetary surfaces, *Journal of Geophysical Research*, 92, 702-710.

Salisbury, J. W., D. M. D'Aria, and E. Jarosewich (1991), Mid-infrared (2.5 - 13.5 μm) reflectance spectra of powdered stony meteorites, *Icarus*, 92, 280-297.

Salisbury, J. W., L. S. Walter, N. Vergo, and D. M. D'Aria (1992), In: *Infrared (2.1-25 μm) spectra of Minerals*. The John Hopkins University Press, Baltimore and London.

Satterfield, C. L., T. K. Lowenstein, R. H. Vreeland, W. D. Rosenzweig, and D. W. Powers (2005), New Evidence for 250 Ma age of halotolerant bacterium from a Permian salt crystal, *Geology (33)*, 265-268.

Schmidt, M. E., S. W. Ruff, T. J. McCoy, W. H. Farrand, J. R. Johnson, R. Gellert, D. W. Ming, R. V. Morris, N. Cabrol , K. W. Lewis, and C. Schroeder (2008), Hydrothermal origin of halogens at Home Plate, Gusev Crater, *Journal of Geophysical Research, 113*, E06S12, doi:10.1029/2007JE003027.

Schmittbuhl, J., S. Gentier, S. Roux (1993), Field measurements of the roughness of fault surfaces, *Geophysical Research Letters*, 20, 8, 639-641.

Schneider, R. D. and V. E. Hamilton (2006), Evidence for locally derived, ultramafic intracrater materials in Amazonis Planitia, Mars, *Journal of Geophysical Research, 111,* E09007, doi:10.1029/2005JE002611.

Schubert, B. A., T. K., Lowenstein, M. N. Timofeeff and M. A. Parker (2009), How do prokaryotes survive in fluid inclusions in halite for 30 k.y.? *Geology, 37*, 1059-1062, doi:10.1120/G30448A.1

Scott, D. H. and K. L. Tanaka (1986), Geologic map of the western equatorial region of Mars, scale 1:15,000,000, *U.S. Geological Survey Miscellaneous Series Investigation Map, I-1802-A.*

Shepard, M. K., R. A. Brackett, and R. E. Arvidson (1995), Self-affine (fractal) topography: Surface parameterization and radar scattering, *Journal of Geophysical Research*, 100, 11,709-11,718, doi:10.1029/95JE00664.

Siegel, R. and J. Howell (1968), Thermal Radiation Heat Transfer, vol.1, *NASA Special Publication*, NASA SP-164.

Singer, R. B., T. B. McCord, R. N. Clark, J. B. Adams, and R. L. Huguenin (1979), Mars surface composition from reflectance spectroscopy: A summary, *Journal of Geophysical Research,* 84, B14, 8415-8426.

Smith, D. E., M. T. Zuber, H. V. Frey, J. B. Garvin, J. W. Head, D. O. Muhleman, G. H. Pettengill, R. J. Phillips, S. C. Solomon, H. J. Zwally, W. B. Banerdt, T. C. Duxbury, M. P. Golombek, F. G. Memoine, G. A. Neumann, D. D. Rowlands, O. Aharonson, R. G. Ford, A. B. Ivanov, C. L. Johnson, P. J. McGovern, J. B. Abshire, R. S. Afzal, and X. Sun (2001), Mars Orbiter Laser Altimeter: Experiment summary after the first year of global mapping of Mars, *Journal of Geophysical Research, 106*(E10), 23689-23722, doi:10.1029/2000JE001364.

Smith, D., G. Neumann, R. E. Arvidson, E. A. Guinness, and S. Slavney (2003), Mars Global Surveyor Laser Altimeter Mission Experiment Gridded Data Record, *NASA Planetary Data System*, MGS-M-MOLA-MEGDR-L3-V1.0.

Sqyures, S. W., J. P. Grotzinger, R. E. Arvidson, J. F. Bell III, W. Calvin, P. R. Christensen, B. C. Clark, J. A. Crisp, W. H. Farrand, K. E. Herkenhoff, J. R> Johnson, G. Klingelhöfer, A. H. Knoll, S. M. McLennan, H. Y. McSween Jr., R. V. Morris, J. W. Rice, Jr., R. Rieder, and L. A. Soderblom (2004), In situ evidence for an ancient aqueous environment at Meridiani Planum, Mars, *Science*, 306, 1709, doi:10.1126/science.1104559.

Squyres, S. W., O. Aharonson, B. C. Clark, B. A. Cohen, L. Crumpler, P. A. de Souza, W. H. Farrand, R. Gellert, J. Grant, J. P. Grotzinger, A. R. C.

Haldermann, J. R. Johnson, G. Klingerlhöfer, K. W. Lewis, R. Li, T. McCoy, A. S. McEwen, H. Y. McSween, D. W. Ming, J. M. Moore, R. V. Morris, T. J., Parker, J. W. Rice, Jr., S. Ruff, M. Schmidt, C. Schröder, L. A. Soderblom and A. Yen (2007), Pyroclastic activity at Home Plate in Gusev Crater, Mars, *Science*, 316, 738, doi:10.1126/science.1139045.

Stemp, W. J. and M. Stemp (2003), Documenting stages of polish development on experimental stone tools: Surface characterization by fractal geometry using USM laser profilometry, *Journal of Archaeological Sciences*, 30, p. 287-296, doi:10.1006/jasc.2002.0837.

Stivaletta, N., R. Barbieri, C. Picard, and M. Bosco (2009), Astrobiological significance of the sabkha life and environments of southern Tunisia, *Planetary and Space Science, 57,* 597-605, doi:10.1016/j.pss.2008.10.002.

Stockstill-Cahill, K. R., F. S. Anderson, V. E. Hamilton (2008), A study of low-albedo deposits within Amazonis Planitia craters: Evidence for locally derived ultramafic to mafic materials, *Journal of Geophysical Research, 113*, E07008, doi:10.1029/2007JE003026.

Sullivan, R., D. Banfield, J. F. Bell III, W. Calvin, D. Fike, M. Golombek, R. Greeley, J. Grotzinger, K. Herkenhoff, D. Jerolmack, M. Malin, D. Ming, L. A. Soderblom, S. W. Squyres, S. Thompson, W. A. Watter, C. M. Weitz, and A. Yen (2005), Aeolian processes at the Mars Exploration Rover Meridiani Planum landing site, *Nature*, 436, 58-61, doi:10.1038/nature03641.

Sullivan, R., A. Arvidson, J. F. Bell III, R. Gellert, M. Golombek, R. Greeley, K. Herkenhoff, J. Johnson, S. Thompson, P. Whelley, and J. Wray (2008), Wind-driven particle mobility on Mars: Insights from Mars Exploration Rover observations at "El Dorado" and surroundings at Gusev Crater, *Journal of Geophysical Research*, 113, E06S07, doi:10.1029/2008JE003101.

Tanaka, K. L. (1986), The stratigraphy of Mars, *Journal of Geophysical Research, 91*, E139-E158, doi:10.1029/JB091iB13p0E139.

Tanaka, K. L. and W. K. Hartmann (2008), The planetary timescale, in *The Concise Geologic Time Scale*, edited by J. G. Ogg, G. M. Ogg, and F. M. Gradstein, pp. 13-22, Cambridge University Press, New York.

Tanaka, K. L., J. M. Dohm, R. Irwin, E. J. Kolb, J. A. Skinner, Jr. and T. M. Hare (2009) Progress in global geologic mapping of Mars, *Lunar and Planetary Science Conference, XL.,* Abstract #1975

Taylor, G. J., J. D. Stopar, W. V. Boynton, S. Karunatillake, J. M. Keller, J. Brückner, H. Wänke, G. Dreibus, K. E. Kerry, R. C. Reedy, L. G. Evans, R. D. Starr, L.

M. V. Martel, S.W. Squyres, O. Gasnault, S. Maurice, C. d'Uston, P. Englert, J. M. Dohm, V. R. Baker, D. Hamara, D. Janes, A. L. Sprague, K. J. Kim, D. M. Drake, S. M. McLennan, and B. C. Hahn (2006), Variations in K/Th on Mars, *Journal of Geophysical Research, 111,* E03S06, doi:10.1029/2005JE002645.

Thomson, J. L. and J. W. Salisbury (1993), The mid-infrared reflectance of mineral mixtures (7-14 μm), *Remote Sensing of the Environment*, 45,1, 1-13, doi:10.1016/0034-4256(93)90077-B.

Tornabene, L. L., J. E. Moersch, H. Y. McSween Jr., V. E. Hamilton, J. L. Piatek, and P. R. Christensen (2008), Surface and crater-exposed lithologic units of the Isidis Basin as mapped by coanalysis of THEMIS and TES derived data products, *Journal of Geophysical Research, 113*, E10001, doi:10.1029/2007JR002988.

Tosca, N. J., and S. M. McLennan (2006), Chemical divides and evaporite assemblages on Mars, *Earth and Planetary Science Letters, 21*, 21-31, doi:10.1016/j.epsl.2005.10.021.

Tosca, N. J., A. H. Knoll, and S. M. McLennan (2008), Water Activity and the Challenge for Life on Early Mars, *Science, 320*, 1204, doi:10.1126/science.1155432

Vincent, R. K. and G. R. Hunt (1968), Infrared reflectance from mat surfaces, *Applied Optics*, 7,1, p. 53-59.

Vincent, R. K., and F. Thompson (1972), Spectral composition imaging of igneous rocks in the 8- to 12- μm region, *Journal of Geophysical Research*, 94, p. 9203-9213.

Vreeland, R. H., W. D. Rosenzweig, and D. W. Powers (2000), Isolation of a 250 million-year-old halotolerant bacterium from a primary salt crystal, *Nature, 407*, 897-900.

Wänke, H., J. Brückner, G. Dreibus, R. Rieder, and I. Ryabchikov (2001), Chemical composition of rocks and soils at the Pathfinder site, *Space Science Reviews*, 96, 317-330

Ward, A. W. (1979) Yardangs on Mars: Evidence of Recent Wind Erosion, *Journal of Geophysical Research, 84*, B14, 8147-8166

White, A. F. and S. L. Brantley (2003), The effect of time on the weathering of silicate minerals: why do weathering rates differ in the laboratory and field, *Chemical Geology*, 202, 479-506, doi:10.1016/j. chemgeo.2003.03.001.

Wilson, E. B. Jr., J. C. Decius, and P. C. Cross (1955), *Molecular Vibrations: The Theory of Infrared and Raman Vibrational Spectra*, McGraw-Hill.

Williams, C. S. (1961), Discussion of the theories of cavity-type sources of radiant energy, *Journal of the Optical Society of America*, 51, 564-571.

Wiseman, S. M., R. E. Arvidson, J. C. Andrews-Hanna, R. N. Clark, N. L. Lanza, D. Des Marais, G. A. Marzon, R. V. Morris, S. L. Murchie, H. E. Newsom, E. Z. Noe Dobrea, A. M. Ollila, F. Poulet, T. L. Roush, F. P. Seelos, and G. A. Swayze (2008a), Phyllosilicate and sulfate-hematite deposits within Miyamoto crater in southern Sinus Meridiani, Mars, *Geophysical Research Letters, 35*, L19204, doi:10.1029/2008GL035363.

Wiseman, S. M., R. E. Arvidson, S. Murchie, F. Poulet, J. C. Andrews-Hanna, R. V. Morris, F. P. Seelos, and the CRISM Team (2008b), Phyllosilicate and hydrated sulfate deposits in Meridiani, *Lunar and Planetary Science Conference, XXXIX*, Abstract # 1806.

Wray, J. J., S. L. Murchie, S. W. Squyres, F. P. Seelos, and L. L. Tornabene (2009), Diverse aqueous environments on ancient Mars revealed in the southern highlands, *Geology, 37,* 1043-1046, doi:10.1130/G30331A.1.

Wyatt, M. B., V. E. Hamilton, H. Y. McSween Jr., P. R. Christensen, and L. A. Taylor (2001), Analysis of terrestrial and Martian volcanic compositions using thermal emission spectroscopy. 1. Determination of mineralogy, chemistry, and classification strategies, *Journal of Geophysical Research*, 106, E7, p. 14,711-14,732.

Yen, A. S., R. Gellert, C. Schröder, R. V. Morris, J. F. Bell III, A. T. Knudson, B. C. Clark, D. W. Ming, J. A. Crisp, R. E. Arvidson, D. Blaney, J. Brückner, P. R. Christensen, D. J. Des Marais, P. A. deSouza Jr., T. E. Economou, A. Ghosh, B. C. Hahn, K. E. Herkenhoff. L. A. Haskin, J. A. Hurowitz, B. L. Jolliff, J. R. Johnson, G. Klingelhöfer, M. Bo Madsen, S. M. McLennan, H. Y. McSween, L. Richter, R. Rieder, D. Rodionov, L. Soderblom, S. W. Squyres, N. J. Tosca, A. Wang, M. Wyatt, and J. Zipfel (2005), An integrated view of the chemistry and mineralogy of martian soils, *Nature, 436*, 49-54, doi:10.1038/nature03637.

Yen, A. S., J. Grotzinger, R. Gellert, B. C. Clark, S. M. McLennan, R. V. Morris, C. Schröder, G. Klingelhöfer, K. E. Herkenhoff, J. R. Johnson, and the Athena Science Team (2006), Evidence for halite at Meridiani Planum, *Lunar and Planetary Science Conference, XXXVII*, Abstract #2128.

Yen, A. S., R. V. Morris, B. C. Clark, R. Gellert, A. T. Knudson, S. Squyres, D. W. Mittlefehldt, D. W. Ming, R. Arvidson, T. McCoy, M. Schmidt, J. Hurowitz, R. Li, and J. R. Johnson (2008), Hydrothermal processes at Gusev Crater: An evaluation of Paso Robles class soils, *Journal of Geophysical Research, 113*, E06S10, doi:10.1029/2007JE002978.

Zuber, M. T., D. E. Smith, S. C. Solomon, D. O. Muhleman, J. W. Head, J. B. Garvin, J. B. Abshire, and J. L. Bufton (1992), The Mars Observer Laser Altimeter Investigation, *Journal of Geophysical Research, 97*, E5, 7781-7797.